

# Google matrix analysis of directed networks

Leonardo Ermann

*Departamento de Física Teórica, GlyA, Comisión Nacional de Energía Atómica,  
Buenos Aires, Argentina*

Klaus M. Frahm and Dima L. Shepelyansky

*Laboratoire de Physique Théorique du CNRS, IRSAMC, Université de Toulouse, UPS,  
31062 Toulouse, France*

(published 2 November 2015; corrected 17 August 2016)

In the past decade modern societies have developed enormous communication and social networks. Their classification and information retrieval processing has become a formidable task for the society. Because of the rapid growth of the World Wide Web, and social and communication networks, new mathematical methods have been invented to characterize the properties of these networks in a more detailed and precise way. Various search engines extensively use such methods. It is highly important to develop new tools to classify and rank a massive amount of network information in a way that is adapted to internal network structures and characteristics. This review describes the Google matrix analysis of directed complex networks demonstrating its efficiency using various examples including the World Wide Web, Wikipedia, software architectures, world trade, social and citation networks, brain neural networks, DNA sequences, and Ulam networks. The analytical and numerical matrix methods used in this analysis originate from the fields of Markov chains, quantum chaos, and random matrix theory.

DOI: [10.1103/RevModPhys.87.1261](https://doi.org/10.1103/RevModPhys.87.1261)

PACS numbers: 89.20.Hh, 89.75.Hc, 89.75.Fb

## CONTENTS

I. Introduction	1261	D. Top people of Wikipedia	1280
II. Scale-free Properties of Directed Networks	1263	E. Multilingual Wikipedia editions	1281
III. Construction of Google Matrix and its Properties	1263	F. Networks and entanglement of cultures	1283
A. Construction rules	1263	X. Google Matrix of Social Networks	1285
B. Markov chains and Perron-Frobenius operators	1264	A. Twitter network	1285
C. Invariant subspaces	1265	B. Poisson statistics of PageRank probabilities	1286
D. Arnoldi method for numerical diagonalization	1266	XI. Google Matrix Analysis of World Trade	1287
E. General properties of eigenvalues and eigenstates	1266	A. Democratic ranking of countries	1287
IV. CheiRank Versus PageRank	1267	B. Ranking of countries by trade in products	1288
A. Probability decay of PageRank and CheiRank	1267	C. Ranking time evolution and crises	1288
B. Correlator between PageRank and CheiRank	1267	D. Ecological ranking of world trade	1289
C. PageRank-CheiRank plane	1268	E. Remarks on world trade and banking networks	1292
D. 2DRank	1268	XII. Networks with Nilpotent Adjacency Matrix	1293
E. Historical notes on spectral ranking	1268	A. General properties	1293
V. Complex Spectrum and Fractal Weyl Law	1269	B. PageRank of integers	1294
VI. Ulam Networks	1269	C. Citation network of Physical Review	1295
A. Ulam method for dynamical maps	1269	XIII. Random Matrix Models of Markov Chains	1297
B. Chirikov standard map	1270	A. Albert-Barabási model of directed networks	1297
C. Dynamical maps with strange attractors	1271	B. Random matrix models of directed networks	1297
D. Fractal Weyl law for Perron-Frobenius operators	1272	C. Anderson delocalization of PageRank?	1299
E. Intermittency maps	1272	XIV. Other Examples of Directed Networks	1300
F. Chirikov typical map	1272	A. Brain neural networks	1300
VII. Linux Kernel Networks	1273	B. Google matrix of DNA sequences	1301
A. Ranking of software architecture	1273	C. Gene regulation networks	1304
B. Fractal dimension of Linux Kernel networks	1274	D. Networks of game go	1305
VIII. WWW Networks of UK Universities	1275	E. Opinion formation on directed networks	1305
A. Cambridge and Oxford University networks	1275	XV. Discussion	1307
B. Universal emergence of PageRank	1276	Acknowledgments	1308
C. Two-dimensional ranking for university networks	1277	References	1308
IX. Wikipedia Networks	1278		
A. Two-dimensional ranking of Wikipedia articles	1278	<b>I. INTRODUCTION</b>	
B. Spectral properties of the Wikipedia network	1279	In the past ten years, modern societies have developed enormous communication and social networks. The World	
C. Communities and eigenstates of the Google matrix	1279		

Wide Web (WWW) alone has about  $50 \times 10^9$  indexed web pages, so that their classification and information retrieval processing becomes a formidable task. Various search engines have been developed by private companies such as Google, Yahoo!, and others which are extensively used by Internet users. In addition, social networks (Facebook, LiveJournal, Twitter, etc.) have gained much popularity in the last few years. In addition, the use of social networks has spread beyond their initial purpose, making them important for political or social events.

To handle such massive databases, fundamental mathematical tools and algorithms related to centrality measures and network matrix properties are actively being developed. Indeed, the PageRank algorithm, which was initially at the basis of the development of the Google search engine (Brin and Page, 1998; Langville and Meyer, 2006), is directly linked to the mathematical properties of Markov chains (Markov, 1906) and Perron-Frobenius operators (Brin and Stuck, 2002; Langville and Meyer, 2006). Because of its mathematical foundation, this algorithm determines a ranking order of nodes that can be applied to various types of directed networks. However, the recent rapid development of WWW and communication networks requires the creation of new tools and algorithms to characterize the properties of these networks on a more detailed and precise level. For example, such networks contain weakly coupled or secret communities which may correspond to very small values of the PageRank and are hard to detect. It is therefore highly important to have new methods to classify and rank large amounts of network information in a way adapted to internal network structures and characteristics.

This review describes matrix tools and algorithms which facilitate classification and information retrieval from large networks recently created by human activity. The Google matrix, formed by links of the network, is typically huge (a few tens of billions of Web pages). Thus, the analysis of its spectral properties including complex eigenvalues and eigenvectors represents a challenge for analytical and numerical methods. It is rather surprising, but the class of such matrices, which belong to the class of Markov chains and Perron-Frobenius operators, has been essentially overlooked in physics. Indeed, physical problems typically belong to the class of Hermitian or unitary matrices. Their properties have been actively studied in the frame of random matrix theory (RMT) (Guhr, Mueller-Groeling, and Weidenmueller, 1998; Mehta, 2004; Akemann, Baik, and Francesco, 2011) and quantum chaos (Haake, 2010). The analytical and numerical tools developed in these research fields have paved the way for understanding many universal and peculiar features of such matrices in the limit of large matrix size corresponding to many-body quantum systems (Guhr, Mueller-Groeling, and Weidenmueller, 1998), quantum computers (Shepelyansky, 2001), and a semiclassical limit of large quantum numbers in the regime of quantum chaos (Haake, 2010). In contrast to the Hermitian problem, the Google matrices of directed networks have complex eigenvalues. The only physical systems where similar matrices had been studied analytically and numerically correspond to models of quantum chaotic scattering whose spectrum is known to have such unusual properties as the fractal Weyl law (Sjöstrand, 1990; Zworski, 1999;

Nonnenmacher and Zworski, 2007; Shepelyansky, 2008; Gaspard, 2014).

In this review we present an extensive analysis of a variety of Google matrices emerging from real networks in various sciences including the WWW of United Kingdom universities, Wikipedia, the Physical Review citation network, the Linux Kernel network, the world trade network (WTN) from the UN COMTRADE database, brain neural networks, networks of DNA sequences, and many others. As an example, the Google matrix of the Wikipedia network of English articles (August 2009) is shown in Fig. 1. We demonstrate that the analysis of the spectrum and eigenstates of a Google matrix of a given network provides a detailed understanding about the information flow and ranking. We also show that such types of matrices naturally appear for Ulam networks of dynamical maps (Shepelyansky and Zhirov, 2010a; Frahm and Shepelyansky, 2012a) in the framework of the Ulam method (Ulam, 1960).

Currently, Wikipedia, a free online encyclopedia, stores more and more information and has become the largest database of human knowledge. In this respect it is similar to *The Library of Babel*, described by Borges (1962), and “The Library exists *ab aeterno*.” The understanding of hidden relations between various areas of knowledge on the basis of Wikipedia can be improved with the help of a Google matrix analysis of directed hyperlink networks of Wikipedia articles as described in this review.

The specific tools of RMT and quantum chaos, combined with the efficient numerical methods for large matrix diagonalization like the Arnoldi method (Stewart, 2001), allow

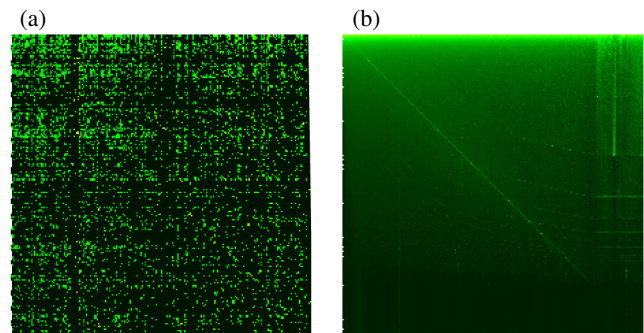


FIG. 1 (color online). Google matrix of the network Wikipedia English articles for August 2009 in the basis of the PageRank index  $K$  (and  $K'$ ). Matrix  $G_{K,K'}$  corresponds to the  $x$  (and  $y$ ) axis with (a)  $1 \leq K, K' \leq 200$ , and with (b)  $1 \leq K, K' \leq N$ ; all nodes are ordered by the PageRank index  $K$  of matrix  $G$  and thus we have two matrix indices  $K, K'$  for matrix elements in this basis. (a) The first  $200 \times 200$  matrix elements of the  $G$  matrix (see Sec. III). (b) The density of all matrix elements coarse grained on  $500 \times 500$  cells where its elements  $G_{K,K'}$  are written in the PageRank basis  $K(i)$  with indices  $i \rightarrow K(i)$  (in the  $x$  axis) and  $j \rightarrow K'(j)$  (in a usual matrix representation with  $K = K' = 1$  on the top-left corner). The color shows the density of matrix elements changing from black for the minimum value  $[(1 - \alpha)/N]$  to white for the maximum value via green (gray) and yellow (light gray); here the damping factor is  $\alpha = 0.85$ . This and other color figures are available in open access arXiv preprint (Ermann, Frahm, and Shepelyansky, 2015). From Ermann, Chepelianskii, and Shepelyansky, 2012.

one to analyze the spectral properties of such large matrices as the entire Twitter network of 41 million users (Frahm and Shepelyansky, 2012a). In 1998 Brin and Page pointed out that “despite the importance of large-scale search engines on the Web, very little academic research has been done on them” (Brin and Page, 1998). The Google matrix of a directed network, like *The Library of Babel* of Borges (1962), contains all the information about a network. The PageRank eigenvector of this matrix finds a broad range of applications being at the mathematical foundation of the Google search engine (Brin and Page, 1998; Langville and Meyer, 2006). We show that the spectrum of this matrix and its other eigenvectors also provide interesting information about network communities and the formation of the PageRank vector. We hope that this review yields a solid scientific basis of matrix methods for efficient analysis of directed networks emerging in various sciences. The described methods will find broad interdisciplinary applications in mathematics, physics, and computer science with the cross fertilization of different research fields. Our aim is to combine the analytical tools and numerical analysis of concrete directed networks to gain a better understanding of the properties of these complex systems.

An interested reader can find a general introduction about complex networks (see also Sec. II) in well-established papers, reviews, and books (Watts and Strogatz, 1998; Albert and Barabási, 2002; Caldarelli, 2003; Newman, 2003, 2010; Dorogovtsev, Goltsev, and Mendes, 2008; Castellano, Fortunato, and Loreto, 2009; Dorogovtsev, 2010; Fortunato, 2010). Descriptions of Markov chains and Perron-Frobenius operators are given by Brin and Page (1998), Gantmacher (2000), Brin and Stuck (2002), and Langville and Meyer (2006), while the properties of RMT and quantum chaos are described by Guhr, Mueller-Groeling, and Weidenmueller (1998), Mehta (2004), Haake (2010), and Akemann, Baik, and Francesco (2011).

The data sets for the main part of the networks considered here are available from the FETNADINE database at <http://www.quantware.ups-tlse.fr/FETNADINE/datasets.htm> from the Quantware group. All color figures are available in open access arXiv preprint (Ermann, Frahm, and Shepelyansky, 2015).

## II. SCALE-FREE PROPERTIES OF DIRECTED NETWORKS

The distributions of the number of ingoing or outgoing links per node for directed networks with  $N$  nodes and  $N_\ell$  links are well known as indegree and outdegree distributions in the community of computer science (Caldarelli, 2003; Donato *et al.*, 2004; Pandurangan, Raghavan, and Upfal, 2006). A network is described by an adjacency matrix  $A_{ij}$  of size  $N \times N$  with  $A_{ij} = 1$  when there is a link from a node  $j$  to a node  $i$  in the network, i.e., “ $j$  points to  $i$ ,” and  $A_{ij} = 0$  otherwise. Real networks are often characterized by power law distributions for the number of ingoing and outgoing links per node  $w_{\text{in,out}}(k) \propto 1/k^{\mu_{\text{in,out}}}$  with typical exponents  $\mu_{\text{in}} \approx 2.1$  and  $\mu_{\text{out}} \approx 2.7$  for the WWW. For example, for the Wikipedia network of Fig. 1 one finds  $\mu_{\text{in}} = 2.09 \pm 0.04$ ,  $\mu_{\text{out}} = 2.76 \pm 0.06$  as shown in Fig. 2 (Zhironov, Zhironov, and Shepelyansky, 2010).

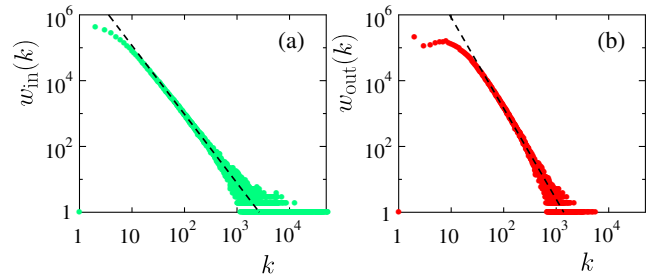


FIG. 2 (color online). Distribution  $w_{\text{in,out}}(k)$  of the number of (a) ingoing and (b) outgoing links  $k$  for  $N = 3\,282\,257$  Wikipedia English articles (August 2009) of Fig. 1 with the total number of links  $N_\ell = 71\,012\,307$ . The straight dashed fit lines show the slopes with (a)  $\mu_{\text{in}} = 2.09 \pm 0.04$  and (b)  $\mu_{\text{out}} = 2.76 \pm 0.06$ . From Zhironov, Zhironov, and Shepelyansky, 2010.

Statistical preferential attachment models were initially developed for undirected networks (Albert and Barabási, 2000). Their generalization to directed networks (Giraud, Georgeot, and Shepelyansky, 2009) generates a power law distribution for ingoing links with  $\mu_{\text{in}} \approx 2$  but the distribution of outgoing links is closer to an exponential decay. We will see that these models are not able to reproduce the spectral properties of  $G$  in real networks.

The most recent studies of WWW, crawled by the Common Crawl Foundation in 2012 (Meusel *et al.*, 2015) for  $N \approx 3.5 \times 10^9$  nodes and  $N_\ell \approx 1.29 \times 10^{11}$  links, provide the exponents  $\mu_{\text{in}} \approx 2.24$ ,  $\mu_{\text{out}} \approx 2.77$ , even if these distributions describe probabilities at the tails which capture only about 1% of nodes. Thus, at present the existing statistical models of networks capture only in an approximate manner the real situation in large networks even if certain models are able to generate a power law decay of PageRank probability.

## III. CONSTRUCTION OF GOOGLE MATRIX AND ITS PROPERTIES

### A. Construction rules

The matrix  $S_{ij}$  of Markov transitions (Markov, 1906) is constructed from the adjacency matrix  $A_{ij} \rightarrow S_{ij}$  by normalizing elements of each column so that their sum is equal to unity ( $\sum_i S_{ij} = 1$ ) and replacing columns with only zero elements (*dangling nodes*) by  $1/N$ . Such matrices with columns sum normalized to unity and  $S_{ij} \geq 0$  belong to the class of Perron-Frobenius operators with a possibly degenerate unit eigenvalue  $\lambda = 1$  and other eigenvalues obeying  $|\lambda| \leq 1$  (see Sec. III.B). Then the Google matrix of the network is introduced as (Brin and Page, 1998)

$$G_{ij} = \alpha S_{ij} + (1 - \alpha)/N. \quad (1)$$

The damping factor  $\alpha$  in the WWW context describes the probability  $(1 - \alpha)$  to jump to any node for a random surfer. At a given node a random surfer follows the available direction of links making a random choice between them with probability proportional to the weight of links. For WWW the Google search engine uses  $\alpha \approx 0.85$  (Langville and Meyer, 2006). For  $0 \leq \alpha \leq 1$  the matrix  $G$  also belongs to

the class of Perron-Frobenius operators as  $S$  and with its columns sum normalized. However, for  $\alpha < 1$  its largest eigenvalue  $\lambda = 1$  is not degenerate and the other eigenvalues lie inside a smaller circle of radius  $\alpha$ , i.e.,  $|\lambda| \leq \alpha$  (Brin and Stuck, 2002; Langville and Meyer, 2006).

The right eigenvector at  $\lambda = 1$ , which is called the PageRank, has real non-negative elements  $P(i)$  and gives the stationary probability  $P(i)$  to find a random surfer at site  $i$ . The PageRank can be efficiently determined by the power iteration method which consists of repeatedly multiplying  $G$  by an iteration vector which is initially chosen as a given random or uniform initial vector. Developing the initial vector in a basis of eigenvectors of  $G$  one finds that the other eigenvector coefficients decay as  $\sim \lambda^n$  and only the PageRank component, with  $\lambda = 1$ , survives in the limit  $n \rightarrow \infty$ . The finite gap  $1 - \alpha \approx 0.15$  between the largest eigenvalue and other eigenvalues ensures, after several tens of iterations, the fast exponential convergence of the method also called the “PageRank algorithm.” Multiplication of  $G$  by a vector requires only  $O(N_\ell)$  multiplications due to the links and the additional contributions due to dangling nodes and the damping factor can be efficiently performed with  $O(N)$  operations. Since often the average number of links per node is of the order of a few tens for WWW and many other networks, one has effectively  $N_\ell$  and  $N$  of the same order of magnitude. At  $\alpha = 1$  the matrix  $G$  coincides with the matrix  $S$  and we see in Sec. VIII that for this case the largest eigenvalue  $\lambda = 1$  is usually highly degenerate due to many invariant subspaces which define many independent Perron-Frobenius operators with at least one eigenvalue  $\lambda = 1$  for each of them.

Once the PageRank is found, e.g., at  $\alpha = 0.85$ , all nodes can be sorted by decreasing probabilities  $P(i)$ . The node rank is then given by the index  $K(i)$  which reflects the relevance of the node  $i$ . The top PageRank nodes, with largest probabilities, are located at small values of  $K(i) = 1, 2, \dots$ .

It is known that on average the PageRank probability is proportional to the number of ingoing links (Langville and Meyer, 2006; Litvak, Scheinhardt, and Volkovich, 2008), characterizing how popular or known a given node is. Assuming that the PageRank probability decays algebraically as  $P_i \sim 1/K_i^\beta$  we obtain that the number of nodes  $N_P$  with PageRank probability  $P$  scales as  $N_P \sim 1/P^{\mu_{in}}$  with  $\mu_{in} = 1 + 1/\beta$  so that  $\beta \approx 0.9$  for  $\mu_{in} \approx 2.1$  being in agreement with the numerical data for the WWW (Donato *et al.*, 2004; Pandurangan, Raghavan, and Upfal, 2006; Meusel *et al.*, 2015) and the Wikipedia network (Zhirov, Zhirov, and Shepelyansky, 2010). More recent mathematical studies on the relation between PageRank probability decay and ingoing links are reported by Jelenkovic and Olvera-Cravioto (2013) and Chen, Litvak, and Olvera-Cravioto (2014). At the same time the proportionality relation between PageRank probability and ingoing links assumes certain statistical properties of networks and works only on average. We note that there are examples of Ulam networks generated by dynamical maps where such proportionality is not working [see, e.g., Ermann and Shepelyansky (2010a) and Sec. VI.E].

In addition to a given directed network with adjacency matrix  $A$  it is useful to analyze an inverse network where links are inverted and whose adjacency matrix  $A^*$  is the transpose of

$A$ , i.e.,  $A_{ij}^* = A_{ji}$ . The matrices  $S^*$  and the Google matrix  $G^*$  of the inverse network are then constructed in the same way from  $A^*$  as described previously and according to Eq. (1) using the same value of  $\alpha$  as for the  $G$  matrix. The right eigenvector of  $G^*$  at eigenvalue  $\lambda = 1$  is called CheiRank giving a complementary rank index  $K^*(i)$  of network nodes (Chepelienskii, 2010; Zhirov, Zhirov, and Shepelyansky, 2010; Ermann, Chepelienskii, and Shepelyansky, 2012). The CheiRank probability  $P^*(K^*)$  is proportional to the number of outgoing links highlighting node communicativity (Zhirov, Zhirov, and Shepelyansky, 2010; Ermann, Chepelienskii, and Shepelyansky, 2012). In analogy with the PageRank we obtain the fact that  $P^* \sim 1/K^{*\beta}$  with  $\beta = 1/(\mu_{out} - 1) \approx 0.6$  for typical  $\mu_{out} \approx 2.7$ . The statistical properties of distribution of nodes on the PageRank-CheiRank plane are described by Ermann, Chepelienskii, and Shepelyansky (2012) for various directed networks. We discuss them later.

We consider an example of a simple network of five nodes shown in Fig. 3(a). The corresponding adjacency matrices  $A$  and  $A^*$  are shown in Fig. 4 for the indices given in Fig. 3(a). The matrices of Markov transitions  $S, S^*$  and Google matrices are computed as described previously and from Eq. (1). The distribution of nodes on the  $(K, K^*)$  plane is shown in Fig. 3(b). After permutations the matrix  $G$  can be rewritten in the basis of PageRank index  $K$  as done in Fig. 1.

## B. Markov chains and Perron-Frobenius operators

Matrices with real non-negative elements and column sums normalized to unity belong to the class of Markov chains (Markov, 1906) and Perron-Frobenius operators (Gantmacher, 2000; Brin and Stuck, 2002; Langville and Meyer, 2006), which have been used in a mathematical analysis of dynamical systems and theory of matrices. A numerical analysis of finite size approximants of such operators is closely linked with the Ulam method (Ulam, 1960) which naturally generates such matrices for dynamical maps (Ermann and Shepelyansky,

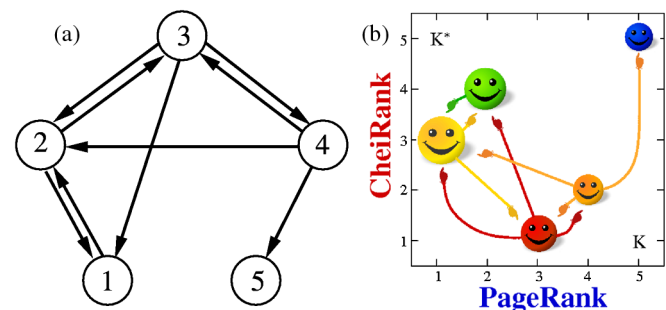


FIG. 3 (color online). (a) Example of a simple network with directed links between five nodes. (b) Distribution of five nodes from (a) on the PageRank-CheiRank plane  $(K, K^*)$ , where the size of a node is proportional to the PageRank probability  $P(K)$  and the color of a node is proportional to the CheiRank probability  $P^*(K^*)$ , with the maximum at gray (red) and the minimum at black (blue). The locations of the nodes of (a) on the  $(K_i, K_i^*)$  plane are (2,4), (1,3), (3,1), (4,2), and (5,5) for the original nodes  $i = 1, 2, 3, 4$ , and 5, respectively. PageRank and CheiRank vectors are computed from the Google matrices  $G$  and  $G^*$  shown in Fig. 4 at a damping factor  $\alpha = 0.85$ .

$$\begin{aligned}
\text{(a)} \quad A &= \begin{pmatrix} 0 & 1 & 1 & 0 & 0 \\ 1 & 0 & 1 & 1 & 0 \\ 0 & 1 & 0 & 1 & 0 \\ 0 & 0 & 1 & 0 & 0 \\ 0 & 0 & 0 & 1 & 0 \end{pmatrix} & \text{(b)} \quad A^* &= \begin{pmatrix} 0 & 1 & 0 & 0 & 0 \\ 1 & 0 & 1 & 0 & 0 \\ 1 & 1 & 0 & 1 & 0 \\ 0 & 1 & 1 & 0 & 1 \\ 0 & 0 & 0 & 0 & 0 \end{pmatrix} \\
\text{(c)} \quad S &= \begin{pmatrix} 0 & 1/2 & 1/3 & 0 & 1/5 \\ 1 & 0 & 1/3 & 1/3 & 1/5 \\ 0 & 1/2 & 0 & 1/3 & 1/5 \\ 0 & 0 & 1/3 & 0 & 1/5 \\ 0 & 0 & 0 & 1/3 & 1/5 \end{pmatrix} & \text{(d)} \quad S^* &= \begin{pmatrix} 0 & 1/3 & 0 & 0 & 0 \\ 1/2 & 0 & 1/2 & 0 & 0 \\ 1/2 & 1/3 & 0 & 1 & 0 \\ 0 & 1/3 & 1/2 & 0 & 1 \\ 0 & 0 & 0 & 0 & 0 \end{pmatrix} \\
\text{(e)} \quad G &= \begin{pmatrix} 0.03 & 0.455 & 0.313 & 0.03 & 0.2 \\ 0.88 & 0.03 & 0.313 & 0.313 & 0.2 \\ 0.03 & 0.455 & 0.03 & 0.313 & 0.2 \\ 0.03 & 0.03 & 0.313 & 0.03 & 0.2 \\ 0.03 & 0.03 & 0.03 & 0.313 & 0.2 \end{pmatrix} & \text{(f)} \quad G^* &= \begin{pmatrix} 0.03 & 0.313 & 0.03 & 0.03 & 0.03 \\ 0.455 & 0.03 & 0.455 & 0.03 & 0.03 \\ 0.455 & 0.313 & 0.03 & 0.88 & 0.03 \\ 0.03 & 0.313 & 0.455 & 0.03 & 0.88 \\ 0.03 & 0.03 & 0.03 & 0.03 & 0.03 \end{pmatrix}
\end{aligned}$$

FIG. 4. (a) Adjacency matrix  $A$  of the network of Fig. 3(a) with indices used there, (b) adjacency matrix  $A^*$  for the network with inverted links; (c) matrices  $S$  and (d)  $S^*$  corresponding to the matrices  $A$  and  $A^*$ ; the Google matrices (e)  $G$  and (f)  $G^*$  corresponding to matrices  $S$  and  $S^*$  for  $\alpha = 0.85$  (only three digits of matrix elements are shown).

2010a, 2010b; Shepelyansky and Zhirov, 2010a). The Ulam method generates Ulam networks whose properties are discussed in Sec. VI.

Matrices  $G$  of this type have at least (one) unit eigenvalue  $\lambda = 1$  since the vector  $e^T = (1, \dots, 1)$  is a left eigenvector for this eigenvalue. Furthermore, one easily verifies that for any vector  $v$  the inequality  $\|Gv\|_1 \leq \|v\|_1$  holds where the norm is the standard 1-norm. From this inequality one immediately obtains that all eigenvalues  $\lambda$  of  $G$  lie in a circle of radius unity  $|\lambda| \leq 1$ . For the Google matrix  $G$  as given in Eq. (1) one can furthermore show for  $\alpha < 1$  that the unity eigenvalue is not degenerate and the other eigenvalues obey even  $|\lambda| \leq \alpha$  (Langville and Meyer, 2006). These and other mathematical results about properties of matrices of such type can be found in Gantmacher (2000) and Langville and Meyer (2006).

It should be pointed out that due to the asymmetry of links on directed networks such matrices have in general a complex eigenvalue spectrum and sometimes they are not even diagonalizable, i.e., there may also be generalized eigenvectors associated with nontrivial Jordan blocks. Matrices of this type rarely appear in physical problems which are usually characterized by Hermitian or unitary matrices with real eigenvalues or located on the unitary circle. The universal spectral properties of such Hermitian or unitary matrices are well described by RMT (Guhr, Mueller-Groeling, and Weidenmueller, 1998; Haake, 2010; Akemann, Baik, and Francesco, 2011). In contrast to this nontrivial complex spectra appear in physical systems only in problems of quantum chaotic scattering and systems with absorption. In such cases it may happen that the number of states  $N_\gamma$ , with finite values  $0 < \lambda_{\min} \leq |\lambda| \leq 1$  ( $\gamma = -2 \ln |\lambda|$ ), can grow algebraically  $N_\gamma \propto N^\nu$  with increasing matrix size  $N$ , with an exponent  $\nu < 1$  corresponding to a fractal Weyl law proposed first in mathematics (Sjöstrand, 1990). Therefore, most eigenvalues drop to  $\lambda = 0$  with  $N \rightarrow \infty$ . We discuss this unusual property in Sec. V.

### C. Invariant subspaces

For typical networks the set of nodes can be decomposed in invariant *subspace* nodes and fully connected *core space* nodes leading to a block structure of the matrix  $S$  in Eq. (1)

which can be represented as (Frahm, Georgeot, and Shepelyansky, 2011)

$$S = \begin{pmatrix} S_{ss} & S_{sc} \\ 0 & S_{cc} \end{pmatrix}. \quad (2)$$

The core space block  $S_{cc}$  contains the links between core space nodes and the coupling block  $S_{sc}$  may contain links from certain core space nodes to certain invariant subspace nodes. By construction there are no links from nodes of invariant subspaces to the nodes of core space. Thus the subspace-subspace block  $S_{ss}$  is actually composed of many diagonal blocks for many invariant subspaces whose number can generally be rather large. Each of these blocks corresponds to a column sum normalized matrix with positive elements of the same type as  $G$  and has therefore at least one unit eigenvalue. This leads to a high degeneracy  $N_1$  of the eigenvalue  $\lambda = 1$  of  $S$ , for example,  $N_1 \sim 10^3$  as for the case of UK universities (see Sec. VIII).

In order to obtain the invariant subspaces, we determine iteratively for each node the set of nodes that can be reached by a chain of nonzero matrix elements of  $S$ . If this set contains all nodes (or at least a macroscopic fraction) of the network, the initial node belongs to the core space  $V_c$ . Otherwise, the limit set defines a subspace which is invariant with respect to applications of the matrix  $S$ . At a second step all subspaces with common members are merged resulting in a sequence of disjoint subspaces  $V_j$  of dimension  $d_j$  and which are invariant by applications of  $S$ . This scheme, which can be efficiently implemented in a computer program, provides a subdivision over  $N_c$  core space nodes (70%–80% of  $N$  for UK university networks) and  $N_s = N - N_c$  subspace nodes belonging to at least one of the invariant subspaces  $V_j$ . This procedure generates the block triangular structure of Eq. (2). Note that since a dangling node is connected by construction to all other nodes it belongs to the core space as well as all nodes which are linked (directly or indirectly) to a dangling node. As a consequence the invariant subspaces do not contain dangling nodes nor nodes linked to dangling nodes.

The detailed algorithm for an efficient computation of the invariant subspaces is described by Frahm, Georgeot, and Shepelyansky (2011). As a result the total number of all subspace nodes  $N_s$ , the number of independent subspaces  $N_d$ , the maximal subspace dimension  $d_{\max}$ , etc. can be determined. The statistical properties for the distribution of subspace dimensions are discussed in Sec. VIII for UK universities and Wikipedia networks. Furthermore it is possible to numerically determine with a very little effort the eigenvalues of  $S$  associated with each subspace by separate diagonalization of the corresponding diagonal blocks in the matrix  $S_{ss}$ . For this, either exact diagonalization or, in rare cases of quite large subspaces, the Arnoldi method (see Sec. III.D) can be used.

After the subspace eigenvalues are determined one can apply the Arnoldi method to the projected core space matrix block  $S_{cc}$  to determine the leading core space eigenvalues. In this way one obtains accurate eigenvalues because the Arnoldi method does not need to compute the numerically problematic highly degenerate unit eigenvalues of  $S$  since the latter are already obtained from the separate and cheap subspace

diagonalization. Actually the alternative and naive application of the Arnoldi method on the full matrix  $S$ , without computing the subspaces first, does not provide the correct number  $N_1$  of degenerate unit eigenvalues and also the obtained clustered eigenvalues, close to unity, are not very accurate. Similar problems hold for the full matrix  $G$  (with damping factor  $\alpha < 1$ ) since here only the first eigenvector, the PageRank, can be accurately determined but there are still many degenerate (or clustered) eigenvalues at (or close to)  $\lambda = \alpha$ .

Since the column sums of  $S_{cc}$  are less than unity, due to nonzero matrix elements in the block  $S_{sc}$ , the leading core space eigenvalue of  $S_{cc}$  is also below unity  $|\lambda_1^{(\text{core})}| < 1$  even though in certain cases the gap to unity may be very small (see Sec. VIII).

We consider concrete examples of such decompositions in Sec. VIII and show in this review spectra with subspace and core space eigenvalues of matrices  $S$  for several network examples. The mathematical results for properties of the matrix  $S$  are discussed by Serra-Capizzano (2005).

#### D. Arnoldi method for numerical diagonalization

The most adapted numerical method to determine the largest eigenvalues of large sparse matrices is the Arnoldi method (Arnoldi, 1951; Stewart, 2001; Golub and Greif, 2006; Frahm and Shepelyansky, 2010). Indeed, usually the matrix  $S$  in Eq. (1) is very sparse with only a few tens of links per node  $\zeta = N_\ell/N \sim 10$ . Thus, a multiplication of a vector by  $G$  or  $S$  is numerically cheap. The Arnoldi method is similar in spirit to the Lanczos method, but is adapted to non-Hermitian or nonsymmetric matrices. Its main idea is to recursively determine an orthonormal set of vectors  $\xi_0, \dots, \xi_{n_A-1}$ , which define a *Krylov space*, by orthogonalizing  $S\xi_k$  on the previous vectors  $\xi_0, \dots, \xi_k$  by the Gram-Schmidt procedure to obtain  $\xi_{k+1}$  and where  $\xi_0$  is some normalized initial vector. The dimension  $n_A$  of the Krylov space (in the following called the *Arnoldi dimension*) should be “modest” but not too small. During the Gram-Schmidt procedure one obtains furthermore the explicit expression  $S\xi_k = \sum_{j=0}^{k+1} h_{jk}\xi_j$  with matrix elements  $h_{jk}$  of the Arnoldi representation matrix of  $S$  on the Krylov space, given by the scalar products or inverse normalization constants calculated during the orthogonalization. In order to obtain a closed representation matrix one needs to replace the last coupling element  $h_{n_A, n_A-1} \rightarrow 0$  which introduces a mathematical approximation. The eigenvalues of the  $n_A \times n_A$  matrix  $h$  are called the *Ritz eigenvalues* and often represent accurate approximations of the exact eigenvalues of  $S$ , at least for a considerable fraction of the Ritz eigenvalues with largest modulus.

In certain particular cases, when  $\xi_0$  belongs to an  $S$  invariant subspace of small dimension  $d$ , the element  $h_{d, d-1}$  vanishes automatically (if  $d \leq n_A$  and assuming that numerical rounding errors are not important) and the Arnoldi iteration stops at  $k = d$  and provides  $d$  exact eigenvalues of  $S$  for the invariant subspace. Note that there are more sophisticated variants of the Arnoldi method (Stewart, 2001) where one applies (implicit) modifications on the initial vector  $\xi_0$  in order to force this vector to be in some small dimensional invariant subspace which results in such a vanishing coupling matrix

element. These variants known as (implicitly) restarted Arnoldi methods allow one to concentrate on certain regions on the complex plane to determine a few but very accurate eigenvalues in these regions. However, for the cases of Google matrices, where one is typically interested in the largest eigenvalues close to the unit circle, only the basic variant described above was used but choosing larger values of  $n_A$  as would have been possible with the restarted variants. The initial vector was typically chosen to be random or as the vector with unit entries.

Concerning the numerical resources the Arnoldi method requires  $\zeta N$  double-precision registers to store the nonzero matrix elements of  $S$ ,  $n_A N$  registers to store the vectors  $\xi_k$ , and  $\text{const} \times n_A^2$  registers to store  $h$  (and various copies of  $h$ ). The computational time scales as  $\zeta n_A N_d$  for the computation of  $S\xi_k$ , with  $N_d n_A^2$  for the Gram-Schmidt orthogonalization procedure (which is typically dominant) and with  $\text{const} \times n_A^3$  for the diagonalization of  $h$ .

The details of the Arnoldi method are described in references given previously. This method has problems with degenerate or strongly clustered eigenvalues and therefore for typical examples of Google matrices it is applied to the core space block  $S_{cc}$  where the effects of the invariant subspaces, being responsible for most of the degeneracies, are exactly taken out according to the previous discussion. In typical examples it is possible to find about  $n_A \approx 640$  eigenvalues with largest  $|\lambda|$  for the entire Twitter network with  $N \approx 4.1 \times 10^7$  (see Sec. X) and about  $n_A \approx 6000$  eigenvalues for Wikipedia networks with  $N \approx 3.2 \times 10^6$  (see Sec. IX). For the two university networks of Cambridge and Oxford 2006 with  $N \approx 2 \times 10^5$  it is possible to compute  $n_A \approx 20\,000$  eigenvalues (see Sec. VIII). For the case of the citation network of Physical Review (see Sec. XII) with  $N \approx 4.6 \times 10^5$  it is even possible and necessary to use high-precision computations (with up to 768 binary digits) to accurately determine the Arnoldi matrix  $h$  with  $n_A \approx 2000$  (Frahm, Eom, and Shepelyansky, 2014).

#### E. General properties of eigenvalues and eigenstates

According to the Perron-Frobenius theorem all eigenvalues  $\lambda_i$  of  $G$  are distributed inside the unitary circle  $|\lambda| \leq 1$ . It can be shown that at  $\alpha < 1$  there is only one eigenvalue  $\lambda_0 = 1$  and all other  $|\lambda_i| \leq \alpha$  having a simple dependence on  $\alpha$ :  $\lambda_i \rightarrow \alpha \lambda_i$  (Langville and Meyer, 2006). The right eigenvectors  $\psi_i(j)$  are defined by

$$\sum_j G_{jj'} \psi_i(j') = \lambda_i \psi_i(j). \quad (3)$$

Only the PageRank vector is affected by  $\alpha$  while other eigenstates are independent of  $\alpha$  due to their orthogonality to the left unit eigenvector at  $\lambda = 1$ . Left eigenvectors are orthonormal to right eigenvectors (Langville and Meyer, 2006).

It is useful to characterize the eigenvectors by their inverse participation ratio (IPR)  $\xi_i = [\sum_j |\psi_i(j)|^2]^2 / \sum_j |\psi_i(j)|^4$  which gives an effective number of nodes populated by an eigenvector  $\psi_i$ . This characteristic is broadly used for a

description of localized or delocalized eigenstates of electrons in a disordered potential with Anderson transition (Guhr, Mueller-Groeling, and Weidenmueller, 1998; Evers and Mirlin, 2008). We discuss the specific properties of eigenvectors in Secs. IV, and VI–XIV.

#### IV. CHEIRANK VERSUS PAGERANK

It is established that the ranking of network nodes based on PageRank order works reliably not only for WWW but also for other directed networks. As an example it is possible to quote the citation network of Physical Review (Redner, 1998, 2005; Radicchi *et al.*, 2009), the Wikipedia network (Zhirov, Zhirov, and Shepelyansky, 2010; Aragón *et al.*, 2012; Eom and Shepelyansky, 2013; Skiena and Ward, 2014), and even the network of world commercial trade (Ermann and Shepelyansky, 2011). Here we describe the main properties of PageRank and CheiRank probabilities using a few real networks. A more detailed presentation for concrete networks follows in Secs. VI–XI.

##### A. Probability decay of PageRank and CheiRank

Wikipedia is a useful example of a scale-free network. An article quotes other Wikipedia articles that generates a network of directed links. For Wikipedia of English articles dated August 2009 we have  $N = 3\,282\,257$  and  $N_\ell = 71\,012\,307$  (Zhirov, Zhirov, and Shepelyansky, 2010). The dependences of PageRank  $P(K)$  and CheiRank  $P^*(K^*)$  probabilities on indices  $K$  and  $K^*$  are shown in Fig. 5. In a large range the decay can be satisfactorily described by an algebraic law with

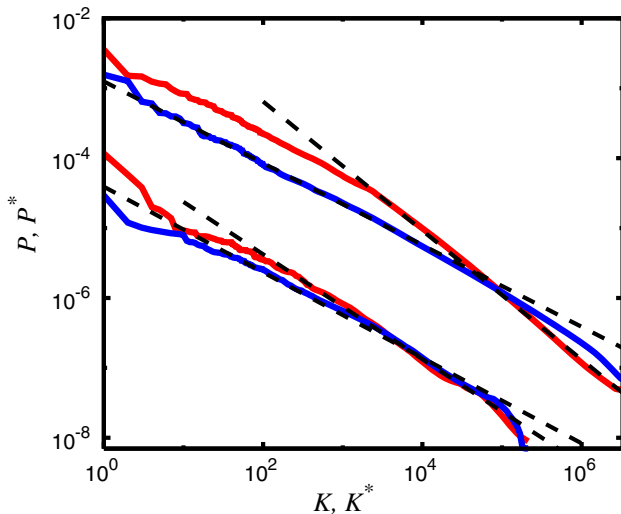


FIG. 5 (color online). Dependence of probabilities of PageRank  $P$  [gray (red) curves] and CheiRank  $P^*$  [black (blue) curves] vectors on the corresponding rank indices  $K$  and  $K^*$  for networks of Wikipedia August 2009 (top curves) and University of Cambridge (bottom curves, moved down by a factor of 100). The straight dashed lines show the power law fits for PageRank and CheiRank with the slopes  $\beta = 0.92$  and  $0.58$ , respectively, corresponding to  $\beta = 1/(\mu_{\text{in,out}} - 1)$  for Wikipedia (see Fig. 2), and  $\beta = 0.75$  and  $0.61$  for Cambridge. From Zhirov, Zhirov, and Shepelyansky, 2010 and Frahm, Georgeot, and Shepelyansky, 2011.

an exponent  $\beta$ . The obtained  $\beta$  values are in reasonable agreement with the expected relation  $\beta = 1/(\mu_{\text{in,out}} - 1)$  with the exponents of the distribution of links given previously. However, the decay is algebraic only on a tail, showing certain nonlinear variations well visible for  $P^*(K^*)$  at large values of  $P^*$ .

Similar data for the network of the University of Cambridge (2006) with  $N = 212\,710$  and  $N_\ell = 2\,015\,265$  (Frahm, Georgeot, and Shepelyansky, 2011) are shown in the same Fig. 5. Here the exponents  $\beta$  have different values with approximately the same statistical accuracy of  $\beta$ .

Thus we come to the same conclusion as Meusel *et al.* (2015): the probability decay of PageRank and CheiRank is only approximately algebraic, the relation between exponents  $\beta$  and  $\mu$  also works only approximately.

##### B. Correlator between PageRank and CheiRank

Each network node  $i$  has both PageRank  $K(i)$  and CheiRank  $K(i)^*$  indices so that it is interesting to know what is the correlation between the corresponding vectors of PageRank and CheiRank. It is convenient to characterize this by a correlator introduced in Chepelienskii (2010):

$$\kappa = N \sum_{i=1}^N P(K(i))P^*(K^*(i)) - 1. \quad (4)$$

Even if all the networks from Fig. 6 have similar algebraic decay of PageRank probability with  $K$  and similar  $\beta \sim 1$  exponents we see that the correlations between PageRank and CheiRank vectors are drastically different in these networks. Thus the networks of UK universities and nine different language editions of Wikipedia have the correlator  $\kappa \sim 1-8$  while all other networks have  $\kappa \sim 0$ . This means that there are significant differences hidden in the network architecture which are not visible from a PageRank analysis. We discuss

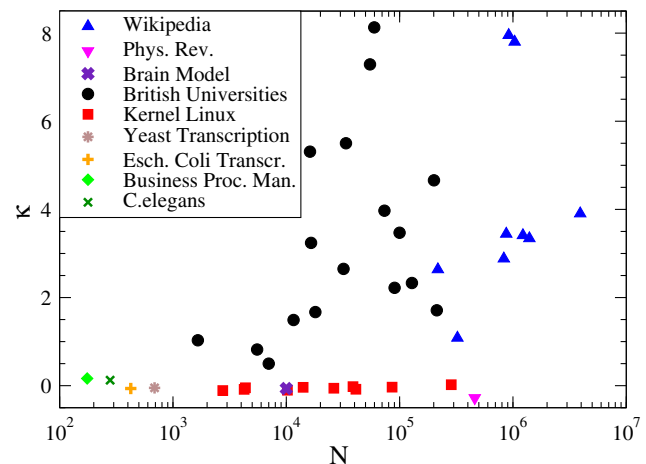


FIG. 6 (color online). Correlator  $\kappa$  as a function of the number of nodes  $N$  for different networks: From Ermann, Chepelienskii, and Shepelyansky, 2012, with additional data from Abel and Shepelyansky, 2011, Eom and Shepelyansky, 2013, Kandiah and Shepelyansky, 2014, and Frahm, Eom, and Shepelyansky, 2014.

the possible origins of such a difference for the above networks in Secs. VIII, IX, and X.

### C. PageRank-CheiRank plane

A more detailed characterization of correlations between PageRank and CheiRank vectors can be obtained from a distribution of network nodes on the two-dimensional plane (2D) of indices  $(K, K^*)$ . Two examples for Wikipedia and Linux networks are shown in Fig. 7. A qualitative difference between the two networks is obvious. For Wikipedia we have a maximum of density along the line  $\ln K^* \approx 5 + (\ln K)/3$  that results from a strong correlation between PageRank and CheiRank with  $\kappa = 4.08$ . In contrast to that for the Linux network V2.4 we have a homogeneous density distribution of nodes along lines  $\ln K^* = \ln K + \text{const}$  corresponding to uncorrelated probabilities  $P(K)$  and  $P^*(K^*)$  and an even slightly negative value of  $\kappa = -0.034$ . Note that if for Wikipedia we generate nodes with independent probabilities distributions  $P$  and  $P^*$ , obtained from this network at the corresponding value of  $N$ , then we obtain a homogeneous node distribution in the  $(K, K^*)$  plane [in the  $(\log K, \log K^*)$  plane it takes a triangular form, see Fig. 4 by Zhironov, Zhironov, and Shepelyansky (2010)].

In Fig. 7(a) we also show the distribution of the top 100 persons from PageRank and CheiRank compared with the top 100 persons from Hart (1992). There is a significant overlap between the PageRank and Hart ranking of persons while CheiRank generates mainly another listing of people. We discuss the Wikipedia ranking of historical figures in Sec. IX.

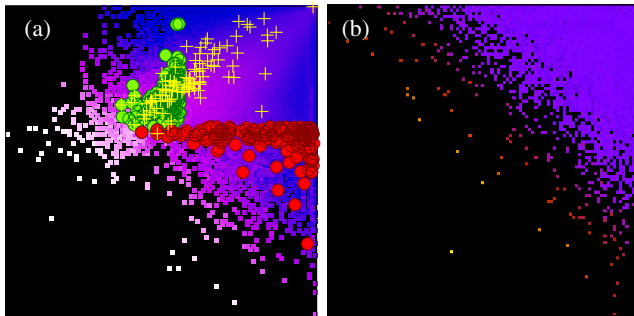


FIG. 7 (color online). Density distribution of network nodes  $W(K, K^*) = dN_i/dKdK^*$  shown on the plane of PageRank and CheiRank indices in log scale  $(\log_N K, \log_N K^*)$  for all  $1 \leq K, K^* \leq N$ , density is computed over equidistant grid in plane  $(\log_N K, \log_N K^*)$  with  $100 \times 100$  cells; color shows the average value of  $W$  in each cell, the normalization condition is  $\sum_{K, K^*} W(K, K^*) = 1$ . Density  $W(K, K^*)$  is shown by color with dark gray (blue) for the minimum in (a) and (b) and (a) white and (b) white (yellow) for the maximum (black for zero). (a) Data for Wikipedia August 2009,  $N = 3\,282\,257$  light gray/dark gray (green/red), points show the top 100 persons from PageRank and CheiRank white (yellow) pluses show the top 100 persons from Hart (1992). From Zhironov, Zhironov, and Shepelyansky, 2010. (b) Density distribution  $W(K, K^*) = dN_i/dKdK^*$  for the Linux Kernel V2.4 network with  $N = 85\,757$ . From Ermann, Chepelianskii, and Shepelyansky, 2012.

### D. 2DRank

PageRank and CheiRank indices  $K_i K_i^*$  order all network nodes according to a monotonous decrease of corresponding probabilities  $P(K_i)$  and  $P^*(K_i^*)$ . While top  $K$  nodes are most popular or known in the network, top  $K^*$  nodes are most communicative nodes with many outgoing links. It is useful to consider an additional ranking  $K_2$ , called 2DRank, which combines properties of both ranks  $K$  and  $K^*$  (Zhironov, Zhironov, and Shepelyansky, 2010).

The ranking list  $K_2(i)$  is constructed by increasing  $K \rightarrow K + 1$  and increasing the 2DRank index  $K_2(i)$  by 1 if a new entry is present in the list of first  $K^* < K$  entries of CheiRank, then the one unit step is done in  $K^*$  and  $K_2$  is increased by 1 if the new entry is present in the list of first  $K < K^*$  entries of CheiRank. More formally, 2DRank  $K_2(i)$  gives the ordering of the sequence of sites that appear inside the squares  $[1, 1; K = k, K^* = k; \dots]$  when one runs progressively from  $k = 1$  to  $N$ . In fact, at each step  $k \rightarrow k + 1$  there are three possibilities: (i) no new sites on two edges of the square, (ii) only one site is on these two edges and it is added in the listing of  $K_2(i)$ , and (iii) two sites are on the edges and both are added in the listing  $K_2(i)$ , first with  $K > K^*$  and second with  $K < K^*$ . For (iii) the choice of order of addition in the list  $K_2(i)$  affects only some pairs of neighboring sites and does not change the main structure of ordering. An illustration example of the 2DRank algorithm is given in Fig. 7 of Zhironov, Zhironov, and Shepelyansky (2010). For Wikipedia a 2DRanking of persons is discussed in Sec. IX.

### E. Historical notes on spectral ranking

Starting with the work of Markov (1906) many scientists contributed to the development of the spectral ranking of Markov chains. The research of Perron (1907) and Frobenius (1912) led to the Perron-Frobenius theorem for square matrices with positive entries (Brin and Stuck, 2002). A detailed historical description of spectral ranking research is reviewed by Franceschet (2011) and Vigna (2013). As described there, the important steps have been done by researchers in psychology, sociology, and mathematics including J. R. Seeley (1949), T.-H. Wei (1952), L. Katz (1953), and C. H. Hubbell (1965) (Franceschet, 2011; Vigna, 2013). In the WWW context, the Google matrix in Eq. (1), with regularization of dangling nodes and damping factor  $\alpha$ , was introduced by Brin and Page (1998).

A PageRank vector of a Google matrix  $G^*$  with inverted directions of links was considered by Fogaras (2003) and Hrisitidis, Hwang, and Papakonstantinou (2008), but no systematic statistical analysis of 2DRanking was presented there. An important step was done by Chepelianskii (2010) who analyzed the  $\lambda = 1$  eigenvectors of  $G$  for the directed network and of  $G^*$  for the network with inverted links. The comparative analysis of the Linux Kernel network and the WWW of the University of Cambridge demonstrated significant differences in correlator  $\kappa$  values on these networks and different functions of top nodes in  $K$  and  $K^*$ . The term CheiRank was coined by Zhironov, Zhironov, and Shepelyansky (2010) to have a clear distinction between eigenvectors of  $G$  and  $G^*$ . We note that top PageRank and



Cheirank nodes have certain similarities with authorities and hubs appearing in the Hiperlink-Induced Topic Search (HITS) algorithm (Kleinberg, 1999). However, the HITS is query dependent while the rank probabilities  $P(K_i)$  and  $P^*(K_i^*)$  classify all nodes of the network.

## V. COMPLEX SPECTRUM AND FRACTAL WEYL LAW

The Weyl law (Weyl, 1912) gives a fundamental link between the properties of quantum eigenvalues in closed Hamiltonian systems, the Planck constant  $\hbar$ , and the classical phase space volume. The number of states in this case is determined by the phase volume of a system with dimension  $d$ . The case of Hermitian operators is now well understood on both mathematical and physical grounds (Landau and Lifshitz, 1989; Dimassi and Sjöstrand, 1999). Surprisingly, only recently it has been realized that the case of nonunitary operators describing open systems in the semiclassical limit has a number of new interesting properties and the concept of the fractal Weyl law (Sjöstrand, 1990; Zworski, 1999) has been introduced to describe the dependence of the number of resonant Gamow eigenvalues (Gamow, 1928) on  $\hbar$ .

The Gamow eigenstates found important applications for the decay of radioactive nuclei, quantum chemistry reactions, chaotic scattering and microlasers with chaotic resonators, and open quantum maps (Gaspard, 1998, 2014; Shepelyansky, 2008). The spectrum of corresponding operators has a complex spectrum  $\lambda$ . The spread width  $\gamma = -2 \ln |\lambda|$  of eigenvalues  $\lambda$  determines the lifetime of a corresponding eigenstate. The understanding of the spectral properties of related operators in the semiclassical limit represents an important challenge.

According to the fractal Weyl law (Sjöstrand, 1990; Lu, Sridhar, and Zworski, 2003) the number of Gamow eigenvalues  $N_\gamma$ , which have escape rates  $\gamma$  in a finite bandwidth  $0 \leq \gamma \leq \gamma_b$ , scales as

$$N_\gamma \propto \hbar^{-d/2} \propto N^{d/2}, \quad (5)$$

where  $d$  is a fractal dimension of a classical strange repeller formed by classical orbits nonescaping in future and past times. In the context of eigenvalues  $\lambda$  of the Google matrix we have  $\gamma = -2 \ln |\lambda|$ . By numerical simulations it has been shown that the law (5) works for a scattering problem in a three-disk system (Lu, Sridhar, and Zworski, 2003) and quantum chaos maps with absorption when the fractal dimension  $d$  is changed in a broad range  $0 < d < 2$  (Shepelyansky, 2008; Ermann and Shepelyansky, 2010b).

The fractal Weyl law (5) of open systems with a fractal dimension  $d < 2$  leads to a striking consequence: only a relatively small fraction of eigenvalues  $\mu_W \sim N_\gamma/N \propto \hbar^{(2-d)/2} \propto N^{(d-2)/2} \ll 1$  has finite values of  $|\lambda|$  while almost all eigenstates of the matrix operator of size  $N \propto 1/\hbar$  have  $\lambda \rightarrow 0$ . The eigenstates with finite  $|\lambda| > 0$  are related to the classical fractal sets of orbits nonescaping neither in the future nor in the past. A fractal structure of these quantum fractal eigenstates was investigated by Shepelyansky (2008).

There it was conjectured that the eigenstates of a Google matrix with finite  $|\lambda| > 0$  will select interesting specific communities of a network. We see later that the fractal Weyl law can indeed be observed in certain directed networks and, in particular, we show in Sec. VI that it naturally appears for Perron-Frobenius operators of dynamical systems and Ulam networks.

It is interesting to note that nontrivial complex spectra also naturally appear in systems of quantum chaos in the presence of a contact with a measurement device (Bruzda *et al.*, 2010). The properties of complex spectra of small size orthostochastic (unistochastic) matrices are analyzed by Zyczkowski *et al.* (2003). In such matrices the elements can be presented in a form  $S_{ij} = O_{ij}^2$  ( $S_{ij} = |U_{ij}|^2$ ), where  $O$  is an orthogonal matrix ( $U$  is a unitary matrix). We will see certain similarities of their spectra with the spectra of directed networks discussed in Sec. VIII.

Recent mathematical results for the fractal Weyl law are presented in Nonnenmacher and Zworski (2007) and Nonnenmacher, Sjostrand, and Zworski (2014).

## VI. ULAM NETWORKS

By construction the Google matrix belongs to the class of Perron-Frobenius operators which naturally appear in ergodic theory (Cornfeld, Fomin, and Sinai, 1982) and dynamical systems with Hamiltonian or dissipative dynamics (Brin and Stuck, 2002). Ulam (1960) proposed a method, now known as the Ulam method, for a construction of finite size approximants for the Perron-Frobenius operators of dynamical maps. The method is based on discretization of the phase space and construction of a Markov chain based on probability transitions between such discrete cells given by the dynamics. Using as an example a simple chaotic map, Ulam made a conjecture that the finite size approximation converges to the continuous limit when the cell size goes to zero. Indeed, it has been proven that for hyperbolic maps in 1 and higher dimensions the Ulam method converges to the spectrum of a continuous system (Li, 1976; Blank, Keller, and Liverani, 2002). The probability flows in dynamical systems have rich and nontrivial features of general importance, like simple and strange attractors with localized and delocalized dynamics governed by simple dynamical rules (Lichtenberg and Lieberman, 1992). Such objects are generic for nonlinear dissipative dynamics and hence can have relevance for actual WWW structure. The analysis of Ulam networks, generated by the Ulam method, allows one to obtain better intuition about the spectral properties of a Google matrix. The term Ulam networks was introduced by Shepelyansky and Zhironov (2010a).

### A. Ulam method for dynamical maps

In Fig. 8 we show how the Ulam method works. The phase space of a dynamical map is divided in equal cells and a number of trajectories  $N_c$  is propagated by a map iteration. Thus the number of trajectories  $N_{ij}$  arrived from cell  $j$  to cell  $i$  is determined. Then the matrix of the Markov transition is defined as  $S_{ij} = N_{ij}/N_c$ . By construction this matrix belongs

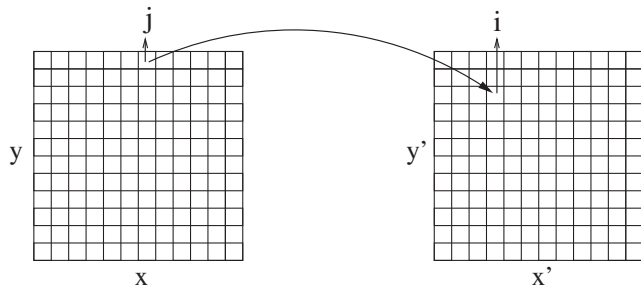


FIG. 8. Illustration of the operation of the Ulam method: the phase space  $(x, y)$  is divided in  $N = N_x \times N_y$  cells,  $N_c$  trajectories start from cell  $j$  and the number of trajectories  $N_{ij}$  arrived to a cell  $i$  from a cell  $j$  is collected after a map iteration. Then the matrix of Markov transitions is defined as  $S_{ij} = N_{ij}/N_c$ , by construction  $\sum_{i=1}^N S_{ij} = 1$ .

to the class of Perron-Frobenius operators which includes the Google matrix.

The physical meaning of the coarse grain description by a finite number of cells is that it introduces in the system a noise of cell size amplitude. Because of that an exact time reversibility of dynamical equations of chaotic maps is destroyed due to exponential instability of chaotic dynamics. This time reversibility breaking is illustrated by an example of the Arnold cat map by Ermann and Shepelyansky (2012). For the Arnold cat map on a long torus it is shown that the spectrum of the Ulam approximate of the Perron-Frobenius (UPFO) is composed of a large group of complex eigenvalues with  $\gamma \sim 2h \approx 2$ , and real eigenvalues with  $|1 - \lambda| \ll 1$  corresponding to a statistical relaxation to the ergodic state at  $\lambda = 1$  described by the Fokker-Planck equation [here  $h$  is the Kolmogorov-Sinai entropy of the map being here equal to the Lyapunov exponent, see, e.g., Chirikov (1979)].

For fully chaotic maps the finite cell size, corresponding to added noise, does not significantly affect the dynamics and the discrete UPFO converges to the limiting case of the continuous Perron-Frobenius operator (Li, 1976; Blank, Keller, and Liverani, 2002). The Ulam method finds useful applications in the studies of dynamics of molecular systems and coherent structures in dynamical flows (Froyland and Padberg, 2009); see also Frahm and Shepelyansky (2010).

## B. Chirikov standard map

However, for symplectic maps with a divided phase space, a noise present in the Ulam method significantly affects the original dynamics leading to a destruction of islands of stable motion and Kolmogorov-Arnold-Moser (KAM) curves. A famous example of such a map is the Chirikov standard map which describes the dynamics of many physical systems (Chirikov, 1979; Chirikov and Shepelyansky, 2008):

$$\bar{y} = \eta y + \frac{K_s}{2\pi} \sin(2\pi x), \quad \bar{x} = x + \bar{y} \pmod{1}. \quad (6)$$

Here bars mark the variables after one map iteration and we consider the dynamics to be periodic on a torus so that  $0 \leq x \leq 1$ ,  $-1/2 \leq y \leq 1/2$ ;  $K_s$  is a dimensionless parameter of chaos. At  $\eta = 1$  we have an area-preserving symplectic

map, considered in this section; for  $0 < \eta < 1$  we have a dissipative dynamics analyzed in Sec. VI.C.

Since the finite cell size generates noise and destroys the KAM curves in the map (6) at  $\eta = 1$ , one should use the generalized Ulam method (Frahm and Shepelyansky, 2010), where the transition probabilities  $N_{ij}/N_c$  are collected along one chaotic trajectory. In this construction a trajectory visits only those cells which belong to one connected chaotic component. Therefore the noise induced by the discretization of the phase space does not lead to a destruction of invariant curves, in contrast to the original Ulam method (Ulam, 1960), which uses all cells in the available phase space. Since a trajectory is generated by a continuous map it cannot penetrate inside the stability islands and on a physical level of rigor one can expect that, due to ergodicity of dynamics on one connected chaotic component, the UPFO constructed in such a way should converge to the Perron-Frobenius operator of the continuous map on a given subspace of chaotic component. The numerical confirmations of this convergence are presented by Frahm and Shepelyansky (2010).

We consider the map (6) at  $K_s = 0.971\,635\,406$  when the golden KAM curve is critical. Because of the symmetry of the map with respect to  $x \rightarrow 1 - x$  and  $y \rightarrow -y$  we can use only the upper part of the phase space with  $y \geq 0$  dividing it in  $M \times M/2$  cells. At that  $K_s$  we find that the number of cells visited by the trajectory in this half square scales as  $N_d \approx C_d M^2/2$  with  $C_d \approx 0.42$ . This means that the chaotic component contains about 40% of the total area which is in good agreement with the known result of Chirikov (1979).

The spectrum of the UPFO matrix  $S$  for the phase space division by  $280 \times 208/2$  cells is shown in Fig. 9(b). In a first approximation the spectrum  $\lambda$  of  $S$  is more or less homogeneously distributed in the polar angle  $\varphi$  defined as  $\lambda_j = |\lambda_j| \exp(i\varphi_j)$ . With the increase of matrix size  $N_d$  the two-dimensional density of states  $\rho(\lambda)$  converges to a limiting

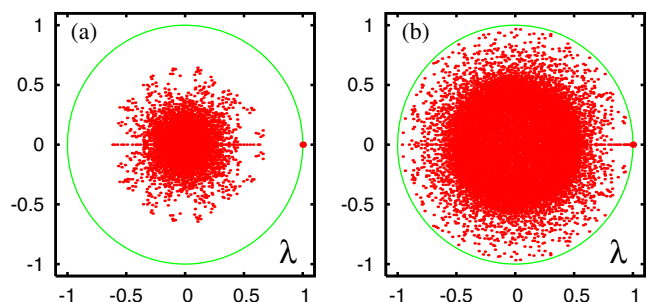


FIG. 9 (color online). Complex spectrum of eigenvalues  $\lambda_j$ , shown by gray (red) dots, for the UPFO of two variants of the Chirikov standard map (6); the unit circle  $|\lambda| = 1$  is shown by a light gray (green) curve, the unit eigenvalue at  $\lambda = 1$  is shown as a gray (larger red) dot. (a) The Chirikov standard map at dissipation  $\eta = 0.3$  and  $K_s = 7$ ; the phase space is covered by  $110 \times 110$  cells and the UPFO is constructed by many trajectories with random initial conditions generating transitions from one cell into another. From Ermann and Shepelyansky, 2010b. (b) The Chirikov standard map without dissipation at  $K_s = 0.971\,635\,406$  with an UPFO constructed from a single trajectory of length  $10^{12}$  in the chaotic domain and  $280 \times 280/2$  cells to cover the phase space. From Frahm and Shepelyansky, 2010.

distribution (Frahm and Shepelyansky, 2010). With the help of the Arnoldi method it is possible to compute a few thousand of eigenvalues with largest absolute values  $|\lambda|$  for maximal  $M = 1600$  with the total matrix size  $N = N_d \approx 5.3 \times 10^5$ .

The eigenstate at  $\lambda = 1$  is homogeneously distributed over the chaotic component at  $M = 25$  (Fig. 10) and higher  $M$  values (Frahm and Shepelyansky, 2010). This results from the ergodicity of motion and the fact that for symplectic maps the measure is proportional to the phase space area (Chirikov, 1979; Cornfeld, Fomin, and Sinai, 1982). Examples of other right eigenvalues of  $S$  at real and complex eigenvalues  $\lambda$  with  $|\lambda| < 1$  are also shown in Fig. 10. For  $\lambda_2$  the eigenstate corresponds to some diffusive mode with two nodal lines, while the other two eigenstates are localized around certain resonant structures in phase space. This shows that eigenstates of the matrix  $G$  (and  $S$ ) are related to specific communities of a network.

With an increase of the number of cells  $M^2/2$  there are eigenvalues which become more and more close to the unit eigenvalue. This is shown to be related to an algebraic statistics of Poincaré recurrences and long time sticking of trajectories in the vicinity of critical KAM curves. At the same time for symplectic maps the measure is proportional to the area so that we have dimension  $d = 2$  and hence we have a usual Weyl law with  $N_\gamma \propto N$ . More details can be found in Frahm and Shepelyansky (2010, 2013).

### C. Dynamical maps with strange attractors

The fractal Weyl law (5) has initially been proposed for quantum systems with chaotic scattering. However, it is natural to assume that it should also work for Perron-Frobenius operators of dynamical systems. Indeed, the

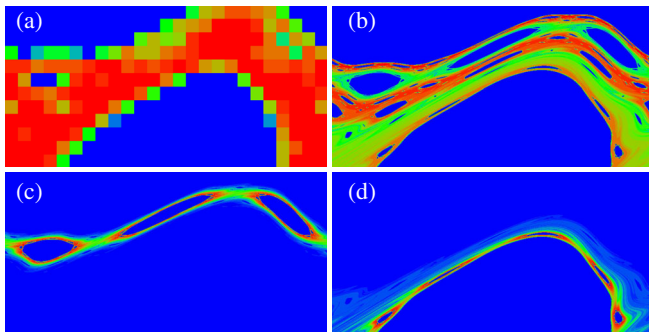


FIG. 10 (color online). Density plots of absolute values of the eigenvectors of the UPFO obtained by the generalized Ulam method with a single trajectory of  $10^{12}$  iterations of the Chirikov standard map at  $K_s = 0.971635406$ . The phase space is shown in the area  $0 \leq x \leq 1$ ,  $0 \leq y \leq 1/2$ ; the UPFO is obtained from  $M \times M/2$  cells placed in this area. (a) Eigenvector  $\psi_0$  with eigenvalue  $\lambda_0 = 1$ ; (b) eigenvector  $\psi_2$  with real eigenvalue  $\lambda_2 = 0.99878108$ ; (c) eigenvector  $\psi_6$  with complex eigenvalue  $\lambda_6 = -0.49699831 + i0.86089756 \approx |\lambda_6|e^{i2\pi/3}$ ; (d) eigenvector  $\psi_{13}$  with complex eigenvalue  $\lambda_{13} = 0.30580631 + i0.94120900 \approx |\lambda_{13}|e^{i2\pi/5}$ . (a) Corresponding to  $M = 25$  while (b)–(d) have  $M = 800$ . Color is proportional to the amplitude with black (blue) for zero and gray (red) for the maximal value. From Frahm and Shepelyansky, 2010.

mathematical results for the Selberg zeta function indicated that the law (5) should remain valid for the UFPO (Nonnenmacher, Sjostrand, and Zworski, 2014). A detailed test of this conjecture (Ermann and Shepelyansky, 2010b) was performed for the map (6) with dissipation at  $0 < \eta < 1$ , when at large  $K_s$  the dynamics converges to a strange attractor in the range  $-2 < y < 2$ , and for the nondissipative case  $\eta = 1$  with absorption, where all orbits leaving the interval  $-aK_s/4\pi \leq y \leq aK_s/4\pi$  are absorbed after one iteration (in both cases there is no modulus in  $y$ ).

An example of the spectrum of UPFO for the model with dissipation is shown in Fig. 9(a). We see that now, in contrast to the symplectic case of Fig. 9(b), the spectrum has a significant gap which separates the eigenvalue  $\lambda = 1$  from the other eigenvalues with  $|\lambda| < 0.7$ . For the case with absorption the spectrum has a similar structure but now with  $|\lambda| < 1$  for the leading eigenvalue  $\lambda$  since the total number of initial trajectories decreases with the number of map iterations due to absorption implying that for this case  $\sum_i S_{ij} < 1$  with  $S$  being the UPFO.

It is established that the distribution of the density of states  $dW/d\gamma$  (or  $dW/d|\lambda|$ ) converges to a fixed distribution in the limit of large  $N$  or cell size going to zero (Ermann and Shepelyansky, 2010b, see Fig. 4). This demonstrates the validity of the Ulam conjecture for considered systems.

Examples of two eigenstates of the UFPO for these two models are shown in Fig. 11. The fractal structure of eigenstates is well visible. For the dissipative case without absorption we have eigenstates localized on the strange attractor. For the case with absorption eigenstates are located on a strange repeller corresponding to an invariant set of nonescaping orbits. The fractal dimension  $d$  of these classical invariant sets can be computed by the usual box-counting method for dynamical systems. It is important to note that for the case with absorption it is more natural to measure the dimension  $d_e$  of the set of orbits nonescaping in the future.

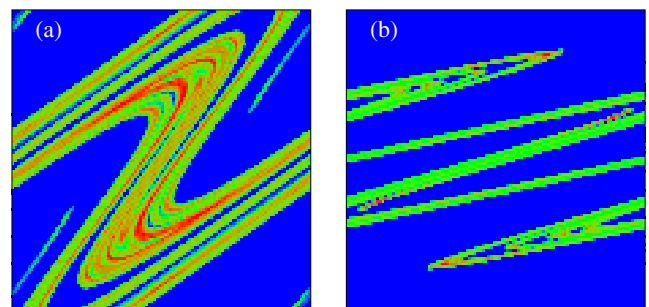


FIG. 11 (color online). Phase space representation of eigenstates of the UFPO  $S$  for  $N = 110 \times 110$  cells (color is proportional to absolute value  $|\psi_i|$  with gray (red) for maximum and black (blue) for zero). (a) An eigenstate with maximum eigenvalue  $\lambda_1 = 0.756$  of the UFPO of map (6) with absorption at  $K_s = 7$ ,  $a = 2$ ,  $\eta = 1$ , the space region is  $(-aK_s/4\pi \leq y \leq aK_s/4\pi, 0 \leq x \leq 1)$ , the fractal dimension of the strange repeller set nonescaping in the future is  $d_e = 1 + d/2 = 1.769$ . (b) An eigenstate at  $\lambda = 1$  of the UFPO of map (6) without absorption at  $K_s = 7$ ,  $\eta = 0.3$ , the shown space region is  $(-1/\pi \leq y \leq 1/\pi, 0 \leq x \leq 1)$ , and the fractal dimension of the strange attractor is  $d = 1.532$ . From Ermann and Shepelyansky, 2010b.

Because of the time reversal symmetry of the continuous map the dimension of the set of orbits nonescaping in the past is also  $d_e$ . Thus the phase space dimension 2 is composed of  $2 = d_e + d_e - d$  and  $d_e = 1 + d/2$ , where  $d$  is the dimension of the invariant set of orbits nonescaping neither in the future nor in the past. For the case with dissipation without absorption all orbits drop on a strange attractor and we have the dimension of invariant set  $d_e = d$ .

#### D. Fractal Weyl law for Perron-Frobenius operators

The direct verification of the validity of the fractal Weyl law (5) is presented in Fig. 12. The number of eigenvalues  $N_\gamma$  in the range with  $0 \leq \gamma \leq \gamma_b$  ( $\gamma = -2 \ln |\lambda|$ ) is numerically computed as a function of matrix size  $N$ . The fit of the dependence  $N_\gamma(N)$ , as shown in Fig. 12(a), allows one to determine the exponent  $\nu$  in the relation  $N_\gamma \propto N^\nu$ . The dependence of  $\nu$  on the fractal dimension  $d$ , computed from the invariant fractal set by the box-counted method, is shown in Fig. 12(b). The numerical data are in good agreement with the theoretical fractal Weyl law dependence  $\nu = d/2$ . This law works for a variety of parameters for the system (6) with absorption and dissipation and also for a strange attractor in the Hénon map ( $\bar{x} = y + 1 - ax^2, \bar{y} = bx$ ). We attribute certain deviations, visible in Fig. 12 especially for  $K_s = 7$ , to the fact that at  $K_s = 7$  there is a small island of stability at  $\eta = 1$ , which can produce a certain influence on the dynamics.

The physical origin of the law (5) can be understood in a simple way: the number of states  $N_\gamma$  with finite values of  $\gamma$  is proportional to the number of cells  $N_f \propto N^{d/2}$  on the fractal set of a strange attractor. Indeed, the results for the overlap measure show that the eigenstates  $N_\gamma$  have a strong overlap

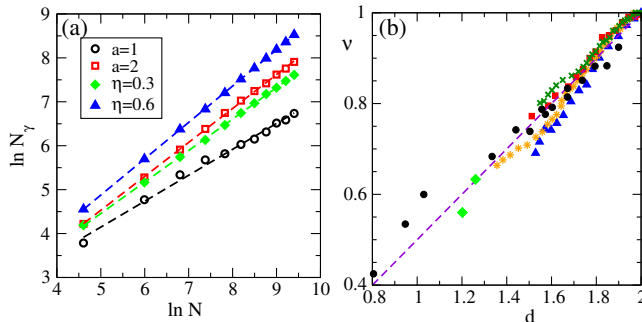


FIG. 12 (color online). (a) The dependence of the integrated number of states  $N_\gamma$  with decay rates  $0 \leq \gamma \leq \gamma_b = 16$  on the size  $N$  of the UFPO matrix  $S$  for the map (6) at  $K_s = 7$ . The fits of numerical data, shown by dashed straight lines, give  $\nu = 0.590$ ,  $d_e = 1 + d/2 = 1.643$  (at  $a = 1$ );  $\nu = 0.772$ ,  $d_e = 1 + d/2 = 1.769$  (at  $a = 2$ );  $\nu = 0.716$ ,  $d = 1.532$  (at  $\eta = 0.3$ );  $\nu = 0.827$ ,  $d = 1.723$  (at  $\eta = 0.6$ ). (b) The fractal Weyl exponent  $\nu$  as a function of fractal dimension  $d$  of the invariant fractal set for the map (6) with a strange attractor ( $\eta < 1$ ) at  $K_s = 15$  [gray (green) crosses],  $K_s = 12$  [gray (red) squares],  $K_s = 10$  [gray (orange) stars], and  $K_s = 7$  [black (blue) triangles]; for a strange repeller ( $\eta = 1$ ) at  $K_s = 7$  (black points) and for a strange attractor for the Hénon map at standard parameters  $a = 1.2$ ,  $b = 0.3$  (green diamonds). The straight dashed line shows the fractal Weyl law dependence  $\nu = d/2$ . From Ermann and Shepelyansky, 2010b.

with the steady state while the states with  $\lambda \rightarrow 0$  have very small overlap. Thus almost all  $N$  states have eigenvalues  $\lambda \rightarrow 0$  and only a small fraction of states on a strange attractor or repeller  $N_\gamma \propto N_f \propto N^{d/2} \ll N$  has finite values of  $\lambda$ . We also checked that the participation ratio  $\xi$  of the eigenstate at  $\lambda = 1$  grows as  $\xi \sim N_f \propto N^{d/2}$  in agreement with the fractal Weyl law (Ermann and Shepelyansky, 2010b).

#### E. Intermittency maps

The properties of the Google matrix generated by one-dimensional intermittency maps have been analyzed by Ermann and Shepelyansky (2010a). It was found that for such Ulam networks there are many eigenstates with eigenvalues  $|\lambda|$  being very close to unity. The PageRank of such networks at  $\alpha = 1$  is characterized by a power law decay with an exponent determined by the parameters of the map. It is interesting to note that usually for the WWW the PageRank probability is proportional to a number of ingoing links distribution (Litvak, Scheinhardt, and Volkovich, 2008). For the case of intermittency maps the decay of PageRank is independent of the number of ingoing links. In addition, for  $\alpha$  close to unity a decay of the PageRank has an exponent  $\beta \approx 1$  but at smaller values  $\alpha \leq 0.9$  the PageRank becomes completely delocalized. It is shown that the delocalization depends on the intermittency exponent of the map. This indicates that a rather dangerous phenomenon of PageRank delocalization can appear for certain directed networks. At the same time the one-dimensional intermittency map still generates a relatively simple structure of links with the typical number of links per node being close to unity. Such a case is probably not very typical for real networks. Therefore it is useful to analyze richer Ulam networks with a larger number of links per node.

#### F. Chirikov typical map

With this aim we consider the Ulam networks generated by the Chirikov typical map with dissipation studied by Shepelyansky and Zhironov (2010a). The map, introduced by Chirikov in 1969 for a description of continuous chaotic flows, has the form

$$y_{t+1} = \eta y_t + k_s \sin(x_t + \theta_t), \quad x_{t+1} = x_t + y_{t+1}. \quad (7)$$

Here the dynamical variables  $x, y$  are taken at integer moments of time  $t$ . Also  $x$  has the meaning of a phase variable and  $y$  is a conjugated momentum or action. The phases  $\theta_t = \theta_{t+T}$  are  $T$  random phases periodically repeated along time  $t$ . We stress that their  $T$  values are chosen and fixed once and they are not changed during the dynamical evolution of  $x, y$ . We consider the map in the region of Fig. 13 ( $0 \leq x < 2\pi, -\pi \leq y < \pi$ ) with the  $2\pi$ -periodic boundary conditions. The parameter  $0 < \eta < 1$  gives a global dissipation. The properties of the symplectic map at  $\eta = 1$  have been studied in detail by Frahm and Shepelyansky (2009). The dynamics is globally chaotic for  $k_s > k_c \approx 2.5/T^{3/2}$  and the Kolmogorov-Sinai entropy is  $h \approx 0.29k_s^{2/3}$  [more details about the Kolmogorov-Sinai entropy can be found in Chirikov (1979), Cornfeld, Fomin, and Sinai (1982), and Brin and Stuck (2002)]. A bifurcation diagram at  $\eta < 1$  shows a series of transitions between fixed

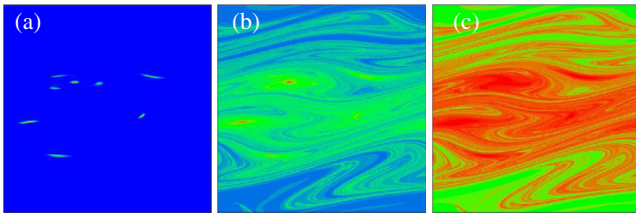


FIG. 13 (color online). PageRank probability  $P_j$  for the Google matrix generated by the Chirikov typical map at  $T = 10$ ,  $k_s = 0.22$ , and  $\eta = 0.99$  with (a)  $\alpha = 1$ , (b)  $\alpha = 0.95$ , and (c)  $\alpha = 0.85$ . The probability  $P_j$  is shown in the phase space region  $0 \leq x < 2\pi$ ;  $-\pi \leq y < \pi$  which is divided in  $N = 3.6 \times 10^5$  cells;  $P_j$  is zero for black (blue) and maximal for gray (red). From Shepelyansky and Zhirov, 2010a.

points, simple and strange attractors. Here we present results for  $T = 10$ ,  $k_s = 0.22$ ,  $\eta = 0.99$  and a specific random set of  $\theta_i$  given in Shepelyansky and Zhirov (2010a).

Because of the exponential instability of motion one cell in the Ulam method gives transitions to  $k_{cl} \approx \exp(hT)$  other cells. According to this relation a large number of cells  $k_{cl}$  can be coupled at large  $T$  and  $h$ . For parameters of Fig. 13 one finds an approximate power law distribution of ingoing and outgoing links in the corresponding Ulam network with the exponents  $\mu_{in} \approx \mu_{out} \approx 1.9$ . The variation of the PageRank vector with the damping factor  $\alpha$  is shown in Fig. 13 on the phase plane  $(x, y)$ . For  $\alpha = 1$  the PageRank is concentrated in a vicinity of a simple attractor composed of several fixed points on the phase plane. Thus the dynamical attractors are the most popular nodes from the network viewpoint. With a decrease of  $\alpha$  down to 0.95, 0.85 values we find a stronger and stronger delocalization of PageRank over the whole phase space.

The delocalization with a decrease of  $\alpha$  is also well seen in Fig. 14, where we show the  $P_j$  dependence on PageRank index  $j$  with a monotonic decreasing probability  $P_j$ . At  $\alpha = 1$  we have an exponential decay of  $P_j$  with  $j$  that corresponds to a Boltzmann-type distribution where a noise produced by a finite cell size in the Ulam method is compensated by dissipation. For  $\alpha = 0.95$  the random jumps of a network surfer, induced by the term  $(1 - \alpha)/N$  in Eq. (1), produce a power law decay of  $P_j \propto 1/j^\beta$  with  $\beta \approx 0.48$ . For  $\alpha = 0.85$  the PageRank probability is flat and completely delocalized over the whole phase space.

The analysis of the spectrum of  $S$  for the map (7) for the parameters of Fig. 14 shows the existence of eigenvalues being very close to  $\lambda = 1$ ; however, there is no exact degeneracy as is the case for UK universities which we discuss later. The spectrum is characterized by the fractal Weyl law with the exponent  $\nu \approx 0.85$ . For eigenstates with  $|\lambda| < 1$  the values of IPR  $\xi$  are less than 300 for a matrix size  $N \approx 1.4 \times 10^4$  showing that eigenstates are localized. However, for the PageRank the computations can be done with larger matrix sizes reaching a maximal value of  $N = 6.4 \times 10^5$ . The dependence of  $\xi$  on  $\alpha$  shows that a delocalization transition of the PageRank vector takes place for  $\alpha < \alpha_c \approx 0.95$ . Indeed, at  $\alpha = 0.98$  we have  $\xi \approx 30$ , while at  $\alpha \approx 0.8$  the IPR value of PageRank becomes comparable with the whole system size

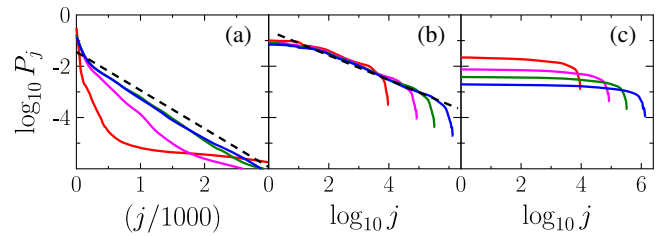


FIG. 14 (color online). Dependence of PageRank probability  $P_j$  on PageRank index  $j$  for number of cells in the UFPO being  $N = 10^4$ ,  $9 \times 10^4$ ,  $3.6 \times 10^5$ , and  $1.44 \times 10^6$  [larger  $N$  have more dark and more long curves in (b) and (c)]. (a) This order of  $N$  is for curves from bottom to top (curves for  $N = 3.6 \times 10^5$  and  $1.44 \times 10^6$  practically coincide in this panel); for the online version we note that the above order of  $N$  values corresponds to red, magenta, green, and blue curves, respectively. The dashed line in (a) shows an exponential Boltzmann decay (see text, the line is shifted in  $j$  for clarity). The dashed straight line in (b) shows the fit  $P_j \sim 1/j^\beta$  with  $\beta = 0.48$ . Other parameters, including the values of  $\alpha$ , and panel order are as in Fig. 13. From Shepelyansky and Zhirov, 2010a.

$\xi \approx 5 \times 10^5 \sim N = 6.4 \times 10^5$  [see Fig. 9 of Shepelyansky and Zhirov (2010a)].

The example of Ulam networks considered here shows that a dangerous phenomenon of PageRank delocalization can take place under certain conditions. This delocalization may represent a serious danger for the efficiency of search engines since for a delocalized flat PageRank the ranking of nodes becomes very sensitive to small perturbations and fluctuations.

## VII. LINUX KERNEL NETWORKS

Modern software codes now represent complex large-scale structures and analysis and optimization of their architecture become a challenge. An interesting approach to this problem, based on a directed network construction, was proposed by Chepelienskii (2010). Here we present results obtained for such networks.

### A. Ranking of software architecture

Following Chepelienskii (2010) we considered the procedure call networks (PCN) for open source programs with emphasis on the code of Linux Kernel (Linux, 2010a) written in the C-programming language (Kernighan and Ritchie, 1978). In this language the code is structured as a sequence of procedures calling each other. Because of that feature the organization of a code can be naturally represented as a PCN, where each node represents a procedure and each directed link corresponds to a procedure call. For the Linux source code such a directed network is built by its lexical scanning with the identification of all the defined procedures. For each of them a list keeps track of the procedure calls inside their definition.

An example of the obtained network for a toy code with two procedures *start\_kernel* and *printk* is shown in Fig. 15. The in and out degrees of this model, noted as  $k$  and  $\bar{k}$ , are shown in Fig. 15. These numbers correspond to the number of outgoing

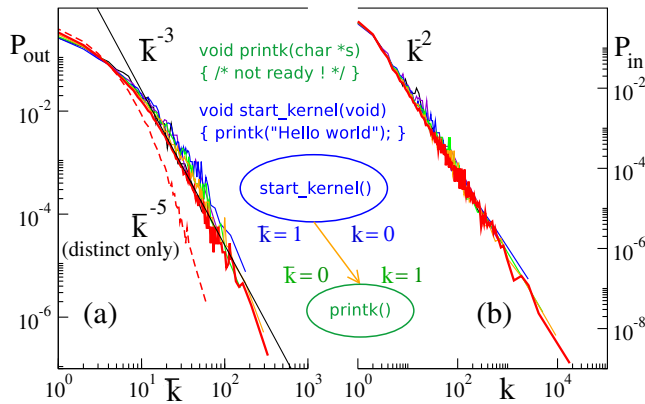


FIG. 15 (color online). The diagram in the center represents the PCN of a toy kernel with two procedures written in the C-programming language. The data in (a) and (b) show outdegree and indegree probability distributions  $P_{\text{out}}(\bar{k})$  and  $P_{\text{in}}(k)$ , respectively. The colors correspond to different Kernel releases. The most recent version 2.6.32, with  $N = 285\,509$  and an average of 3.18 calls per procedure, is represented in gray (red). Older versions (2.4.37.6, 2.2.26, 2.0.40, 1.2.12, and 1.0) with  $N$  respectively equal to (85 756, 38 766, 14 079, 4358, and 2751) follow the same behavior. The dashed curve in (a) shows the outdegree probability distribution if only calls to distinct destination procedures are kept. From [Chepelianskii, 2010](#).

and ingoing calls for each procedure. The obtained in- and outdegree probability distributions  $P_{\text{in}}(k)$  and  $P_{\text{out}}(\bar{k})$  are shown Fig. 15 for different Linux Kernel releases. These distributions are well described by power law dependences  $P_{\text{in}}(k) \propto 1/k^{\mu_{\text{in}}}$  and  $P_{\text{out}}(\bar{k}) \propto 1/\bar{k}^{\mu_{\text{out}}}$  with  $\mu_{\text{in}} = 2.0 \pm 0.02$  and  $\mu_{\text{out}} = 3.0 \pm 0.1$ . These values of exponents are close to those found for the WWW ([Donato et al., 2004](#); [Pandurangan, Raghavan, and Upfal, 2006](#)). If only calls to distinct functions are counted in the outdegree distribution then the exponent drops to  $\mu_{\text{out}} \approx 5$ , whereas  $\mu_{\text{in}}$  remains unchanged. It is important that the distributions for the different kernel releases remain stable even if the network size increases from  $N = 2751$  for version V1.0 to  $N = 285\,509$  for the latest version V2.6.32 taken into account in this study. This confirms the free-scale structure of the software architecture of the Linux Kernel network.

The probability distributions of PageRank and CheiRank vectors are also well described by power laws with exponents  $\beta_{\text{in}} \approx 1$  and  $\beta_{\text{out}} \approx 0.5$  being in good agreement with the usual relation  $\beta = 1/(\mu - 1)$  [see Fig. 2 in [Chepelianskii \(2010\)](#)]. For V2.6.32 the top three procedures of PageRank at  $\alpha = 0.85$  are *printk*, *memset*, and *kfree* with probabilities 0.024, 0.012, and 0.011, respectively, while at the top of CheiRank we have *start\_kernel*, *btfs\_ioctl*, and *menu\_finalize* with, respectively, 0.000 280, 0.000 255, and 0.000 250. These procedures perform rather different tasks with *printk* reporting messages and *start\_kernel* initializing the Kernel and managing the repartition of tasks. This gives an idea that both PageRank and CheiRank order can be useful to highlight different aspects of directed and inverted flows on our network. Of course, in the context of the WWW ingoing links related to PageRank are less vulnerable as compared to outgoing links related to CheiRank, which can be modified by a user rather easily.

However, in other type of networks both directions of links appear in a natural manner and thus both vectors of PageRank and CheiRank play an important and useful role.

For the Linux Kernel network the correlator  $\kappa$  Eq. (4) between PageRank and CheiRank vectors is close to zero (see Fig. 6). This confirms the independence of two vectors. The density distribution of nodes of the Linux Kernel network, shown in Fig. 7(b), has a homogeneous distribution along  $\ln K + \ln K^* = \text{const}$  lines demonstrating once more the absence of correlations between  $P(K_i)$  and  $P^*(K_i^*)$ . Indeed, such homogeneous distributions appear if nodes are generated randomly with factorized probabilities  $P_i P_i^*$  ([Chepelianskii, 2010](#); [Zhirov, Zhirov, and Shepelyansky, 2010](#)). Such a situation seems to be rather generic for software architecture. Indeed, other open software codes also have a small value for a correlator, e.g., OpenSource software including GIMP 2.6.8 has  $\kappa = -0.068$  at  $N = 17\,540$  and X Windows server R7.1-1.1.0 has  $\kappa = -0.027$  at  $N = 14\,887$ . In contrast to these software codes the Wikipedia networks have large values of  $\kappa$  and inhomogeneous distributions in  $(K, K^*)$  plane (see Figs. 6 and 7).

The physical reasons for the absence of correlations between  $P(K)$  and  $P^*(K^*)$  have been explained by [Chepelianskii \(2010\)](#) on the basis of the concept of “separation of concerns” in software architecture ([Dijkstra, 1982](#)). It is argued that a good code should decrease the number of procedures that have high values of both PageRank and CheiRank since such procedures will play a critical role in error propagation since they are both popular and highly communicative at the same time. For example, in the Linux Kernel *do\_fork*, that creates new processes, belongs to this class. Such critical procedures may introduce subtle errors because they entangle otherwise independent segments of code. These observations suggest that the independence between popular procedures, which have high  $P(K_i)$  and fulfill important but well-defined tasks, and communicative procedures, which have high  $P^*(K_i^*)$  and organize and assign tasks in the code, is an important ingredient of well-structured software.

## B. Fractal dimension of Linux Kernel networks

The spectral properties of the Linux Kernel network have been analyzed by [Ermann, Chepelianskii, and Shepelyansky \(2011\)](#). At large  $N$  the spectrum is obtained with the help of the Arnoldi method from the ARPACK library. This allows one to find eigenvalues with  $|\lambda| > 0.1$  for the maximal  $N$  at V2.6.32. An example of the complex spectrum  $\lambda$  of  $G$  is shown in Fig. 16(a). There are clearly visible lines at real axis and polar angles  $\varphi = \pi/2, 2\pi/3, 4\pi/3, 3\pi/2$ . The latter are related to certain cycles in procedure calls, e.g., an eigenstate at  $\lambda_i = 0.85 \exp(i2\pi/3)$  is located only on six nodes. The spectrum of  $G^*$  has a similar structure.

The network size  $N$  grows with the version number of the Linux Kernel corresponding to its evolution in time. We determine the total number of states  $N_\lambda$  with  $0.1 < |\lambda| \leq 1$  and  $0.25 < |\lambda| \leq 1$ . The dependence of  $N_\lambda$  on  $N$ , shown in Fig. 16(b), clearly demonstrates the validity of the fractal Weyl law with an exponent  $\nu \approx 0.63$  for  $G$  (we find  $\nu^* \approx 0.65$  for  $G^*$ ). We take the values of  $\nu$  for  $\lambda = 0.1$ , where the number

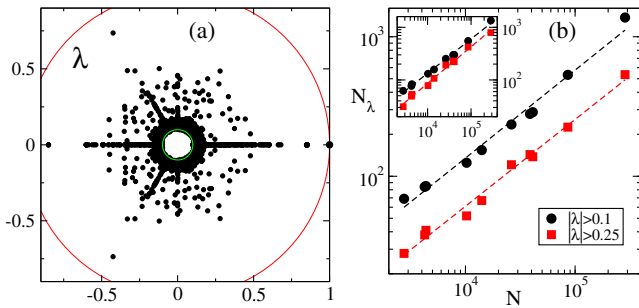


FIG. 16 (color online). (a) Distribution of eigenvalues  $\lambda$  in the complex plane for the Google matrix  $G$  of the Linux Kernel version 2.6.32 with  $N = 285\,509$  and  $\alpha = 0.85$ ; the solid curves represent the unit circle and the lowest limit of computed eigenvalues. (b) The dependence of the integrated number of eigenvalues  $N_\lambda$  with  $|\lambda| > 0.25$  [gray (red) squares] and  $|\lambda| > 0.1$  (black circles) as a function of the total number of processes  $N$  for versions of Linux Kernels. The values of  $N$  correspond (in increasing order) to Linux Kernel versions 1.0, 1.1, 1.2, 1.3, 2.0, 2.1, 2.2, 2.3, 2.4, and 2.6. The power law  $N_\lambda \propto N^\nu$  has fitted values  $\nu_{|\lambda|>0.25} = 0.622 \pm 0.010$  and  $\nu_{|\lambda|>0.1} = 0.630 \pm 0.015$ . The inset shows data for the Google matrix  $G^*$  with inverse link directions; the corresponding exponents are  $\nu_{|\lambda|>0.25}^* = 0.696 \pm 0.010$  and  $\nu_{|\lambda|>0.1}^* = 0.652 \pm 0.007$ . From Ermann, Chepelienskii, and Shepelyansky, 2011.

of eigenvalues  $N_\lambda$  gives better statistics. Within statistical errors the value of  $\nu$  is not sensitive to the cutoff value at small  $\lambda$ . The matrix  $G^*$  has slightly higher values of  $\nu$ . These results show that the PCN of the Linux Kernel has a fractal dimension  $d = 2\nu \approx 1.26$  for  $G$  and  $d = 2\nu \approx 1.3$  for  $G^*$ .

To check that the fractal dimension of the PCN indeed has this value, the dimension of the network is computed by another direct method known as the cluster growing method (Song, Havlin, and Makse, 2005). In this method the average mass or number of nodes  $\langle M_c \rangle$  is computed as a function of the network distance  $l$  counted from an initial seed node with further averaging over all seed nodes. For a dimension  $d$  the mass  $\langle M_c \rangle$  should grow as  $\langle M_c \rangle \propto l^d$  that allows one to determine the value of  $d$  for a given network. Note that this method should be generalized to the case of directed networks. For that the network distance  $l$  is computed following only outgoing links. The average of  $\langle M_c(l) \rangle$  is done over all nodes. Because of global averaging the method gives the same result for the matrix with an inverted link direction (indeed, the total number of outgoing links is equal to the number of ingoing links). However, as established by Ermann, Chepelienskii, and Shepelyansky (2011), the fractal dimension obtained by this generalized method is very different from the case of a converted undirected network, when each directed link is replaced by an undirected one. The average dimension obtained with this method for PCN is  $d = 1.4$  even if a certain 20% increase of  $d$  appears for the latest Linux version V2.6. We attribute this deviation for the version V2.6 to the well-known fact that significant rearrangements in the Linux Kernel have been done after version V2.4 (Linux, 2010a).

Thus in view of these restrictions we consider that there is rather good agreement of the fractal dimension obtained from the fractal Weyl law with  $d \approx 1.3$  and the value obtained with

the cluster growing method which gives an average  $d \approx 1.4$ . The fact that  $d$  is approximately the same for all versions up to V2.4 means that the Linux Kernel is characterized by a self-similar fractal growth in time. The closeness of  $d$  to unity signifies that procedure calls are almost linearly ordered that corresponds to a good code organization. Of course, the fractal Weyl law gives the dimension  $d$  obtained during the time evolution of the network. This dimension is not necessary the same as for a given version of the network of fixed size. However, one can expect that the growth goes in a self-similar way (Dorogovtsev, Goltsev, and Mendes, 2008) and that the static dimension is close to the dimension value emerging during the time evolution. This can be viewed as some kind of ergodicity conjecture. Our data show that this conjecture works with good accuracy up to the Linux Kernel V.2.6.

Thus the results obtained by Ermann, Chepelienskii, and Shepelyansky (2011) and described here confirm the validity of the fractal Weyl law for the Linux Kernel network with the exponent  $\nu \approx 0.65$  and the fractal dimension  $d \approx 1.3$ . It is important to note that the fractal Weyl exponent  $\nu$  is not sensitive to the exponent  $\beta$  characterizing the decay of the PageRank. Indeed, the exponent  $\beta$  remains practically the same for the WWW (Donato *et al.*, 2004) and the PCN of the Linux Kernel (Chepelienskii, 2010), while the values of fractal dimension are different with  $d \approx 4$  for the WWW and  $d \approx 1.3$  for the PCN (Ermann, Chepelienskii, and Shepelyansky, 2011).

The analysis of the eigenstates of  $G$  and  $G^*$  shows that their IPR values remain small ( $\xi < 70$ ) compared to the matrix size  $N \approx 2.8 \times 10^5$  showing that they are well localized on certain selected nodes.

## VIII. WWW NETWORKS OF UK UNIVERSITIES

The WWW networks of certain UK universities for the years between 2002 and 2006 are publicly available at <http://cybermetrics.wlv.ac.uk/database/>. Because of their modest size, these networks are well suitable for a detailed study of PageRank, CheiRank, complex eigenvalue spectra, and eigenvectors (Frahm, Geogot, and Shepelyansky, 2011).

### A. Cambridge and Oxford University networks

We start our analysis of WWW university networks from those of Cambridge and Oxford 2006. For example, in Fig. 5 we show the dependence of PageRank (CheiRank) probabilities  $P$  ( $P^*$ ) on rank index  $K$  ( $K^*$ ) for the WWW of Cambridge 2006 at  $\alpha = 0.85$ . The decay is satisfactorily described by a power law with the exponent  $\beta = 0.75$  ( $\beta = 0.61$ ).

The complex eigenvalue spectrum and the invariant subspace structure (see Sec. III.C) have been studied in great detail for the cases of Cambridge 2006 and Oxford 2006. For Cambridge 2006 (Oxford 2006) the network size is  $N = 212\,710$  (200 823) and the number of links is  $N_\ell = 2\,015\,265$  (1 831 542). There are  $n_{\text{inv}} = 1543$  (1889) invariant subspaces, with maximal dimension  $d_{\text{max}} = 4656$  (1545), together they contain  $N_s = 48\,239$  (30 579) subspace nodes leading to 3508 (3275) eigenvalues (of the matrix  $S$ ) with  $|\lambda_j| = 1$  of which  $n_1 = 1832$  (2360) are at  $\lambda_j = 1$  (about 1% of  $N$ ). The last number  $n_1$  is larger than the number of invariant subspaces

$n_{\text{inv}}$  since each of the subspaces has at least one unit eigenvalue because each subspace is described by a full representation matrix of the Perron-Frobenius type. To determine the complex eigenvalue spectrum one can apply exact diagonalization on each subspace and the Arnoldi method on the remaining core space.

The spectra of all subspace eigenvalues and  $n_A = 20000$  core space eigenvalues of the matrices  $S$  and  $S^*$  are shown in Fig. 17. Even if the decay of PageRank and CheiRank probabilities with rank index is rather similar for both universities [see Fig. 1 in Frahm, Georgeot, and Shepelyansky (2011)] the spectra of two networks are very different. Thus the spectrum contains much more detailed information about the network features compared to the rank vectors.

At the same time the spectra of two universities have certain similar features. Indeed, one can identify cross and triple-star structures. These structures are very similar to those seen in the spectra of random orthostochastic matrices of small size  $N = 3, 4$  shown in Fig. 18 from Zyczkowski *et al.* (2003) (spectra of unistochastic matrices have a similar structure). The spectrum borders, determined analytically by Zyczkowski

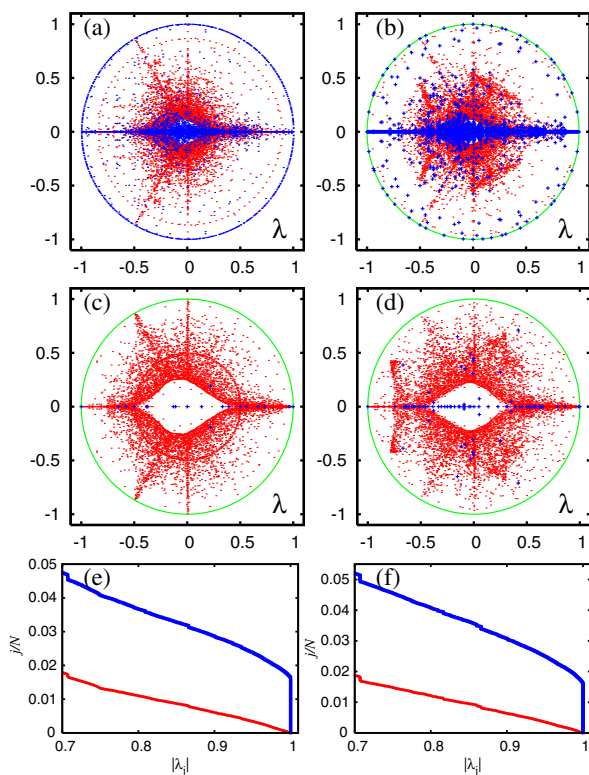


FIG. 17 (color online). (a), (b) The complex eigenvalue spectrum  $\lambda$  of matrix  $S$  for the University of Cambridge 2006 and Oxford 2006, respectively. (c), (d) The spectrum  $\lambda$  of matrix  $S^*$  for Cambridge 2006 and Oxford 2006. Eigenvalues  $\lambda$  of the core space are shown by gray (red) points, eigenvalues of isolated subspaces are shown by black (blue) points, and the gray (green) curve (when shown) is the unit circle. (e), (f) The fraction  $j/N$  of eigenvalues with  $|\lambda| > |\lambda_j|$  for the core space eigenvalues [gray (red) bottom curve] and all eigenvalues [black (blue) top curve] from top row data for Cambridge 2006 and Oxford 2006. From Frahm, Georgeot, and Shepelyansky, 2011.

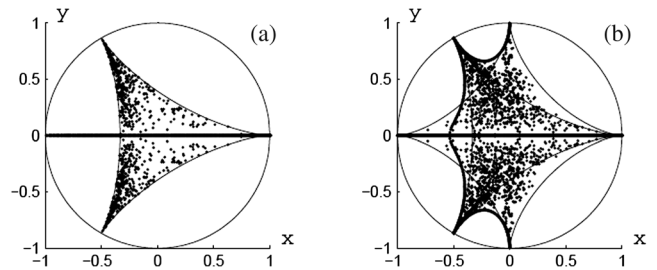


FIG. 18. Spectra  $\lambda$  of 800 random orthostochastic matrices of size (a)  $N = 3$  and (b)  $N = 4$  ( $\text{Re}\lambda = x, \text{Im}\lambda = y$ ). Thin lines denote 3- and 4-hypocycloids, while the thick lines represent the 3-4 interpolation arc. From Zyczkowski *et al.*, 2003.

*et al.* (2003) for these  $N$  values, are also shown. The similarity is more visible for the spectrum of the  $S^*$  case of Figs. 17(c) and 17(d). We attribute this to a larger randomness in outgoing links which have more fluctuations compared to ingoing links, as discussed by Eom *et al.* (2013). The similarity of spectra of Fig. 17 with those of random matrices in Fig. 18 indicates that there are dominant triple and quadruple structures of nodes present in the university networks which are relatively weakly connected to other nodes.

The core space submatrix  $S_{cc}$  of Eq. (2) does not obey the column sum normalization due to nonvanishing elements in the block  $S_{sc}$  which allow for a small but finite escape probability from core space to subspace nodes. Therefore the maximum eigenvalue of the core space (of the matrix  $S_{cc}$ ) is below unity. For Cambridge 2006 (Oxford 2006) it is given by  $\lambda_1^{(\text{core})} = 0.999\,874\,353\,718$  ( $0.999\,982\,435\,081$ ) with a quite clear gap  $1 - \lambda_1^{(\text{core})} \sim 10^{-4}$  ( $\sim 10^{-5}$ ).

## B. Universal emergence of PageRank

For  $\alpha = 1$  the leading eigenvalue  $\lambda = 1$  is highly degenerate due to the subspace structure. This degeneracy is lifted for  $\alpha < 1$  with a unique eigenvector, the PageRank, for the leading eigenvalue. The question arises how does the PageRank emerge if  $1 - \alpha \ll 1$ . Following Frahm, Georgeot, and Shepelyansky (2011), an answer is obtained from a formal matrix expression:

$$P = (1 - \alpha)(I - \alpha S)^{-1} e/N, \quad (8)$$

where the vector  $e$  has unit entries on each node and  $I$  is the unit matrix. Then, assuming that  $S$  is diagonalizable (with no nontrivial Jordan blocks) we can use the expansion

$$P = \sum_{\lambda_j=1} c_j \psi_j + \sum_{\lambda_j \neq 1} \frac{1 - \alpha}{(1 - \alpha) + \alpha(1 - \lambda_j)} c_j \psi_j, \quad (9)$$

where  $\psi_j$  are the eigenvectors of  $S$  and  $c_j$  coefficients determined by the expansion  $e/N = \sum_j c_j \psi_j$ . Thus Eq. (9) indicates that in the limit  $\alpha \rightarrow 1$  the PageRank converges to a particular linear combination of the eigenvectors with  $\lambda_j = 1$ , which are all localized in one of the subspaces. For a finite but very small value of  $1 - \alpha \ll 1 - \lambda_1^{(\text{core})}$  the corrections for the contributions of the core space nodes



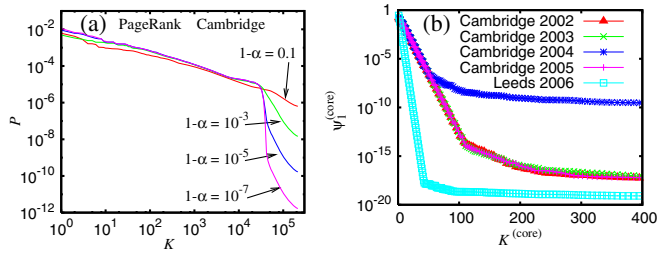


FIG. 19 (color online). (a) PageRank  $P(K)$  of Cambridge 2006 for  $1 - \alpha = 0.1, 10^{-3}, 10^{-5}$ , and  $10^{-7}$ . (b) First core space eigenvector  $\psi_1^{(\text{core})}$  vs its rank index  $K^{(\text{core})}$  for the UK university networks with a small core space gap  $1 - \lambda_1^{(\text{core})} < 10^{-8}$ . From Frahm, Georgeot, and Shepelyansky, 2011.

are  $\sim (1 - \alpha)/(1 - \lambda_1^{(\text{core})})$ . This behavior is indeed confirmed by Fig. 19(a) showing the evolution of the PageRank for different values of  $1 - \alpha$  for the case of Cambridge 2006 and using a particular method, based on an alternate combination of the power iteration method and the Arnoldi method (Frahm, Georgeot, and Shepelyansky, 2011), to numerically determine the PageRank for very small values of  $1 - \alpha \sim 10^{-8}$ .

However, for certain of the university networks the core space gap  $1 - \lambda_1^{(\text{core})}$  is particularly small, for example,  $1 - \lambda_1^{(\text{core})} \sim 10^{-17}$ , such that in standard double-precision arithmetic the Arnoldi method, applied to the matrix  $S_{cc}$ , does not allow one to determine this small gap. For these particular cases it is possible to determine rather accurately the core space gap and the corresponding eigenvector by another numerical approach called the “projected power method” (Frahm, Georgeot, and Shepelyansky, 2011). These eigenvectors, shown in Fig. 19(b), are strongly localized on a modest number of nodes  $\sim 10^2$  and with very small but nonvanishing values on the other nodes. Technically these vectors extend to the whole core space but practically they define small quasisubspaces (in the core space domain), where the escape probability is extremely small (Frahm, Georgeot, and Shepelyansky, 2011) and in the range  $1 - \alpha \sim 10^{-8}$  they still contribute to the PageRank according to Eq. (9).

In Fig. 20(b) we show that for several of the university networks the PageRank at  $1 - \alpha = 10^{-8}$  has actually a universal form when using the rescaled variables  $PN_s$  vs  $K/N_s$  with a power law behavior close to  $P \propto K^{-2/3}$  for  $K/N_s < 1$ . The rescaled data of Fig. 20(a) show that the fraction of subspaces with dimensions larger than  $d$  is well described by the power law  $F(x) \approx (1 + 2x)^{-1.5}$  with the dimensionless variable  $x = d/\langle d \rangle$ , where  $\langle d \rangle$  is an average subspace dimension computed for the WWW of a given university. The tables of all considered UK universities with the parameters of their WWW are given in Frahm, Georgeot, and Shepelyansky (2011). We note that the CheiRank of  $S^*$  of Wikipedia 2009 also approximately follows the above universal distributions. However, for the  $S$  matrix of Wikipedia the number of subspaces is small and statistical analysis cannot be performed for this case.

The origin of the universal distribution  $F(x)$  still remains a puzzle. Possible links with a percolation on directed networks (Dorogovtsev, Goltsev, and Mendes, 2008) are still to be

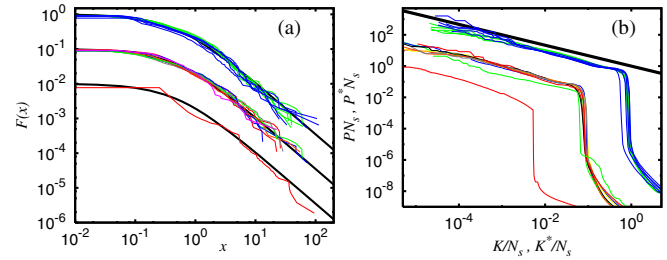


FIG. 20 (color online). (a) Fraction of invariant subspaces  $F$  with dimensions larger than  $d$  as a function of the rescaled variable  $x = d/\langle d \rangle$ . Upper curves correspond to Cambridge (gray/green) and Oxford (black/blue) for years 2002 to 2006 and middle curves (shifted down by a factor of 10) correspond to the university networks of Glasgow, Cambridge, Oxford, Edinburgh, UCL, Manchester, Leeds, Bristol, and Birkbeck for year 2006 with  $\langle d \rangle$  between 14 and 31. Lower curve (shifted down by a factor of 100) corresponds to the matrix  $S^*$  of Wikipedia with  $\langle d \rangle = 4$ . The thick black line is  $F(x) = (1 + 2x)^{-1.5}$ . (b) Rescaled PageRank  $PN_s$  vs rescaled rank index  $K/N_s$  for  $1 - \alpha = 10^{-8}$  and  $3974 \leq N_s \leq 48\,239$  for the same university networks as in (a) (upper and middle curves, the latter shifted down and left by a factor of 10). The lower curve (shifted down and left by a factor of 100) shows the rescaled CheiRank of Wikipedia  $P^*N_s$  vs  $K^*/N_s$  with  $N_s = 21\,198$ . The thick black line corresponds to a power law with exponent  $-2/3$ . From Frahm, Georgeot, and Shepelyansky, 2011.

elucidated. It also remains unclear how stable this distribution really is. It works well for UK university networks 2002–2006. However, for the Twitter network (Frahm and Shepelyansky, 2012a) such a distribution becomes rather approximate. Also for the network of Cambridge in 2011, analyzed by Ermann, Chepelianskii, and Shepelyansky (2012) and Ermann, Frahm, and Shepelyansky (2013) with  $N \approx 8.9 \times 10^5$ ,  $N_\ell \approx 1.5 \times 10^7$ , the number of subspaces is significantly reduced and a statistical analysis of their size distribution is not relevant. It is possible that an increase of the number of links per node  $N_\ell/N$  from a typical value of 10 for UK universities to 35 for Twitter affects this distribution. For Cambridge 2011 the network entered in a regime when many links are generated by robots that apparently leads to a change of its statistical properties.

### C. Two-dimensional ranking for university networks

Two-dimensional ranking of network nodes provides a new characterization of directed networks. Here we consider a density distribution of nodes (see Sec. IV.C) in the PageRank-CheiRank plane for examples of two WWW networks of Cambridge 2006 and ENS Paris 2011 shown in Fig. 21 from Ermann, Chepelianskii, and Shepelyansky (2012).

The density distribution for Cambridge 2006 shows that nodes with high PageRank have low CheiRank that corresponds to zero density at low  $K, K^*$  values. At large  $K, K^*$  values there is a maximum line of density which is located not very far from the diagonal  $K \approx K^*$ . The presence of correlations between  $P(K_i)$  and  $P^*(K_i^*)$  leads to a probability distribution with one main maximum along a diagonal at

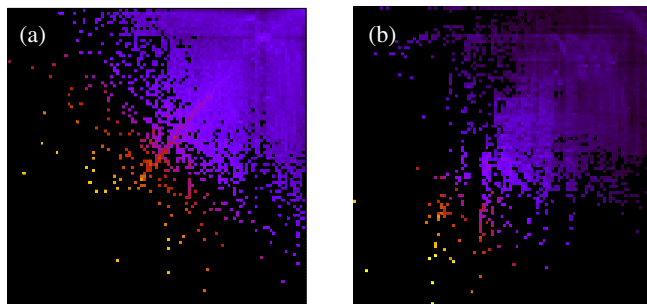


FIG. 21 (color online). Density distribution  $W(K, K^*) = dN_i/dKdK^*$  for networks of universities in the plane of PageRank  $K$  and CheiRank  $K^*$  indices on a log scale ( $\log_N K, \log_N K^*$ ). The density is shown for a  $100 \times 100$  equidistant grid in  $\log_N K, \log_N K^* \in [0, 1]$ , the density is averaged over all nodes inside each cell of the grid, and the normalization condition is  $\sum_{K, K^*} W(K, K^*) = 1$ . Color varies from black for zero to gray (yellow) for maximum density value  $W_M$  with a saturation value of  $W_s^{1/4} = 0.5W_M^{1/4}$  so that the same color is fixed for  $0.5W_M^{1/4} \leq W^{1/4} \leq W_M^{1/4}$  to show in a better way low densities. Networks of the University of Cambridge 2006 with (a)  $N = 212710$  and ENS Paris 2011 for crawling level 7 with (b)  $N = 1820015$ . From Ermann, Chepelianskii, and Shepelyansky, 2012.

In  $K + \ln K^* = \text{const}$ . This is similar to the properties of the density distribution for the Wikipedia network shown in Fig. 7(a).

The 2DRanking might give new possibilities for information retrieval from large databases which are rapidly growing with time. For example, the size of the Cambridge network increased by a factor of 4 from 2006 to 2011. At present, Web robots start automatically to generate new Web pages. These features can be responsible for the appearance of gaps in the density distribution in the  $(K, K^*)$  plane at large  $K, K^* \sim N$  values visible for large-scale university networks such as ENS Paris in 2011 (see Fig. 21). Such an automatic generation of links can change the scale-free properties of networks. Indeed, for ENS Paris a large step in the PageRank distribution appears (Ermann, Chepelianskii, and Shepelyansky, 2012) possibly indicating a delocalization transition tendency of the PageRank that can destroy the efficiency of information retrieval from the WWW.

## IX. WIKIPEDIA NETWORKS

The free online encyclopedia Wikipedia is a large repository of human knowledge. Its size is growing, permanently accumulating a large amount of information and becoming a modern version of *The Library of Babel*, described by Borges (1962). The hyperlink citations between Wikipedia articles provides an important example of directed networks evolving in time for many different languages. In particular, the English edition of August 2009 has been studied in detail (Zhirov, Zhirov, and Shepelyansky, 2010; Ermann, Chepelianskii, and Shepelyansky, 2012; Ermann, Frahm, and Shepelyansky, 2013). The effects of time evolution (Eom *et al.*, 2013) and entanglement of cultures in multilingual Wikipedia editions

have been investigated by Aragón *et al.* (2012), Eom and Shepelyansky (2013), and Eom *et al.* (2015).

### A. Two-dimensional ranking of Wikipedia articles

The statistical distribution of links in Wikipedia networks has been found to follow a power law with the exponents  $\mu_{\text{in}}, \mu_{\text{out}}$  (Capocci *et al.*, 2006; Zlatic *et al.*, 2006; Muchnik *et al.*, 2007; Zhirov, Zhirov, and Shepelyansky, 2010). The probabilities of PageRank and CheiRank are shown in Fig. 5. They are satisfactorily described by a power law decay with exponents  $\beta_{PR, CR} = 1/(\mu_{\text{in}, \text{out}} - 1)$  (Zhirov, Zhirov, and Shepelyansky, 2010).

The density distribution of articles over the PageRank-CheiRank plane ( $\log_N K, \log_N K^*$ ) is shown in Fig. 7(a) for English Wikipedia August 2009. We stress that the density is very different from those generated by the product of independent probabilities of  $P$  and  $P^*$  given in Fig. 5. In the latter case we obtain a density homogeneous along lines  $\ln K^* = -\ln K + \text{const}$  being rather similar to the distribution for the Linux network also shown in Fig. 7. This result is in good agreement with the fact that the correlator  $\kappa$  between PageRank and CheiRank vectors is rather large for Wikipedia  $\kappa = 4.08$  while it is close to zero for the Linux network  $\kappa \approx -0.05$ .

The difference between PageRank and CheiRank is clearly seen from the names of the articles with the highest ranks [ranks of all articles are given in Zhirov, Zhirov, and Shepelyansky (2010)]. At the top of PageRank we have (1) the United States, (2) the United Kingdom, and (3) France, while for CheiRank we find (1) Portal: Contents/Outline of Knowledge/Geography and Places, (2) a list of state leaders by year, and (3) Portal: Contents/Index/Geography and Places. Clearly PageRank selects first articles on a broadly known subject with a large number of ingoing links while CheiRank selects first highly communicative articles with many outgoing links. The 2DRank combines these two characteristics of information flow on a directed network. At the top of 2DRank  $K_2$  we find (1) India, (2) Singapore, and (3) Pakistan. Thus, these articles are most known and popular and most communicative at the same time.

The top 100 articles in  $K, K_2, K^*$  are determined for several categories including countries, universities, people, and physicists. It is shown in Zhirov, Zhirov, and Shepelyansky (2010) that PageRank recovers about 80% of the top 100 countries from the SJR database (SJR, 2007), about 75% of the top 100 universities of Shanghai University ranking,<sup>1</sup> and, among physicists, about 50% of the top 100 Nobel winners in physics. This overlap is lower for 2DRank and even lower for CheiRank. However, as we see in more detail, 2DRank and CheiRank highlight other properties being complementary to PageRank.

We give an example of the top three physicists among those of 754 registered in Wikipedia in 2010: (1) Aristotle, (2) Albert Einstein, and (3) Isaac Newton from PageRank; (1) Albert Einstein, (2) Nikola Tesla, and (3) Benjamin

<sup>1</sup>Shanghai ranking, 2010b, "Academic ranking of world universities," <http://www.shanghairanking.com/>.

Franklin from 2DRank; and (1) Hubert Reeves, (2) Shen Kuo, and (3) Stephen Hawking from CheiRank. It is clear that PageRank gives the most known, 2DRank gives the most known and active in other areas, and CheiRank gives those who are known and contribute to the popularization of science. Indeed, e.g., Hubert Reeves and Stephen Hawking are very well known for their popularization of physics that increases their communicative power and places them at the top of CheiRank. Shen Kuo obtained recognized results in an enormous variety of fields of science that leads to the second top position in CheiRank even if his activity was about 1000 years ago.

According to Wikipedia ranking the top universities are (1) Harvard University, (2) the University of Oxford, and (3) the University of Cambridge in PageRank; and (1) Columbia University, (2) the University of Florida, and (3) Florida State University in 2DRank and CheiRank. CheiRank and 2DRank highlight connectivity degrees of universities that leads to the appearance of a significant number of arts, religious, and military specialized colleges (12% and 13%, respectively, for CheiRank and 2DRank), while PageRank has only 1% of them. CheiRank and 2DRank introduce also a larger number of relatively small universities who are keeping links to their alumni in a significantly better way that gives an increase of their ranks. It is established (Eom *et al.*, 2013) that top 10 PageRank universities from English Wikipedia in years 2003, 2005, 2007, 2009, and 2011 recover correspondingly 9, 9, 8, 7, and 7 from the top 10 of the Shanghai ranking; see footnote 1.

The time evolution of the probability distributions of PageRank, CheiRank, and two-dimensional ranking is analyzed by Eom *et al.* (2013) showing that they become stabilized for the period 2007–2011.

On the basis of these results we conclude that the above algorithms provide correct and important ranking of a large volume of information and knowledge accumulated at Wikipedia. It is interesting that even Dow-Jones companies are ranked via Wikipedia networks in a good manner (Zhirov, Zhirov, and Shepelyansky, 2010). We discuss the ranking of top people of Wikipedia later.

## B. Spectral properties of the Wikipedia network

The complex spectrum of eigenvalues of  $G$  for the English Wikipedia network of August 2009 is shown in Fig. 22. As for university networks, the spectrum also has some invariant subspaces resulting in degeneracies of the leading eigenvalue  $\lambda = 1$  of  $S$  (or  $S^*$ ). However, due to the stronger connectivity of the Wikipedia network these subspaces are significantly smaller compared to university networks (Eom *et al.*, 2013; Ermann, Frahm, and Shepelyansky, 2013). For example, of the August 2009 edition in Fig. 22 there are 255 invariant subspaces (of the matrix  $S$ ) covering 515 nodes with 255 unit eigenvalues  $\lambda_j = 1$  and 381 eigenvalues on the complex unit circle with  $|\lambda_j| = 1$ . For the matrix  $S^*$  of Wikipedia there are 5355 invariant subspaces with 21 198 nodes, 5365 unit eigenvalues, and 8968 eigenvalues on the unit circle (Ermann, Frahm, and Shepelyansky, 2013). The complex spectra of all subspace eigenvalues and the first  $n_A = 6000$  core space eigenvalues of  $S$  and  $S^*$  are shown in Fig. 22. As in the university cases, in the spectrum we can identify cross and

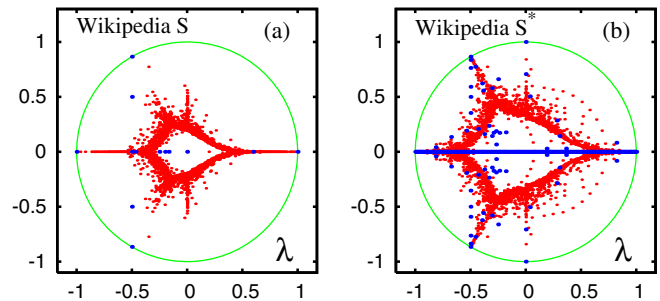


FIG. 22 (color online). Complex eigenvalue spectra  $\lambda$  of (a)  $S$  and (b)  $S^*$  for the English Wikipedia of August 2009 with  $N = 3\,282\,257$  articles and  $N_\ell = 71\,012\,307$  links. The gray (red) dots are the core space eigenvalues, the black (blue) dots are the subspace eigenvalues, and the solid gray (green) curves show the unit circles. The core space eigenvalues are computed by the projected Arnoldi method with Arnoldi dimension  $n_A = 6000$ . From Eom *et al.*, 2013.

triple-star structures similar to those of orthostochastic matrices shown in Fig. 18. However, for Wikipedia (especially for  $S$ ) the largest complex eigenvalues outside the real axis are much farther away from the unit circle. For  $S$  of Wikipedia the two largest core space eigenvalues are  $\lambda_1^{(\text{core})} = 0.999\,987$  and  $\lambda_2^{(\text{core})} = 0.977\,237$  indicating that the core space gap  $|1 - \lambda_1^{(\text{core})}| \sim 10^{-5}$  is much smaller than the secondary gap  $|\lambda_1^{(\text{core})} - \lambda_2^{(\text{core})}| \sim 10^{-2}$ . As a consequence the PageRank of Wikipedia (at  $\alpha = 0.85$ ) is strongly influenced by the leading core space eigenvector and actually both vectors select the same five top nodes.

The time evolution of the spectra of  $G$  and  $G^*$  for the English Wikipedia was studied by Eom *et al.* (2013). It is shown that the spectral structure remains stable for years 2007–2011.

## C. Communities and eigenstates of the Google matrix

The properties of the eigenstates of the Google matrix of Wikipedia August 2009 are analyzed by Ermann, Frahm, and Shepelyansky (2013). The global idea is that the eigenstates with large values of  $|\lambda|$  select certain specific communities. If  $|\lambda|$  is close to unity then a relaxation of probability from such nodes is rather slow and we can expect that such eigenstates highlight some new interesting information even if these nodes are located on a tail of PageRank. The important advantage of the Wikipedia network is that its nodes are Wikipedia articles with a relatively clear meaning allowing us to understand the origins of appearance of certain nodes in one community.

The localization properties of eigenvectors  $\psi_i$  of the Google matrix can be analyzed with the help of IPR  $\xi$  (see Sec. III.E). Another possibility is to fit a decay of an eigenstate amplitude by a power law  $|\psi_i(K_i)| \sim K_i^b$ , where  $K_i$  is the index ordering  $|\psi_i(j)|$  by a monotonically decreasing amplitude [similar to  $P(K)$  for PageRank]. The exponents  $b$  on the tails of  $|\psi_i(j)|$  are found to be typically in the range  $-2 < b < -1$  (Ermann, Frahm, and Shepelyansky, 2013). At the same time the eigenvectors with large complex eigenvalues or real

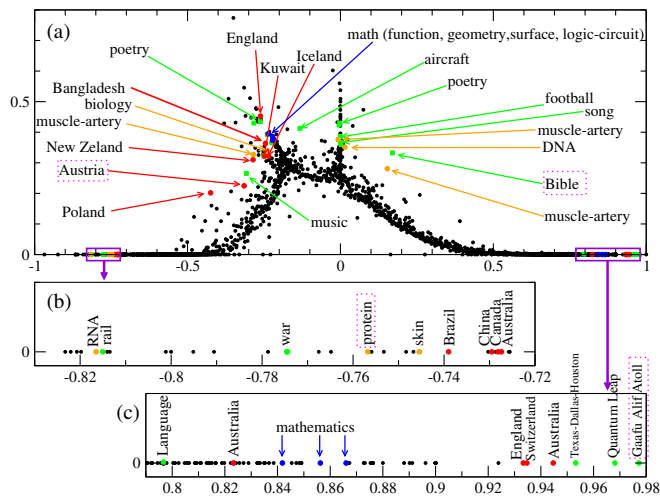


FIG. 23 (color online). Complex eigenvalue spectrum of the matrices  $S$  for the English Wikipedia August 2009. Highlighted eigenvalues represent different communities of Wikipedia and are labeled by the most repeated and important words following word counting of the first 1000 nodes. (a) A complex plane for positive imaginary part of eigenvalues, while (b) and (c) zoom in on the negative and positive real parts. From Ermann, Frahm, and Shepelyansky, 2013.

eigenvalues close to  $\pm 1$  are quite well localized on  $\xi_i \approx 10^2 - 10^3$  nodes that is much smaller than the whole network size  $N \approx 3 \times 10^6$ .

To understand the meaning of other eigenstates in the core space we order selected eigenstates by their decreasing value  $|\psi_i(j)|$  and apply word frequency analysis for the first 1000 articles with  $K_i \leq 1000$ . The most frequent word of a given eigenvector is used to label the eigenvector name. These labels with corresponding eigenvalues are shown in Fig. 23. There are four main categories for the selected eigenvectors belonging to countries (gray/red), biology and medicine (very light gray/orange), mathematics (black/blue), and others (light gray/green). The category of others contains rather diverse articles about poetry, Bible, football, music, American TV series (e.g., Quantum Leap), or small geographical places (e.g., Gaafu Alif Atoll). These eigenstates select certain specific communities which are relatively weakly coupled with the main bulk part of Wikipedia that generates a relatively large modulus of  $|\lambda_i|$ .

For example, for the article Gaafu Alif Atoll the eigenvector is mainly localized on names of small atolls forming Gaafu Alif Atoll. This case represents a well-localized community of articles mainly linked between themselves that gives a slow relaxation rate of this eigenmode with  $\lambda = 0.9772$  being rather close to unity. Another eigenvector has a complex eigenvalue with  $|\lambda| = 0.3733$  and the top article Portal: Bible. Another two articles are Portal: Bible/featured chapter/archives, Portal: Bible/Featured article. These top three articles have very close values of  $|\psi_i(j)|$  that seem to be the reason why we have  $\varphi = \arg(\lambda_i) = 0.3496\pi$  being very close to  $\pi/3$ . Examples of other eigenvectors are discussed by Ermann, Frahm, and Shepelyansky (2013) in detail.

The analysis performed by Ermann, Frahm, and Shepelyansky (2013) for Wikipedia August 2009 shows that

the eigenvectors of the Google matrix of Wikipedia clearly identify certain communities which are relatively weakly connected with the Wikipedia core when the modulus of corresponding eigenvalues is close to unity. For moderate values of  $|\lambda|$  we still have well-defined communities which however have stronger links with some popular articles (e.g., countries) that lead to a more rapid decay of such eigenmodes. Thus the eigenvectors highlight interesting features of communities and network structure. However, *a priori*, it is not evident what is a correspondence between the numerically obtained eigenvectors and the specific community features in which someone has a specific interest. In fact, practically each eigenvector with a moderate value of  $|\lambda| \sim 0.5$  selects a certain community and there are many of them. So it remains difficult to target and select from eigenvalues  $\lambda$  a specific community one is interested.

The spectra and eigenstates of other networks like the WWW of Cambridge 2011, Le Monde, BBC, and PCN of Python are discussed by Ermann, Frahm, and Shepelyansky (2013). It is found that IPR values of eigenstates with large  $|\lambda|$  are well localized with  $\xi \ll N$ . The spectra of each network have significant differences from one another.

#### D. Top people of Wikipedia

There is always significant public interest to know who are the most significant historical figures, or persons, of humanity. The Hart list of the top 100 people who, according to him, most influenced human history is available at Hart (1992). Hart “ranked these 100 persons in order of importance: that is, according to the total amount of influence that each of them had on human history and on the everyday lives of other human beings.” Of course, a human ranking can always be objected arguing that an investigator has his or her own preferences. Also investigators from different cultures can have different viewpoints on the same historical figure. Thus it is important to perform a ranking of historical figures on purely mathematical and statistical grounds which exclude any cultural and personal preferences of investigators.

A detailed two-dimensional ranking of persons of the English Wikipedia August 2009 was done by Zhirov, Zhirov, and Shepelyansky (2010). Earlier studies had been done in a nonsystematic way without any comparison with established top 100 lists (Zhirov, Zhirov, and Shepelyansky, 2010, 2015). Also at those times Wikipedia had not yet entered in its stabilized phase of development.

The top people of Wikipedia August 2009 are found to be (1) Napoleon I of France, (2) George W. Bush, and (3) Elizabeth II of the United Kingdom for PageRank; (1) Michael Jackson, (2) Frank Lloyd Wright, and (3) David Bowie for 2DRank; and (1) Kasey S. Pipes, (2) Roger Calmel, and (3) Yury G. Chernavsky for CheiRank (Zhirov, Zhirov, and Shepelyansky, 2010). For the PageRank list of 100 the overlap with the Hart list is at 35% (PageRank), 10% (2DRank), and almost zero for CheiRank. This is attributed to a very broad distribution of historical figures on a 2D plane, as shown in Fig. 7, and a large variety of human activities. These activities are classified by five main categories: politics, religion, arts, science, and sport. For the top 100 PageRank persons we have the following

distribution over these categories: 58, 10, 17, 15, and 0, respectively. Clearly PageRank overestimates the significance of politicians whose list is dominated by USA presidents not always well known to a broad public. For 2DRank we find, respectively, 24, 5, 62, 7, and 2. Thus this rank highlights artistic sides of human activity. For CheiRank we have 15, 1, 52, 16, and 16 so that the dominant contribution comes from arts, science, and sport. The interesting property of this rank is that it selects many composers, singers, writers, and actors. As an interesting feature of CheiRank we note that among scientists it selects those who are not so well known to a broad public but who discovered new objects, e.g., George Lyell who discovered many Australian butterflies or Nikolai Chernykh who discovered many asteroids. CheiRank also selects persons active in several categories of human activity.

For the English Wikipedia August 2009 the distribution of the top 100 PageRank, CheiRank, and Hart's persons on PageRank-CheiRank plane is shown in Fig. 7(a).

The distribution of Hart's top 100 persons on the  $(K, K^*)$  plane for the English Wikipedia in years 2003, 2005, 2007, August 2009, December 2009, and 2011 is found to be stable for the period 2007–2011 even if certain persons change their ranks (Eom *et al.*, 2013). The distribution of the top 100 persons of the Wikipedia August 2009 remains stable and compact for PageRank and 2DRank for the period 2007–2011 while for CheiRank the fluctuations of positions are large. This is due to the fact that outgoing links are easily modified and fluctuating.

The time evolution of distribution of top persons over fields of human activity has been established by Eom *et al.* (2013). PageRank persons are dominated by politicians whose percentage increases with time, while the percent of arts decreases. For 2DRank the arts are dominant but their percentage decreases with time. We also see the appearance of sports which is absent in PageRank. The mechanism of the qualitative ranking differences between two ranks is related to the fact that 2DRank takes into account via CheiRank a contribution of outgoing links. Because of that singers, actors, and sportsmen improve their CheiRank and 2DRank positions since articles about them contain various music albums, movies, and sport competitions with many outgoing links. Because of that the component of arts gets higher positions in 2DRank in contrast with the dominance of politics in PageRank.

The interest in the ranking of people via the Wikipedia network is growing as shown by the recent study of the English edition (Skiena and Ward, 2014).

### E. Multilingual Wikipedia editions

The English edition allows one to obtain ranking of historical people but as we saw the PageRank list is dominated by USA presidents that probably does not correspond to the global world viewpoint. Hence, it is important to study multilingual Wikipedia editions which now have 287 languages and represent broader cultural views of the world.

One of the first cross-cultural studies was done for the 15 largest language editions constructing a network of links between a set of articles of people biographies for each edition. However, the number of nodes and links in such a

biographical network is significantly smaller compared to the whole network of Wikipedia articles and thus the fluctuations become rather large. For example, from the biographical network of the Russian edition one finds as the top person Napoleon III (and even not Napoleon I) (Aragón *et al.*, 2012), who has a rather low importance for Russia.

Another approach was used by Eom and Shepelyansky (2013) ranking the top 30 persons by PageRank, 2DRank, and CheiRank algorithms for all articles of each of nine editions and attributing each person to her or his native language. The selected editions are English (EN), French (FR), German (DE), Italian (IT), Spanish (ES), Dutch (NL), Russian (RU), Hungarian (HU), and Korean (KO). The aim here is to understand how different cultures evaluate a person. Is an important person in one culture also important in another culture? It is found that local heroes are dominant but also global heroes exist and create an effective network representing entanglement of cultures.

The top article of PageRank is usually USA or the name of a country of a given language (FR, RU, KO). For NL we have at the top beetle, species, and France. The top articles of CheiRank are various listings.

The distributions of articles density and the top 30 persons for each rank algorithm are shown in Fig. 24 for four editions EN, FR, DE, and RU. We see that in global the distributions have a similar shape that can be attributed to the fact that all editions describe the same world. However, local features of distributions are different corresponding to different cultural views on the same world [the other five editions are shown in Fig. 2 in Eom and Shepelyansky (2013)]. The top 30 persons for each edition are selected manually that represents a weak point of this study.

From the lists of top persons, the “fields” of activity are identified for each top 30 rank persons in which he or she is active. The six activity fields are politics, art, science, religion, sports, etc. (here etc. includes all other activities). As shown in Fig. 25, for PageRank, politics is dominant and science is secondarily dominant. The only exception is Dutch where science is the almost dominant activity field (politics has the same number of points). In the case of 2DRank in Fig. 25, art becomes dominant and politics is secondarily dominant. In the case of CheiRank, art and sports are dominant fields [see Fig. 3 in Eom and Shepelyansky (2013)]. Thus, for example, in the CheiRank top 30 list we find astronomers who discovered a lot of asteroids, e.g., Karl Wilhelm Reinmuth (the fourth position in RU and the seventh in DE), who was a prolific discoverer of about 400 of them. As a result, his article contains a long list of asteroids discovered by him and giving him a high CheiRank. The distributions of persons over activity fields are shown in Fig. 25 for nine language editions (marked by the standard two letters used by Wikipedia).

The change of activity priority for different ranks is due to the different balance between incoming and outgoing links there. Usually the politicians are well known to a broad public; hence, the articles about politicians are pointed to by many articles. However, the articles about politicians are not very communicative since they rarely point to other articles. In contrast, articles about persons in other fields like science, art, and sports are more communicative because of listings of

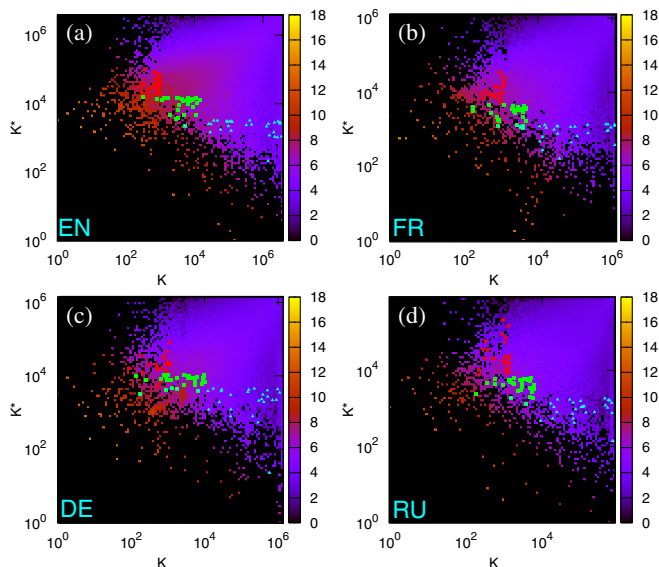


FIG. 24 (color online). Density of the Wikipedia articles in the PageRank-CheiRank plane ( $K, K^*$ ) for four different language Wikipedia editions. The gray (red) points are top PageRank articles of persons, the light gray (green) squares are top 2DRank articles of persons, and the dark gray (cyan) triangles are top CheiRank articles of persons. Wikipedia language editions are (a) English EN, (b) French FR, (c) German DE, and (d) Russian RU. Color bars show a natural logarithm of density, changing from minimal nonzero density (dark) to maximal one (white), and zero density is shown by black. From Eom and Shepelyansky, 2013.

insects, planets, and asteroids they discovered or listings of song albums or sports competitions they gain.

On the basis of this approach one obtains local ranks for each of 30 persons  $1 \leq K_{P,E,A} \leq 30$  for each edition  $E$  and algorithm  $A$ . Then an average ranking score of a person  $P$  is determined as  $\Theta_{P,A} = \sum_E (31 - K_{P,E,A})$  for each algorithm. This method determines the global historical figures. The top global persons are (1) Napoleon, (2) Jesus, and (3) Carl Linnaeus for PageRank; (1) Micheal Jackson, (2) Adolf Hitler, and (3) Julius Caesar for 2DRank. For CheiRank the lists of different editions have rather low overlap and such an averaging is not efficient. The first positions reproduce the top persons from the English edition discussed in Sec. IX.D; however, the next ones are different.

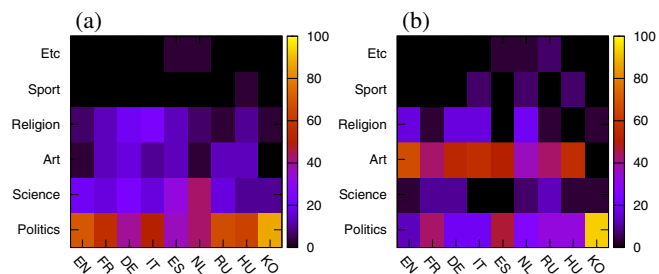


FIG. 25 (color online). Distribution of the top 30 persons over activity fields for (a) PageRank and (b) 2DRank for each of nine Wikipedia editions. The color bars show the values in percent. From Eom and Shepelyansky, 2013.

Since each person is attributed to his or her native language it is also possible for each edition to obtain the top local heroes who have the native language of the edition. For example, we find for PageRank for EN George W. Bush, Barack Obama, and Elizabeth II; for FR Napoleon, Louis XIV of France, and Charles de Gaulle; for DE Adolf Hitler, Martin Luther, and Immanuel Kant; and for RU Peter the Great, Joseph Stalin, and Alexander Pushkin. For 2DRank we have for EN Frank Sinatra, Paul McCartney, and Michael Jackson; for FR Francois Mitterrand, Jacques Chirac, and Honore de Balzac; for DE Adolf Hitler, Otto von Bismarck, and Ludwig van Beethoven; and for RU Dmitri Mendeleev, Peter the Great, and Yaroslav the Wise. These ranking results are rather reasonable for each language. Results for other editions and CheiRank are given in Eom and Shepelyansky (2013).

A weak point of the above study is a manual selection of persons and not a very large number of editions. A significant improvement was reached in a recent study (Eom *et al.*, 2015) where 24 editions were analyzed. These 24 languages cover 59% of the world population, and these 24 editions cover 68% of the total number of Wikipedia articles in all 287 available languages. Also the selection of people from the rank list of each edition is now done in an automatic computerized way. For that a list of approximately  $1.1 \times 10^6$  biographical articles about people with their English names is generated. From this list of persons, with their biographical article title in the English Wikipedia, the corresponding titles in other language editions are determined using the interlanguage links provided by Wikipedia.

Using the corresponding articles, identified by the interlanguage links in different language editions, the top 100 persons are obtained from the rankings of all Wikipedia articles of each edition. A birth place, birth date, and gender of each top 100 ranked person are identified, based on DBpedia or a manual inspection of the corresponding Wikipedia biographical article, when for the considered person no DBpedia data were available. In this way 24 lists of the top 100 persons for each edition are obtained in PageRank with 1045 unique names and in 2DRank with 1616 unique names. Each of the 100 historical figures is attributed to a birth place at the country level, to a birth date in year, to a gender, and to a cultural language group. The birth place is assigned according to the current country borders. The cultural group of historical figures is assigned by the most spoken language of their birth place at the current country level. The considered editions are English EN, Dutch NL, German DE, French FR, Spanish ES, Italian IT, Portuguese PT, Greek EL, Danish DA, Swedish SV, Polish PL, Hungarian HU, Russian RU, Hebrew HE, Turkish TR, Arabic AR, Persian FA, Hindi HI, Malaysian MS, Thai TH, Vietnamese VI, Chinese ZH, Korean KO, and Japanese JA (dated February 2013). The size of network changes from the maximal value  $N = 4\,212\,493$  for EN to the minimal one  $N = 78\,953$  for TH.

All persons are ranked by their average rank score  $\Theta_{P,A} = \sum_E (101 - K_{P,E,A})$  with  $1 \leq K_{P,E,A} \leq 100$  similar to the study of nine editions described previously. For PageRank the top global historical figures are Carl Linnaeus, Jesus, and Aristotle and for 2DRank we obtain Adolf Hitler, Michael

Jackson, and Madonna (entertainer). Thus the averaging over 24 editions modifies the top ranking. The list of top 100 PageRank global persons has an overlap of 43 persons with the Hart list (Hart, 1992). Thus the averaging over 24 editions gives a significant improvement compared to 35 persons overlap for the case of the English edition only (Zhirov, Zhirov, and Shepelyansky, 2010). For comparison we note that the top 100 list of historical figures has also been recently determined by the Pantheon MIT project at <http://pantheon.media.mit.edu> having an overlap of 42 persons with the Hart list. This Pantheon MIT list is established on the basis of the number of editions and the number of clicks on an article of a given person without using rank algorithms discussed here. The overlap between the top 100 PageRank list and the top 100 Pantheon list is 44%. More data are available in Eom *et al.* (2015).

The fact that Carl Linnaeus is the top historical figure of the Wikipedia PageRank list came as a surprise for media and the broad public (Shepelyansky, 2015). This ranking is due to the fact that Carl Linnaeus created a classification of world species including animals, insects, herbs, trees, etc. Thus all articles of these species point to the article Carl Linnaeus in various languages. As a result Carl Linnaeus appears on almost all top positions in all 24 languages. Hence, even if a politician, like Barak Obama, takes the second position in his country language EN (Napoleon is at the first position in EN) he is usually placed at a low ranking in other language editions. As a result Carl Linnaeus takes the first global PageRank position.

The number of appearances of historical persons in 24 lists of the top 100 for each edition can be distributed over present world countries according to the birth place of each person. This geographical distribution is shown in Fig. 26 for PageRank and 2DRank. In PageRank the top countries are DE, USA, and IT and in 2DRank US, DE, and UK. The appearance of many UK and US singers improves the positions of English speaking countries in 2DRank.

The distributions of the top PageRank and 2DRank historical figures over 24 Wikipedia editions for each century are shown in Fig. 27. Each person is attributed to a century according to the birth date covering the range of 35 centuries from BC 15th to AD 20th centuries. For each century the number of persons is normalized to unity to see more clearly the relative contribution of each language for each century.

The Greek edition has more historical figures in the BC fifth century because of Greek philosophers. Also most of the Western-Southern European language editions, including English, Dutch, German, French, Spanish, Italian, Portuguese, and Greek, have more top historical figures because they have Augustine the Hippo and Justinian I in common. The Persian (FA) and the Arabic (AR) Wikipedia have more historical figures compared to other language editions (in particular, European language editions) from the sixth to the 12th century due to Islamic leaders and scholars. The data of Fig. 27 show well-pronounced patterns, corresponding to strong interactions between cultures: from the BC fifth century to the AD 15th century for JA, KO, ZH, and VI; from the AD sixth century to the AD 12th century for FA and AR; and a common birth pattern in EN, EL, PT, IT, ES, DE, and NL (Western European languages) from the BC



FIG. 26 (color online). The number of appearances of historical figures of a given country, obtained from 24 lists of the top 100 persons of (a) PageRank and (b) 2DRank, shown on the world map. Color changes from zero (white) to maximum (black), corresponding to the average number of person appearances per country. From Eom *et al.*, 2015.

fifth century to the AD sixth century. A detailed analysis shows that even in the BC 20th century each edition has a significant fraction of persons of its own language so that even with ongoing globalization there is a significant dominance of local historical figures for certain cultures. More data on the above points and gender distributions are available in Eom *et al.* (2015).

#### F. Networks and entanglement of cultures

We now know how a person of a given language is ranked by editions of other languages. If a top person from a language edition  $A$  appears in another edition  $B$ , we consider this as a “cultural” influence from culture  $A$  to  $B$ . This generates entanglement in a network of cultures. Here we associate a language edition with its corresponding culture considering that a language is the first element of culture, even if a culture is not reduced only to a language. Eom and Shepelyansky (2013) attributed a person to a given language, or culture, according to his or her native language fixed via corresponding Wikipedia article. In Eom *et al.* (2015) the attribution to a culture is done via a birth place of a person, each language considered as a proxy for a cultural group, and a person is assigned to one of these cultural groups based on the most spoken language of his or her birth place at the country level. If a person does not belong to any of the studied editions then he or she is attributed to an additional cultural group world WR.

After such an attribution of all persons the two networks of cultures are constructed based on the top PageRank historical figures and the top 2DRank historical figures, respectively.

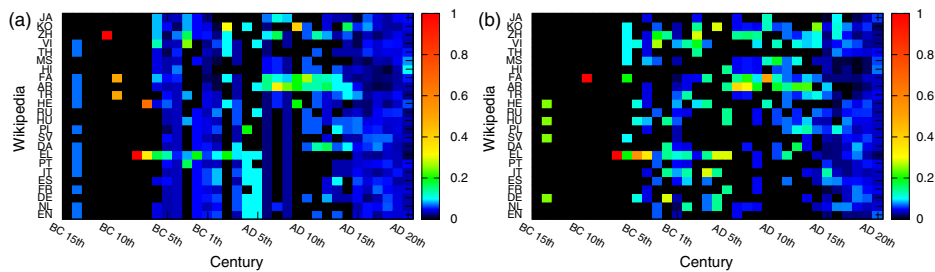


FIG. 27 (color online). Birth date distributions over 35 centuries of the top historical figures from each Wikipedia edition marked by the two letter standard notation of Wikipedia. (a) Column normalized birth date distributions of PageRank historical figures; (b) the same as (a) for 2DRank historical figures. From Eom *et al.*, 2015.

Each culture (i.e., language) is represented as a node of the network, and the weight of a directed link from culture *A* to culture *B* is given by the number of historical figures belonging to culture *B* (e.g., French) appearing in the list of top 100 historical figures for a given culture *A* (e.g., English).

For example, according to Eom *et al.* (2015), there are five French historical figures among the top 100 PageRank historical figures of the English Wikipedia, so we can assign weight 5 to the link from English to French. Thus, Figs. 28(a) and 28(b) represent the constructed networks of cultures defined by appearances of the top PageRank historical figures and top 2DRank historical figures, respectively.

In total we have two networks with 25 nodes which include our 24 editions and an additional node WR for all other world cultures. Persons of a given culture are not taken into account in the rank list of the language edition of this culture. Then following the standard rules (1) the Google matrix of the network of cultures is constructed by the normalization of the sum of all elements in each column to unity. The matrix  $G_{KK'}$ , written in the PageRank indices  $K, K'$ , is shown in Fig. 29 for persons from (a) PageRank and (b) 2DRank lists. The matrix  $G^*$  is constructed in the same way as  $G$  for the network with inverted directions of links.

From the obtained matrices  $G$  and  $G^*$  we determine PageRank and CheiRank vectors and then the PageRank-CheiRank plane ( $K, K^*$ ), shown in Fig. 30, for networks of

cultures from Fig. 28. Here  $K$  indicates the ranking of a given culture ordered by how many of its own top historical figures appear in other Wikipedia editions, and  $K^*$  indicates the ranking of a given culture according to how many of the top historical figures in the considered culture are from other cultures. It is important to note that for 24 editions the world node WR appears on positions  $K = 3$  or  $K = 4$  in Figs. 30(a) and 30(b), signifying that the 24 editions capture the main part of the historical figures born in these cultures. We note that for nine editions in Eom and Shepelyansky (2013) the node WR was at the top position for PageRank so that a significant fraction of historical figures was attributed to other cultures.

From the data of Fig. 30 we obtain at the top positions of  $K$  cultures EN, DE, and IT showing that other cultures strongly point to them. However, we argue that for cultures it is also important to have strong communicative properties and hence it is important to have a 2DRank of cultures at top positions. On the top 2DRank position we have Greek, Turkish, and Arabic (for PageRank persons) in Fig. 30(a) and French, Russian, and Arabic (for 2DRank persons) in Fig. 30(b). This demonstrates the important historical influence of these cultures via both importance (incoming links) and communicative (outgoing links) properties present in a balanced manner.

Thus the described research across Wikipedia language editions suggests a rigorous mathematical way, based on Markov chains and Google matrix, for the recognition of important historical figures and the analysis of interactions of cultures at different historical periods and in different world regions. Such an approach recovers 43% of persons from the

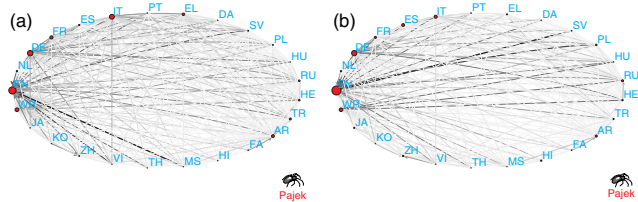


FIG. 28 (color online). Network of cultures, obtained from 24 Wikipedia languages and the remaining world (WR), considering (a) the top 100 PageRank historical figures and (b) the top 100 2DRank historical figures. The link width and darkness are proportional to a number of foreign historical figures quoted in the top 100 of a given culture, the link direction goes from a given culture to cultures of quoted foreign historical figures, and quotations inside cultures are not considered. The size of nodes is proportional to their PageRank. From Eom *et al.*, 2015.

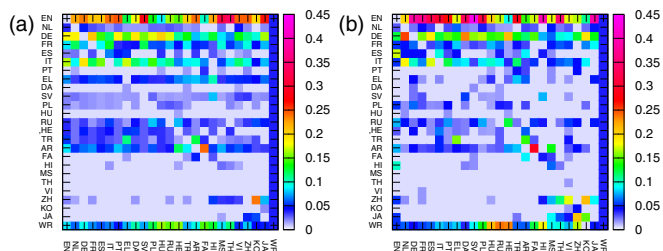


FIG. 29 (color online). A Google matrix of the network of cultures shown in Fig. 28(a) and 28(b), respectively. The matrix elements  $G_{ij}$  are shown by color with the damping factor  $\alpha = 0.85$ . From Eom *et al.*, 2015.



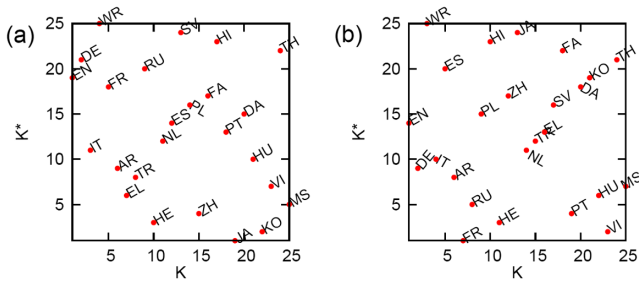


FIG. 30 (color online). PageRank-CheiRank plane of cultures with corresponding indices  $K$  and  $K^*$  obtained from the network of cultures based on (a) the top 100 PageRank historical figures, and (b) the top 100 2DRank historical figures. From Eom *et al.*, 2015.

well-established Hart historical study (Hart, 1992) that demonstrates the reliability of this method. We think that further extension of this approach to a larger number of Wikipedia editions will provide a more detailed and balanced analysis of interactions of world cultures.

## X. GOOGLE MATRIX OF SOCIAL NETWORKS

Social networks like Facebook, LiveJournal, Twitter, and Vkontakte start to play a more and more important role in modern society. The Twitter network is a directed one and here we consider its spectral properties mainly following the analysis reported by Frahm and Shepelyansky (2012a).

### A. Twitter network

Twitter is a rapidly growing online directed social network. For July 2009 a data set of this entire network is available with  $N = 41\,652\,230$  nodes and  $N_\ell = 1\,468\,365\,182$  links [for data sets see Frahm and Shepelyansky (2012a)]. For this case the spectrum and eigenstate properties of the corresponding Google matrix have been analyzed in detail using the Arnoldi method and standard PageRank and CheiRank computations (Frahm and Shepelyansky, 2012a). For the Twitter network the average number of links per node  $\zeta = N_\ell/N \approx 35$  and the general interconnectivity between top PageRank nodes are considerably larger than for other networks such as Wikipedia (Sec. IX) or UK universities (Sec. VIII) as can be seen in Figs. 31 and 32.

The decay of the PageRank probability can be approximately described by an algebraic decay with the exponent  $\beta \approx 0.54$  while for CheiRank we have a larger value  $\beta \approx 0.86$  (Frahm and Shepelyansky, 2012a) that is opposite to the usual situation. The image of top matrix elements of  $G_{KK'}$  with  $1 \leq K, K' \leq 200$  is shown in Fig. 31. The density distribution of nodes on the  $(K, K^*)$  plane is also shown there. It is somewhat similar to those of the Wikipedia case in Fig. 24, but with a larger density concentration along the line  $K \approx K^*$ .

However, the most striking feature of  $G$  matrix elements is a strong interconnectivity between top PageRank nodes. Thus for Twitter the top  $K \leq 1000$  elements fill about 70% of the matrix and about 20% for size  $K \leq 10^4$ . For Wikipedia the filling factor is smaller by a factor of 10–20. In particular, the number  $N_G$  of links between  $K$  top PageRank nodes

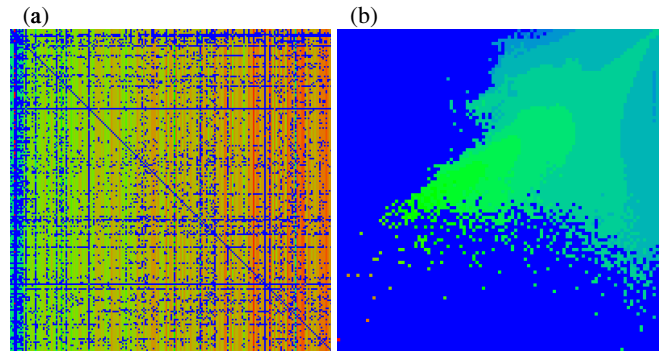


FIG. 31 (color online). (a) Google matrix of Twitter; matrix elements of  $G$  are shown in the basis of PageRank index  $K$  of matrix  $G_{KK'}$ . Here the  $x$  (and  $y$ ) axis show  $K$  (and  $K'$ ) with the range  $1 \leq K, K' \leq 200$ . (b) The density of nodes  $W(K, K^*)$  of Twitter on the PageRank-CheiRank plane  $(K, K^*)$ , averaged over  $100 \times 100$  logarithmically equidistant grids for  $0 \leq \ln K, \ln K^* \leq \ln N$  with the normalization condition  $\sum_{K, K^*} W(K, K^*) = 1$ . The  $x$  axis corresponds to  $\ln K$  and the  $y$  axis to  $\ln K^*$ . In both panels the color varies from black (blue) at the minimal value to gray (red) at the maximal value; here  $\alpha = 0.85$ . From Frahm and Shepelyansky, 2012a.

behaves for  $K \leq 10^3$  as  $N_G \sim K^{1.993}$  while for Wikipedia  $N_G \sim K^{1.469}$ . The exponent for  $N_G$ , being close to 2 for Twitter, indicates that for the top PageRank nodes the Google matrix is macroscopically filled with a fraction 0.6–0.8 of nonvanishing matrix elements (see also Figs. 31 and 32) and the very well-connected top PageRank nodes can be considered as the Twitter elite (Kandiah and Shepelyansky, 2012). For Wikipedia the interconnectivity among top PageRank nodes has an exponent 1.5 being somewhat reduced but still stronger as compared to certain university networks where typical exponents are close to unity (for the range  $10^2 \leq K \leq 10^4$ ). The strong interconnectivity of Twitter is also visible in its global logarithmic density distribution of nodes in the PageRank-CheiRank plane  $(K, K^*)$  [Fig. 31(b)] which shows a maximal density along a certain ridge along a

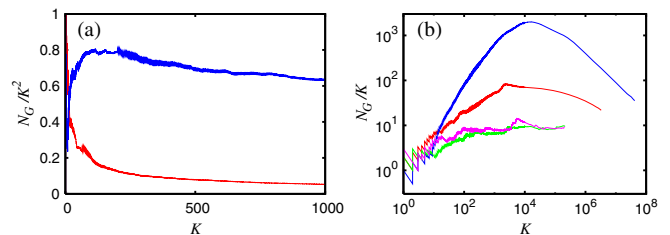


FIG. 32 (color online). (a) Dependence of the area density  $g_K = N_G/K^2$  of nonzero elements of the adjacency matrix among top PageRank nodes on the PageRank index  $K$  for Twitter [black (blue curve) and Wikipedia [gray (red) curve] networks; data are shown in linear scale. (b) Linear density  $N_G/K$  of the same matrix elements shown for the whole range of  $K$  in log-log scale for Twitter (blue curve), Wikipedia (red curve), Oxford University 2006 (magenta curve), and Cambridge University 2006 (green curve) (curves from top to bottom at  $K = 100$ ). From Frahm and Shepelyansky, 2012a.

line  $\ln K^* = \ln K + \text{const}$  with a significant large number of nodes at small values  $K$ ,  $K^* < 1000$ .

The decay exponent of the PageRank is for Twitter  $\beta = 0.540$  (for  $1 \leq K \leq 10^6$ ), which indicates a precursor of a delocalization transition as compared to Wikipedia ( $\beta = 0.767$ ) or the WWW ( $\beta \approx 0.9$ ), caused by the strong interconnectivity (Frahm and Shepelyansky, 2012a). The Twitter network is also characterized by a large value of PageRank-CheiRank correlator  $\kappa = 112.6$  that is by a factor of 30–60 larger than this value for Wikipedia and university networks. Such a larger value of  $\kappa$  results from certain individual large values  $\kappa_i = NP(K(i))P^*(K^*(i)) \sim 1$ . It is argued that this is related to a strong interconnectivity between top  $K$  PageRank users of the Twitter network (Frahm and Shepelyansky, 2012a).

The spectra of matrices  $S$  and  $S^*$  are obtained with the help of the Arnoldi method for a relatively modest Arnoldi dimension due to a very large matrix size. The largest  $n_A$  modulus eigenvalues  $|\lambda|$  are shown in Fig. 33. The invariant subspaces (see Sec. III.C) for the Twitter network cover about  $N_s = 4 \times 10^4$  ( $1.8 \times 10^5$ ) nodes for  $S$  ( $S^*$ ) leading to

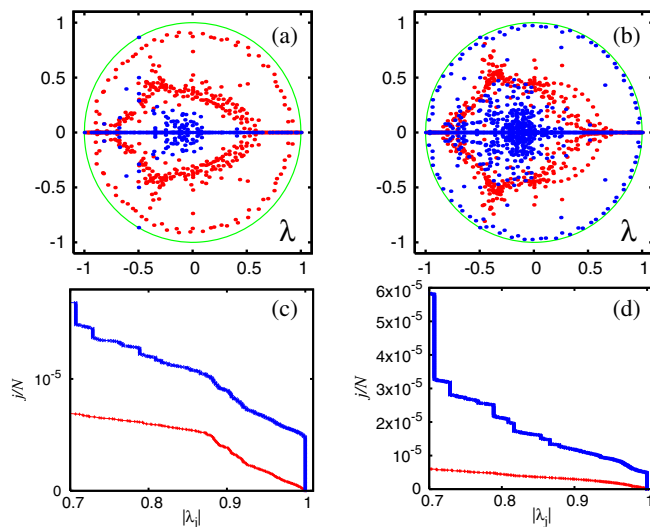


FIG. 33 (color online). Spectrum of the Twitter matrix (a), (c)  $S$ , and (b), (d)  $S^*$ . (a), (b) Subspace eigenvalues [black (blue) dots] and core space eigenvalues [gray (red) dots] in the  $\lambda$  plane [the gray (green) curve shows the unit circle]; there are 17 504 (66 316) invariant subspaces, with maximal dimension 44 (2959) and the sum of all subspace dimensions is  $N_s = 40 307$  (180 414). The core space eigenvalues are obtained from the Arnoldi method applied to the core space sub-block  $S_{cc}$  of  $S$  with Arnoldi dimension  $n_A = 640$ . (c), (d) The fraction  $j/N$  of eigenvalues with  $|\lambda| > |\lambda_j|$  for the core space eigenvalues [gray (red) bottom curve] and all eigenvalues [black (blue) top curve] from raw data [(a), (b), respectively]. The number of eigenvalues with  $|\lambda_j| = 1$  is 34 135 (129 185) of which 17 505 (66 357) are at  $\lambda_j = 1$ ; this number is (slightly) larger than the number of invariant subspaces which have each at least one unit eigenvalue. Note that in (c) and (d) the number of eigenvalues with  $|\lambda_j| = 1$  is artificially reduced to 200 in order to have a better scale on the vertical axis. The correct numbers of those eigenvalues correspond to (c)  $j/N = 8.195 \times 10^{-4}$  and (d)  $3.102 \times 10^{-3}$  which are strongly outside the vertical panel scale. From Frahm and Shepelyansky, 2012a.

$1.7 \times 10^4$  ( $6.6 \times 10^4$ ) eigenvalues with  $\lambda_j = 1$  or even  $3.4 \times 10^4$  ( $1.3 \times 10^5$ ) eigenvalues with  $|\lambda_j| = 1$ . However, for Twitter the fraction of subspace nodes  $g_1 = N_s/N \approx 10^{-3}$  is smaller than the fraction  $g_1 \approx 0.2$  for the university networks of Cambridge or Oxford (with  $N \approx 2 \times 10^5$ ) since the size of the whole Twitter network is significantly larger. The complex spectra of  $S$  and  $S^*$  also show the cross and triple-star structures, as in the cases of Cambridge and Oxford 2006 (see Fig. 17), even though for the Twitter network they are significantly less pronounced.

## B. Poisson statistics of PageRank probabilities

From a physical viewpoint one can conjecture that the PageRank probabilities are described by a steady-state quantum Gibbs distribution over certain quantum levels with energies  $E_i$  by the identification  $P(i) = \exp(-E_i/T)/Z$  with  $Z = \sum_i \exp(-E_i/T)$  (Frahm and Shepelyansky, 2014). In some sense this conjecture assumes that the operator matrix  $G$  can be represented as a sum of two operators  $G_H$  and  $G_{NH}$ , where  $G_H$  describes a Hermitian system while  $G_{NH}$  represents a non-Hermitian operator which creates a system thermalization at a certain effective temperature  $T$  with the quantum Gibbs distribution over energy levels  $E_i$  of the operator  $G_H$ .

The identification of PageRank with an energy spectrum allows one to study the corresponding level statistics which represents a well-known concept in the framework of random matrix theory (Guhr, Mueller-Groeling, and Weidenmueller, 1998; Mehta, 2004). The most direct characteristic is the probability distribution  $p(s)$  of unfolded level spacings  $s$ . Here  $s = (E_{i+1} - E_i)/\Delta E$  is a spacing between nearest levels measured in the units of average local energy spacing  $\Delta E$ . The unfolding procedure (Guhr, Mueller-Groeling, and Weidenmueller, 1998; Mehta, 2004) requires the smoothed dependence of  $E_i$  on the index  $K$  which is obtained from a polynomial fit of  $E_i \sim \ln(P_i)$  with  $\ln(K)$  as an argument (Frahm and Shepelyansky, 2014).

The statistical properties of fluctuations of levels have been extensively studied in the fields of RMT (Mehta, 2004), quantum chaos (Haake, 2010), and disordered solid state systems (Evers and Mirlin, 2008). It is known that integrable quantum systems have  $p(s)$  well described by the Poisson distribution  $p_{\text{Pois}}(s) = \exp(-s)$ . In contrast the quantum systems, which are chaotic in the classical limit (e.g., the Sinai billiard), have  $p(s)$  given by the RMT being close to the Wigner surmise  $p_{\text{Wig}}(s) = (\pi/2)s \exp[-(\pi/4)s^2]$  (Bohigas, Giannoni, and Schmit, 1984). Also the Anderson localized phase is characterized by  $p_{\text{Pois}}(s)$  while in the delocalized regime one has  $p_{\text{Wig}}(s)$  (Evers and Mirlin, 2008).

The results for the Twitter PageRank level statistics (Frahm and Shepelyansky, 2014) are shown in Fig. 34. We find that  $p(s)$  is well described by the Poisson distribution. Furthermore, the evolution of energy levels  $E_i$  with the variation of the damping factor  $\alpha$  shows many level crossings which are typical for Poisson statistics. Note that here each level has its own index so that it is rather easy to see if there is a real or avoided level crossing.

The validity of the Poisson statistics for PageRank probabilities is confirmed also for the networks of Wikipedia

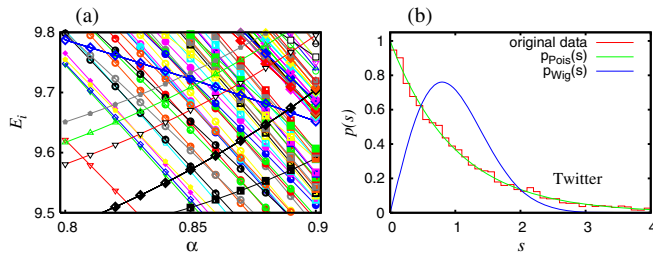


FIG. 34 (color online). (a) The dependence of certain top PageRank levels  $E_i = -\ln(P_i)$  on the damping factor  $\alpha$  for the Twitter network. Data points on curves with one color correspond to the same node  $i$ ; about 150 levels are shown close to the minimal energy  $E \approx 7.5$ . (b) The histogram of unfolded level-spacing statistics for Twitter at  $10 < K \leq 10^4$ . The Poisson distribution  $p_{\text{Pois}}(s) = \exp(-s)$  and the Wigner surmise  $p_{\text{Wig}}(s) = (\pi/2)s \exp[-(\pi/4)s^2]$  are also shown for comparison. From Frahm and Shepelyansky, 2014.

editions in English, French, and German from Fig. 24 (Frahm and Shepelyansky, 2014). We argue that due to the absence of level repulsion the PageRank order of nearby nodes can be easily interchanged. The Poisson law obtained implies that the nearby PageRank probabilities fluctuate as random independent variables.

## XI. GOOGLE MATRIX ANALYSIS OF WORLD TRADE

During the last decades the trade between countries has been developed in an extraordinary way. Usually countries are ranked in the WTN taking into account their exports and imports measured in USD (US dollars) (Central Intelligence Agency, 2009). However, the use of these quantities, which are local in the sense that countries know their total imports and exports, could hide the information of the centrality role that a country plays in this complex network. In this section we present the two-dimensional Google matrix analysis of the WTN introduced in Ermann and Shepelyansky (2011). Some previous studies of global network characteristics were considered by Garlaschelli and Loffredo (2005) and Serrano, Boguna, and Vespignani (2007), degree centrality measures were analyzed by De Benedictis and Tajoli (2011), and a time evolution of network global characteristics was studied by He and Deem (2010). Topological and clustering properties of a multiplex network of various commodities were discussed by Barigozzi, Fagiolo, and Garlaschelli (2010), and an ecological ranking based on the nestedness of countries and products was presented by Ermann and Shepelyansky (2013).

The money exchange between countries defines a directed network. Therefore a Google matrix analysis can be introduced in a natural way. PageRank and CheiRank algorithms can be easily applied to this network with a straightforward correspondence with imports and exports. Two-dimensional ranking, introduced in Sec. IV, gives an illustrative representation of global importance of countries in the WTN. The important element of Google ranking of WTN is its democratic treatment of all world countries, independently of their richness, that follows the main principle of the United Nations (UN).

### A. Democratic ranking of countries

The WTN is a directed network that can be constructed considering countries as nodes and money exchange as links. We follow the definition of the WTN of Ermann and Shepelyansky (2011), where trade information comes from UN COMTRADE (2011). These data include all trades between countries for different products [using the standard international trade classification of goods (SITC1)] from 1962 to 2009.

All useful information of the WTN is expressed via the money matrix  $M$ , whose definition, in terms of its matrix elements  $M_{ij}$ , is defined as the money transfer (in USD) from country  $j$  to country  $i$  in a given year. This definition can be applied to a given specific product or to all commodities, which represent the sum over all products.

In contrast to the binary adjacency matrix  $A_{ij}$  of WWW (as the ones analyzed in Secs. VIII and X, for example)  $M$  has weighted elements. This corresponds to a case when there are in principle multiple numbers of links from  $j$  to  $i$  and this number is proportional to USD amount transfer. Such a situation appears in Sec. VI for Ulam networks and Sec. VII for Linux PCN with the main difference that for the WTN case there is a large variation of mass matrix elements  $M_{ij}$ , related to the fact that there is a strong variation of richness of various countries.

The Google matrices  $G$  and  $G^*$  are constructed according to the usual rules and relation (1) with  $M_{ij}$  and its transposed:  $S_{ij} = M_{ij}/m_j$  and  $S_{ij}^* = M_{ji}/m_j^*$ , where  $S_{ij} = 1/N$  and  $S_{ij}^* = 1/N$ , if for a given  $j$  all elements  $M_{ij} = 0$  and  $M_{ji} = 0$ , respectively. Here  $m_j = \sum_i M_{ij}$  and  $m_j^* = \sum_i M_{ji}$  are the total export and import masses for country  $j$ . Thus the sum in each column of  $G$  or  $G^*$  is equal to unity. In this way the Google matrices  $G$  and  $G^*$  of the WTN allow one to treat all countries on equal grounds independently of the fact if a given country is rich or poor. This kind of analysis treats in a democratic way all world countries in consonance with the standards of the UN.

The probability distributions of ordered PageRank  $P(K)$  and CheiRank  $P^*(K^*)$  depend on their indices in a rather similar way with a power law decay given by  $\beta$ . For the fit of the top 100 countries and all commodities the average exponent value is close to  $\beta = 1$  corresponding to the Zipf law (Zipf, 1949).

The distribution of countries on the PageRank-CheiRank plane for trade in all commodities in year 2008 is shown in Figs. 35(a) and 35(b) at  $\alpha = 0.5$ . Even if the Google matrix approach is based on a democratic ranking of international trade, being independent of the total amount of export and import and the gross domestic product (GDP) for a given country, the top ranks  $K$  and  $K^*$  belong to the group of industrially developed countries. This means that these countries have efficient trade networks with optimally distributed trade flows. Another striking feature of global distribution is that it is concentrated along the main diagonal  $K = K^*$ . This feature is not present in other networks studied before. The origin of this density concentration is related to a simple economy reason: for each country the total import is approximately equal to export since each country should keep on

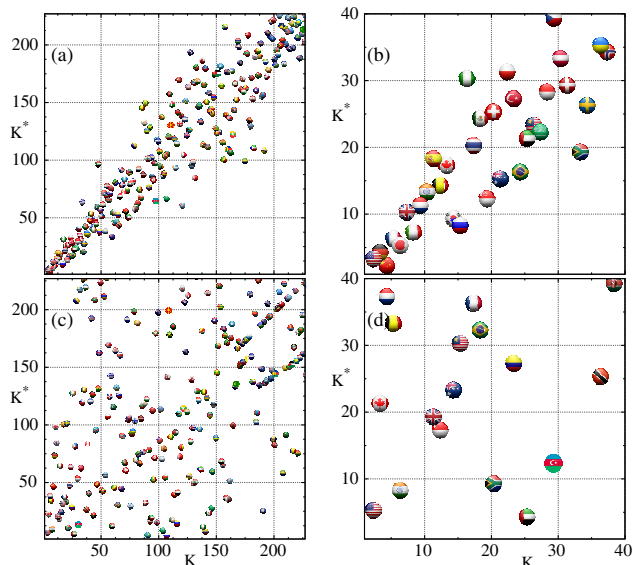


FIG. 35 (color online). Country positions in the PageRank-Cheirank plane  $(K, K^*)$  for world trade in various commodities in 2008. Each country is shown by a circle with its own flag [for better visibility the circle center is slightly displaced from its integer position  $(K, K^*)$  along the direction angle  $\pi/4$ ]. The panels show the ranking for trade in the following commodities: (a), (b) all commodities, and (c), (d) crude petroleum. (a), (c) A global scale with all 227 countries, while (b) and (d) give a zoom in the region of the  $40 \times 40$  top ranks. From Ermann and Shepelyansky, 2011.

average an economic balance. This balance does not imply a symmetric money matrix, used in a gravity model of trade (De Benedictis and Tajoli, 2011; Krugman, Obstfeld, and Melitz, 2011), as can be seen in the significant broadening of distribution of Fig. 35 (especially at the middle values of  $K \sim 100$ ).

For a given country its trade is doing well if its  $K^* < K$  so that the country exports more than it imports. The opposite relation  $K^* > K$  corresponds to a bad trade situation (e.g., Greece being significantly above the diagonal). We also can say that local minima in the curve of  $K^* - K$  vs  $K$  correspond to a successful trade while maxima mark bad traders. In 2008 the most successful were China, Republic of Korea, Russia, Singapore, Brazil, South Africa, and Venezuela (in the order of  $K$  for  $K \leq 50$ ), while among the bad traders we note the UK, Spain, Nigeria, Poland, Czech Republic, Greece, and Sudan with an especially strong export drop for the two last cases.

A comparison between local and global rankings of countries for both imports and exports gives a new tool to analyze the countries economy. For example, in 2008 the most significant differences between Cheirank and the rank given by total exports are for Canada and Mexico with corresponding money export ranks  $\tilde{K}^* = 11$  and 13 and with  $K^* = 16$  and 23, respectively. These variations can be explained in the context that the export of these two countries is too strongly oriented on the USA. In contrast Singapore moves up from the  $\tilde{K}^* = 15$  export position to  $K^* = 11$  that shows the stability and broadness of its export trade; a similar situation appears

for India moving up from  $\tilde{K}^* = 19$  to  $K^* = 12$  [see Ermann and Shepelyansky (2011) for a more detailed analysis].

## B. Ranking of countries by trade in products

If we focus on the two-dimensional distribution of countries in a specific product we obtain very different information. The symmetry approximately visible for all commodities is absolutely absent: the points are scattered practically over the whole square  $N \times N$  (see Fig. 35). The reason for such a strong scattering is clear: e.g., for crude petroleum some countries export this product while other countries import it. Even if there is some flow from exporters to exporters it remains relatively low. This makes the Google matrix very asymmetric. Indeed, the asymmetry of trade flow is well visible in Figs. 35(c) and 35(d).

The same comparison of global and local rankings done before for all commodities can be applied to specific products obtaining even more strong differences. For example, for crude petroleum Russia moves up from a  $\tilde{K}^* = 2$  export position to  $K^* = 1$  showing that its trade network in this product is better and broader than the one of Saudi Arabia which is at the first export position  $\tilde{K}^* = 1$  in money volume. Iran moves in the opposite direction from the  $\tilde{K}^* = 5$  money position down to  $K^* = 14$  showing that its trade network is restricted to a small number of nearby countries. A significant improvement of ranking takes place for Kazakhstan moving up from  $\tilde{K}^* = 12$  to  $K^* = 2$ . A direct analysis shows that this happens due to an unusual fact that Kazakhstan is practically the only country which sells crude petroleum to the Cheirank leader in this product Russia. This puts Kazakhstan in the second position. It is clear that such direction of trade is more of a political or geographical origin and is not based on economic reasons.

The same detailed analysis can be applied to all specific products given by SITC1. For example, for the trade of cars France goes up from the  $\tilde{K}^* = 7$  position in exports to  $K^* = 3$  due to its broad export network.

## C. Ranking time evolution and crises

The WTN has evolved during the period 1962–2009. The number of countries is increased by 38%, while the number of links per country for all commodities is increased in total by 140% with a significant increase from 50% to 140% during the period 1993–2009 corresponding to economy globalization. At the same time for a specific commodity the average number of links per country remains on a level of 3–5 links being by a factor of 30 smaller compared to all commodities trade. During the whole period the total amount  $M_T$  of trade in USD shows an average exponential growth by 2 orders of magnitude.

A statistical density distribution of countries in the plane  $(K^* - K, K^* + K)$  in the period 1962–2009 for all commodities is shown in Fig. 36. The distribution has a form of spindle with maximum density at the vertical axis  $K^* - K = 0$ . We remind one that good exporters are on the lower side of this axis at  $K^* - K < 0$ , while the good importers (bad exporters) are on the upper side at  $K^* - K > 0$ .

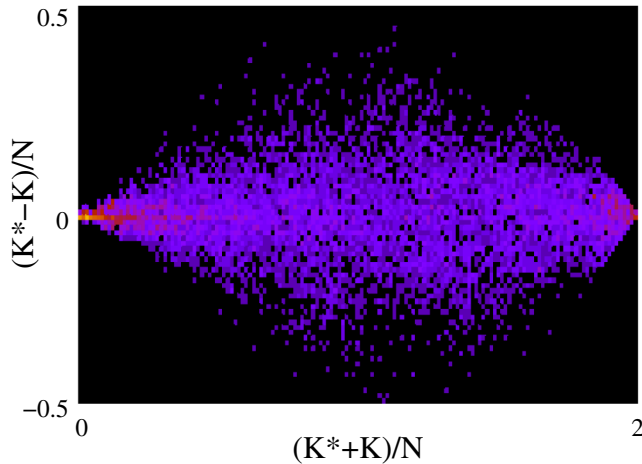


FIG. 36 (color online). Spindle distribution for the WTN of all commodities for all countries in the period 1962–2009 shown in the plane of  $((K^* - K)/N, (K^* + K)/N)$  (coarse graining inside each of the  $76 \times 152$  cells); data from the UN COMTRADE database. From Ermann and Shepelyansky, 2011.

The evolution of the ranking of countries for all commodities reflects their economical changes. The countries that occupy top positions tend to move very little in their ranks and can be associated with a solid phase. On the other hand, the countries in the middle region of  $K^* + K$  have a gaslike phase with strong rank fluctuations.

Examples of ranking evolution  $K$  and  $K^*$  for Japan, France, the Federal Republic of Germany and Germany, Great Britain, the USA, and for Argentina, India, China, the USSR, and the

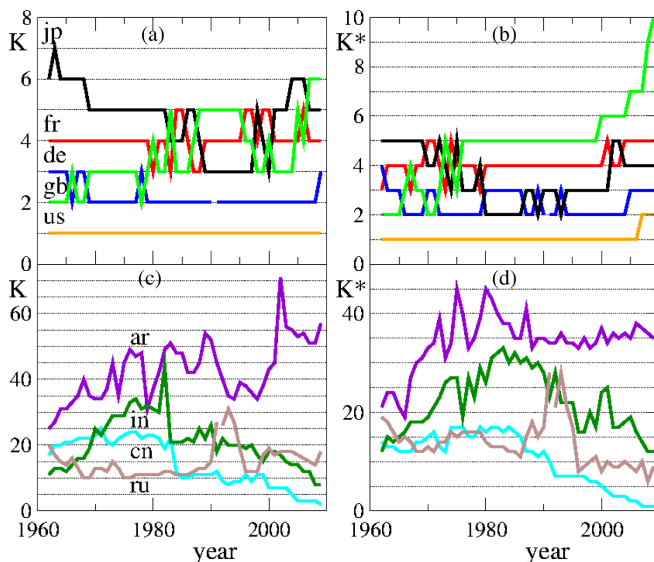


FIG. 37 (color online). Time evolution of CheiRank and PageRank indices  $K$ ,  $K^*$  for some selected countries for all commodities. The countries shown are (a), (b) Japan (jp, black), France (fr, red), Federal Republic of Germany and Germany (de, both blue), Great Britain (gb, green), USA (us, orange) [curves from top to bottom in (a)]. The countries shown are (c), (d) Argentina (ar, violet), India (in, dark green), China (cn, cyan), USSR and Russian Federation (ru, both gray) [curves from top to bottom in (c)]. From Ermann and Shepelyansky, 2011.

Russian Federation are shown in Fig. 37. It is interesting to note that sharp increases in  $K$  mark crises in 1991 and 1998 for Russia and in 2001 for Argentina (import is reduced in a period of crisis). It is also visible that in recent years the solid phase is perturbed by the entrance of new countries such as China and India. Other regional or global crisis could be highlighted due to the large fluctuations in the evolution of ranks. For example, in the range  $81 \leq K + K^* \leq 120$ , during the period of 1992–1998 some financial crises such as Black Wednesday, the Mexico crisis, the Asian crisis, and the Russian crisis are appreciated with this ranking evolution.

#### D. Ecological ranking of world trade

Interesting parallels between multiproduct world trade and interactions between species in ecological systems has been traced by Ermann and Shepelyansky (2013). This approach is based on the analysis of the strength of transitions forming the Google matrix for the multiproduct world trade network.

Ecological systems are characterized by high complexity and biodiversity (May, 2001) linked to nonlinear dynamics and chaos emerging in the process of their evolution (Lichtenberg and Lieberman, 1992). The interactions between species form a complex network whose properties can be analyzed by the modern methods of scale-free networks. The analysis of their properties uses a concept of mutualistic networks and provides detailed understanding of their features being linked to a high nestedness of these networks (Burgos *et al.*, 2007, 2008; Bastolla *et al.*, 2009; Saverda *et al.*, 2011). Using the UN COMTRADE database we show that a similar ecological analysis gives a valuable description of the world trade: countries and trade products are analogous to plants and pollinators, and the whole trade network is characterized by a high nestedness typical for ecological networks.

An important feature of ecological networks is that they are highly structured, being very different from randomly interacting species (Bascompte *et al.*, 2003). Recently it was shown that the mutualistic networks between plants and their pollinators (Bascompte *et al.*, 2003; Memmott, Waser, and Price, 2004; Vázquez and Aizen, 2004; Olesen *et al.*, 2007; Rezende *et al.*, 2007) are characterized by high nestedness which minimizes competition and increases biodiversity (Burgos *et al.*, 2007, 2008; Bastolla *et al.*, 2009; Saverda *et al.*, 2011).

The mutualistic WTN is constructed on the basis of the UN COMTRADE database from the matrix of trade transactions  $M_{c',c}^p$  expressed in USD for a given product (commodity)  $p$  from country  $c$  to country  $c'$  in a given year (from 1962 to 2009). For product classification we use 3-digits SITC Rev1 discussed earlier with the number of products  $N_p = 182$ . All these products are described in UN COMTRADE (2011) in the commodity code document SITC Rev1. The number of countries varies between  $N_c = 164$  in 1962 and  $N_c = 227$  in 2009. The import and export trade matrices are defined as  $M_{p,c}^{(i)} = \sum_{c'=1}^{N_c} M_{c,c'}^p$  and  $M_{p,c}^{(e)} = \sum_{c'=1}^{N_c} M_{c',c}^p$ , respectively. We use the dimensionless matrix elements  $m^{(i)} = M^{(i)}/M_{\max}$  and  $m^{(e)} = M^{(e)}/M_{\max}$ , where for a given year  $M_{\max} = \max\{\max[M_{p,c}^{(i)}], \max[M_{p,c}^{(e)}]\}$ . The distributions of

matrix elements  $m^{(i)}$  and  $m^{(e)}$  in the plane of indices  $p$  and  $c$ , ordered by the total amount of import and export in a decreasing order, are shown and discussed by Ermann and Shepelyansky (2013). In global, the distributions of  $m^{(i)}$  and  $m^{(e)}$  remain stable in time especially in view of 100 times growth of the total trade volume during the period 1962–2009. The fluctuations of  $m^{(e)}$  are larger compared to the  $m^{(i)}$  case since certain products, e.g., petroleum, are exported by only a few countries while it is imported by almost all countries.

To use the methods of ecological analysis we construct the mutualistic network matrix for import  $Q^{(i)}$  and export  $Q^{(e)}$  whose matrix elements take binary value 1 or 0 if corresponding elements  $m^{(i)}$  and  $m^{(e)}$  are, respectively, larger or smaller than a certain trade threshold value  $\mu$ . The fraction  $\varphi$  of nonzero matrix elements varies smoothly in the range  $10^{-6} \leq \mu \leq 10^{-2}$  and further analysis is not really sensitive to the actual  $\mu$  value inside this broad range.

In contrast to ecological systems (Bastolla *et al.*, 2009) the world trade is described by a directed network and hence we characterize the system by two mutualistic matrices  $Q^{(i)}$  and  $Q^{(e)}$  corresponding to import and export. Using the standard nestedness BINMATNEST algorithm (Rodríguez-Gironés and Santamaría, 2006) we determine the nestedness parameter  $\eta$  of the WTN and the related nestedness temperature  $T = 100(1 - \eta)$ . The algorithm reorders lines and columns of a mutualistic matrix concentrating nonzero elements as much as possible in the top left corner and thus providing information about the role of immigration and extinction in an ecological system. A high level of nestedness and ordering can be reached only for systems with low  $T$ . It is argued that the nested architecture of real mutualistic networks increases their biodiversity.

The nestedness matrices generated by the BINMATNEST algorithm (Rodríguez-Gironés and Santamaría, 2006) are shown in Fig. 38 for ecology networks ARR1 ( $N_{\text{pl}} = 84$ ,  $N_{\text{anim}} = 101$ ,  $\varphi = 0.043$ , and  $T = 2.4$ ) and WES ( $N_{\text{pl}} = 207$ ,  $N_{\text{anim}} = 110$ ,  $\varphi = 0.049$ , and  $T = 3.2$ ) from Rezende *et al.* (2007). Using the same algorithm we generate the nestedness matrices of the WTN using the mutualistic matrices for import  $Q^{(i)}$  and export  $Q^{(e)}$  for the WTN in years 1968 and 2008 with a fixed typical threshold  $\mu = 10^{-3}$  (see Fig. 38). As for ecological systems, for the WTN data we also obtain a rather small nestedness temperature ( $T \approx 6$  and 8 for import and export in 1968 and  $T \approx 4$  and 8 in 2008, respectively). These values are by factors of 9 and 4 times smaller than the corresponding  $T$  values for import and export from random generated networks with the corresponding values of  $\varphi$ .

The small value of nestedness temperature obtained for the WTN confirms the validity of the ecological analysis of the WTN structure: trade products play the role of pollinators which produce exchange between world countries, which play the role of plants. As in ecology the WTN evolves to the state with a very low nestedness temperature that satisfies the ecological concept of system stability appearing as a result of high network nestedness (Bastolla *et al.*, 2009).

The nestedness algorithm creates an effective ecological ranking (EcoloRanking) of all UN countries. The evolution of the 20 top ranks throughout the years is shown in Fig. 39 for

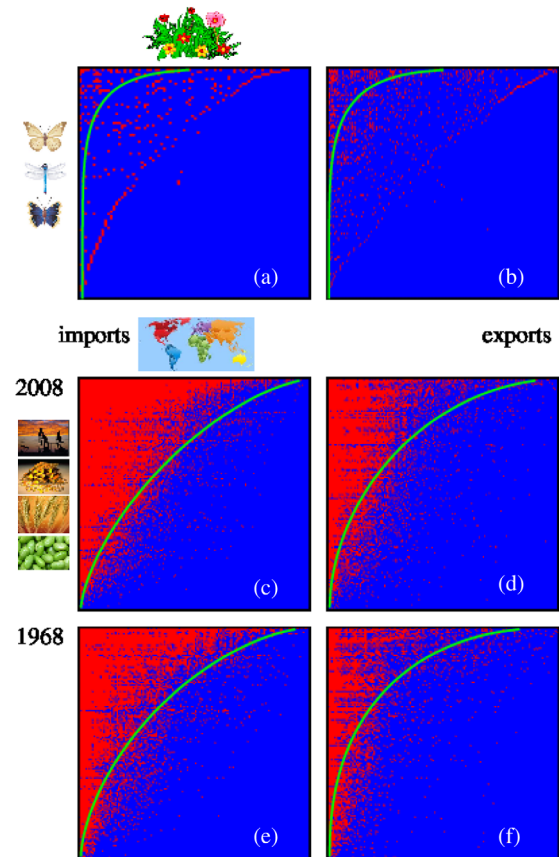


FIG. 38 (color online). Nestedness matrices for the plant-animal mutualistic networks in the top panels, and for the WTN of countries and products in the middle and bottom panels. (a), (b) Data of ARR1 and WES networks. From Rezende *et al.*, 2007. The WTN matrices are computed with the threshold  $\mu = 10^{-3}$  and corresponding  $\varphi \approx 0.2$  for years (c), (d) 2008 and (e), (f) 1968 and 2008 for (c), (e) import and (d), (f) export. Gray (red) and black (blue) represent unit and zero elements, respectively; only lines and columns with nonzero elements are shown. The order of plants and animals, countries and products is given by the nestedness algorithm (Rodríguez-Gironés and Santamaría, 2006); the perfect nestedness is shown by gray (green) curves for the corresponding values of  $\varphi$ . From Ermann and Shepelyansky, 2013.

import and export. This ranking is quite different from the more commonly applied ranking of countries by their total import and export monetary trade volume (Central Intelligence Agency, 2009) (see the corresponding data in Fig. 40) or the democratic ranking of the WTN based on the Google matrix analysis discussed previously. Indeed, in 2008 China is at the top rank for total export volume but it is only at the fifth position in EcoloRank (see Figs. 39 and 40). In a similar way Japan moves down from the fourth to the 17th position while the USA raises up from the third to the first rank.

The same nestedness algorithm generates not only the ranking of countries but also the ranking of trade products for import and export which is presented in Fig. 41. For comparison we also show the standard ranking of products by their trade volume. In Fig. 41 the color of symbols marks the first SITC digit described in the figure (UN COMTRADE, 2011) and Table 2 in Ermann and Shepelyansky (2013).

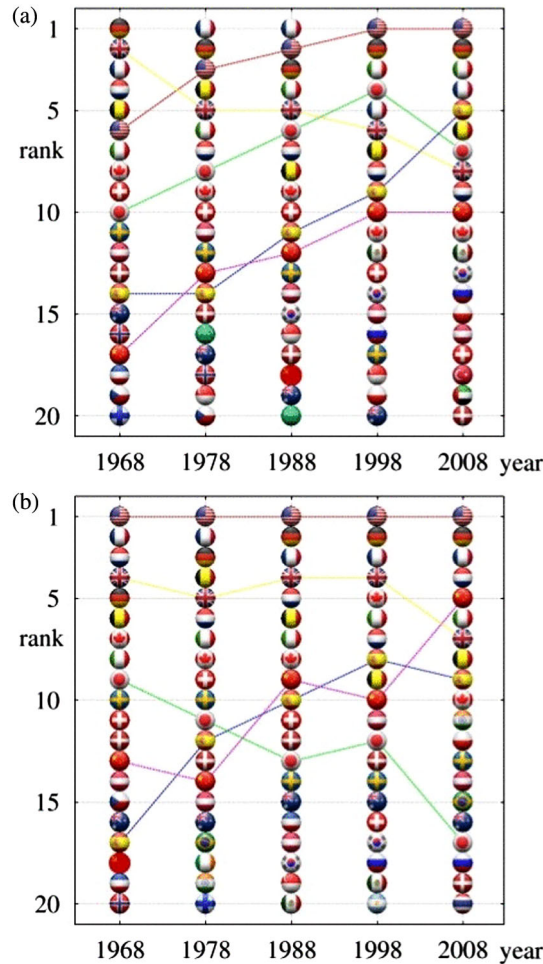


FIG. 39 (color online). Top 20 EcoloRank countries as a function of the years for the WTN (a) import and (b) export panels. The ranking is given by the nestedness algorithm for the trade threshold  $\mu = 10^{-3}$ ; each country is represented by its corresponding flag. As an example, dashed lines show a time evolution of the following countries: USA, UK, Japan, China, and Spain. From Ermann and Shepelyansky, 2013.

The origin of such a difference between the EcoloRanking and the trade volume ranking of countries is related to the main idea of mutualistic ranking in ecological systems: the nestedness ordering stresses the importance of mutualistic pollinators (products for the WTN) which generate links and exchange between plants (countries for the WTN). In this way generic products, which participate in the trade between many countries, become of primary importance even if their trade volume is not at the top lines of import or export. In fact, such mutualistic products glue the skeleton of the world trade while the nestedness concept allows one to rank them in order of their importance. The time evolution of this EcoloRanking of products of the WTN is shown in Fig. 41 for import and export in comparison with the product ranking by the monetary trade volume (since the trade matrix is diagonal in the product index the ranking of products in the latter case is the same for import and export). The top and middle panels have dominate colors corresponding to machinery (SITC Rev1 code 7, blue) and mineral fuels (3, black) with a moderate contribution of

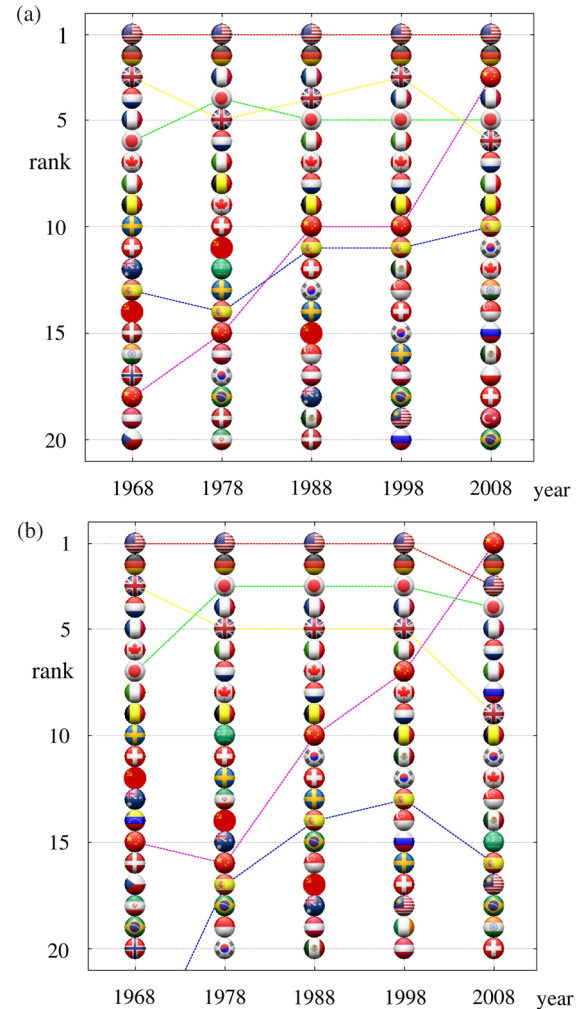


FIG. 40 (color online). The top 20 countries as a function of years ranked by the total monetary trade volume of the WTN in (a) import and (b) export, respectively; each country is represented by its corresponding flag. Dashed lines show time evolution of the same countries as in Fig. 39. From Ermann and Shepelyansky, 2013.

chemicals (5, yellow) and manufactured articles (8, cyan) and a small fraction of goods classified by material (6, green). Even if the global structure of product ranking by trade volume has certain similarities with import EcoloRanking there are also important new elements. Indeed, in 2008 the mutualistic significance of petroleum products (code 332), *machindus* (machines for special industries code 718), and *medpharm* (medical-pharmaceutical products code 541) is much higher compared to their volume ranking, while petroleum crude (code 331) and office machines (code 714) have smaller mutualistic significance compared to their volume ranking.

The new element of EcoloRanking is that it differentiates between import and export products while for trade volume they are ranked in the same way. Indeed, the dominant colors for export (Fig. 41, bottom panel) correspond to food (SITC Rev1 code 0, red) with the contribution of black import and crude materials (code 2, violet); followed by cyan import and a more pronounced presence of *finnotclass* (commodities and

transactions not classified in code 9, brown). EcoloRanking of export shows a clear decrease tendency of dominance of SITC codes 0 and 2 with time and increase of importance of codes 3 and 7. It is interesting to note that the code 332 of petroleum products is very vulnerable in volume ranking due to significant variations of petroleum prices but in EcoloRanking this product keeps the stable top positions in all years showing its mutualistic structural importance for the world trade. EcoloRanking of export shows also the importance of fish (code 031), clothing (code 841), and fruits (code 051) which are placed on higher positions compared to their volume ranking. At the same time *roadvehic* (code 732), which is at the top volume ranking, has relatively low ranking in export since only a few countries dominate the production of road vehicles.

It is interesting to note that in Fig. 41 petroleum crude is at the top of the trade volume ranking, e.g., in 2008 (top panel), but it is absent in import EcoloRanking (middle panel) and it is only in the sixth position in export EcoloRanking (bottom

panel). A similar feature is visible for years 1968 and 1978. At first glance this looks surprising but in fact for mutualistic EcoloRanking it is important that a given product is imported from top EcoloRank countries: this is definitely not the case for petroleum crude which practically is not produced inside the top 10 import EcoloRank countries (the only exception is USA, which however also does not export much). Because of that reason this product has low mutualistic significance.

The mutualistic concept of product importance is at the origin of a significant difference of EcoloRanking of countries compared to the usual trade volume ranking (see Figs. 39 and 40). Indeed, in the latter case China and Japan are at the dominant positions but their trade is concentrated in specific products in which their mutualistic role is relatively low. In contrast, USA, Germany, and France keep the top three EcoloRank positions during almost 40 years, demonstrating their mutualistic power and importance for the world trade. Thus our results show the universal features of ecologic ranking of complex networks with promising future applications to trade, finance, and other areas.

### E. Remarks on world trade and banking networks

The new approach to the world trade, based on the Google matrix analysis, gives a democratic type of ranking being independent of the trade amount of a given country. In this way rich and poor countries are treated on equal democratic grounds. In a certain sense PageRank probability for a given country is proportional to its rescaled import flows while CheiRank is proportional to its rescaled export flows inside of the WTN.

The global characteristics of the world trade are analyzed on the basis of this new type of ranking. Even if all countries are treated now on equal democratic grounds still we find at the top rank the group of industrially developed countries approximately corresponding to *G-20* and recover 74% of countries listed in *G-20*. The Google matrix analysis demonstrates an existence of two solid state domains of rich and poor countries which remain stable during the years of consideration. Other countries correspond to a gas phase with ranking strongly fluctuating in time. We propose a simple random matrix model which well describes the statistical properties of rank distribution for the WTN (Ermann and Shepelyansky, 2011).

The comparison between usual ImportRank-ExportRank (Central Intelligence Agency, 2009) and our PageRank-CheiRank approach shows that the latter highlights the trade flows in a new and useful manner which is complementary to the usual analysis. The important difference between these two approaches is due to the fact that the ImportRank-ExportRank method takes into account only a global amount of money exchange between a country and the rest of the world, while the PageRank-CheiRank approach takes into account all links and money flows between all countries.

The future developments should consider a matrix with all countries and all products whose size becomes significantly larger ( $N \sim 220 \times 10^4 \sim 2 \times 10^6$ ) compared to a modest size  $N \approx 227$  considered here. However, some new problems of this multiplex network analysis should be resolved combining a democracy in countries with volume importance of products in which the role is not democratic. It is quite possible that such

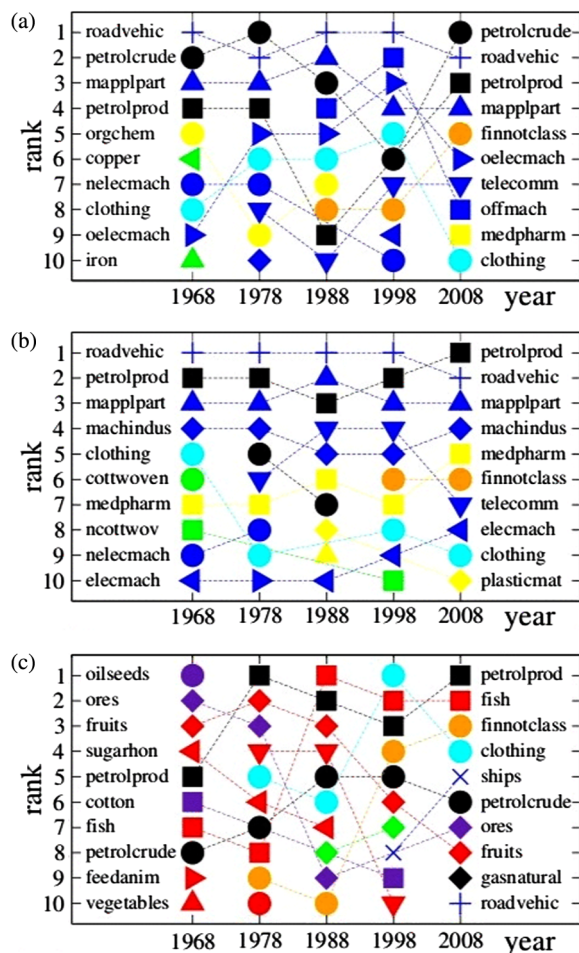


FIG. 41 (color online). The top 10 ranks of trade products as a function of years for the WTN. (a) Ranking of products by monetary trade volume. (b), (c) Ranking is given by the nestedness algorithm for (b) import and (c) export with the trade threshold  $\mu = 10^{-3}$ . Each product is shown by its own symbol with a short name written at years 1968 and 2008; the symbol color marks the first SITC digit. The SITC codes of products and their names are given in the UN COMTRADE (2011) and Table 2 of Ermann and Shepelyansky (2013). From Ermann and Shepelyansky, 2013.



an improved analysis will generate an asymmetric ranking of products in contrast to their symmetric ranking by volume in export and import. The ecological ranking of the WTN discussed in Sec. XI.D indicates preferences and asymmetry of trade in multiple products (Ermann and Shepelyansky, 2013). The first steps in the Google matrix analysis of the multiproduct world trade network, with 61 products and up to 227 countries, were done recently by Ermann and Shepelyansky (2015) confirming this asymmetry. It is established there that such multifunctional networks can be analyzed by the Google matrix approach, using a certain personalized vector, so that the world countries are treated on democratic equal grounds while the contribution of products remains proportional to their trade volume. Such a multiproduct world trade network allows one to investigate the sensitivity of trade to price variation of various products. This approach can also be applied to the world network of economic activities obtained from the Organization for Economic Co-operation and Development and the World Trade Organization (OECD-WTO) database (Kandiah, Escaith, and Shepelyansky, 2015). It allows one to determine the sensitivities of the economic balance of world countries with respect to labor cost variations in certain selected countries. In difference from the multiproduct WTN of UN COMTRADE, where there are no direct transitions between products, the OECD-WTO database contains interactions between various activity sectors of various countries that opens new possibilities for a more advanced analysis.

It is also important to note that usually in economy researchers analyze time evolution of various indexes studying their correlations. The results presented previously for the WTN show that in addition to time evolution there is also evolution in space of the network. As for waves in an ocean, time and space are both important, and we think that time and space study of trade captures important geographical factors which will play a dominant role for the analysis of contamination propagation over the WTN in case of crisis. We think that the WTN data capture many essential elements which will play a rather similar role for financial flows in the interbank payment networks. We expect that the analysis of financial flows between bank units would prevent an important financial crisis shaking the world in the last years. Unfortunately, in contrast to the WWW and the UN COMTRADE, the banks keep their financial flows hidden. Because of this secrecy of banks the society is still suffering from financial crises. And all this for a network of very small size estimated on a level of 50 000 bank units for the whole world being by a factor  $1 \times 10^6$  smaller than the present size of the WWW [e.g., the Fedwire interbank payment network of the USA contains only 6600 nodes (Soramäki *et al.*, 2007)]. In a drastic contrast with bank networks the WWW provided a public access to its nodes changing the world on a scale of 20 years. A creation of the World Bank Web (WBW) with information accessible for authorized investigators allows one to understand and control financial flows in an efficient manner preventing the society from bank crises. We note that the methods of network analysis and ranking start to attract the interest of researchers in various banks (Craig and von Peter, 2010; Garratt, Mahadeva, and Svirydzhenka, 2011).

## XII. NETWORKS WITH NILPOTENT ADJACENCY MATRIX

### A. General properties

In certain networks (Frahm, Chepelienskii, and Shepelyansky, 2012; Frahm, Eom, and Shepelyansky, 2014) it is possible to identify an ordering scheme for the nodes such that the adjacency matrix has nonvanishing elements  $A_{mn}$  only for nodes  $m < n$  providing a triangular matrix structure. In these cases it is possible to provide a semianalytical theory (Frahm, Chepelienskii, and Shepelyansky, 2012; Frahm, Eom, and Shepelyansky, 2014) which allows one to simplify the numerical calculation of the nonvanishing eigenvalues of the matrix  $S$  introduced in Sec. III.A. It is useful to write this matrix in the form

$$S = S_0 + (1/N)ed^T, \quad (10)$$

where the vector  $e$  has unit entries for all nodes and the *dangling vector*  $d$  has unit entries for dangling nodes and zero entries for the other nodes. The extra contribution  $ed^T/N$  just replaces the empty columns (of  $S_0$ ) with  $1/N$  entries at each element. For a triangular network structure the matrix  $S_0$  is nilpotent, i.e.,  $S_0^l = 0$  for some integer  $l > 0$  and  $S_0^{l-1} \neq 0$ . Furthermore, for the network examples studied previously (Frahm, Chepelienskii, and Shepelyansky, 2012; Frahm, Eom, and Shepelyansky, 2014) we have  $l \ll N$  which has important consequences for the eigenvalue spectrum of  $S$ .

There are two groups of (right) eigenvectors  $\psi$  of  $S$  with eigenvalue  $\lambda$ . For the first group the quantity  $C = d^T\psi$  vanishes and  $\psi$  is also an eigenvector of  $S_0$  and if  $S_0$  is nilpotent we have  $\lambda = 0$  (there are also many higher order generalized eigenvectors associated with  $\lambda = 0$ ). For the second group we have  $C \neq 0$ ,  $\lambda \neq 0$ , and the eigenvector is given by  $\psi = (\lambda\mathbb{1} - S_0)^{-1}Ce/N$ . Expanding the matrix inverse in a finite geometric series (for nilpotent  $S_0$ ) and applying the condition  $C = d^T\psi$  on this expression one finds that the eigenvalue must be a zero of the *reduced polynomial* of degree  $l$ :

$$\mathcal{P}_r(\lambda) = \lambda^l - \sum_{j=0}^{l-1} \lambda^{l-1-j} c_j = 0, \quad c_j = d^T S_0^j e/N. \quad (11)$$

This shows that there are at most  $l$  nonvanishing eigenvalues of  $S$  with eigenvectors  $\psi \propto \sum_{j=0}^{l-1} \lambda^{-j-1} v^{(j)}$ , where  $v^{(j)} = S_0^j e/N$  for  $j = 0, \dots, l-1$ . Actually, the vectors  $v^{(j)}$  generate an  $S$ -invariant  $l$ -dimensional subspace and from  $Sv^{(j)} = c_j v^{(0)} + v^{(j+1)}$  (using the identification  $v^{(l)} = 0$ ) one directly obtains the  $l \times l$  representation matrix  $\bar{S}$  of  $S$  with respect to  $v^{(j)}$  (Frahm, Chepelienskii, and Shepelyansky, 2012). Furthermore, the characteristic polynomial of  $\bar{S}$  is indeed given by the reduced polynomial (11) and the sum rule  $\sum_{j=0}^{l-1} c_j = 1$  ensures that  $\lambda = 1$  is indeed a zero of  $\mathcal{P}_r(\lambda)$  (Frahm, Chepelienskii, and Shepelyansky, 2012). The corresponding eigenvector (PageRank  $P$  at  $\alpha = 1$ ) is given by  $P \propto \sum_{j=0}^{l-1} v^{(j)}$ . The remaining  $N - l$  (generalized)

eigenvectors of  $S$  are associated with many different Jordan blocks of  $S_0$  for the eigenvalue  $\lambda = 0$ .

These  $l$  nonvanishing complex eigenvalues can be numerically computed as the zeros of the reduced polynomial by the Newton-Maehly method, by a numerical diagonalization of the “small” representation matrix  $\tilde{S}$  (or better a more stable transformed matrix with identical eigenvalues) or by the Arnoldi method using the uniform vector  $e$  as the initial vector. In the latter case the Arnoldi method should theoretically (in the absence of rounding errors) exactly explore the  $l$ -dimensional subspace of the vectors  $v^{(j)}$  and break off after  $l$  iterations with  $l$  exact eigenvalues.

However, numerical rounding errors may have a strong effect due to the Jordan blocks for the zero eigenvalue (Frahm, Chepelienskii, and Shepelyansky, 2012). Indeed, an error  $\epsilon$  appearing in the bottom left corner of a Jordan matrix of size  $D$  with zero eigenvalue leads to numerically induced eigenvalues on a complex circle of radius

$$|\lambda_\epsilon| = \epsilon^{1/D}. \quad (12)$$

Such an error can become significant with  $|\lambda| > 0.1$  even for  $\epsilon \sim 10^{-15}$  as soon as  $D > 15$ . We call this phenomenon the Jordan error enhancement. Furthermore, also the numerical determination of the zeros of  $\mathcal{P}_r(\lambda)$  for large values of  $l \sim 10^2$  can be numerically rather difficult. Thus, it may be necessary to use a high-precision library such as the GNU Multiple Precision Arithmetic Library (see <https://gmplib.org/>) either for the determination of the zeros of  $\mathcal{P}_r(\lambda)$  or for the Arnoldi method (Frahm, Eom, and Shepelyansky, 2014).

## B. PageRank of integers

A network for integer numbers (Frahm, Chepelienskii, and Shepelyansky, 2012) can be constructed by linking an integer number  $n \in \{1, \dots, N\}$  to its divisors  $m$  different from 1 and  $n$  itself by an adjacency matrix  $A_{mn} = M(n, m)$ , where the multiplicity  $M(n, m)$  is the number of times we can divide  $n$  by  $m$ , i.e., the largest integer such that  $m^{M(n,m)}$  is a divisor of  $n$ , and  $A_{mn} = 0$  for all other cases. The number 1 and the prime numbers are not linked to any other number and correspond to dangling nodes. The total size  $N$  of the matrix is fixed by the maximal considered integer. According to numerical data the number of links  $N_\ell = \sum_{mn} A_{mn}$  is given by  $N_\ell = N(a_\ell + b_\ell \ln N)$  with  $a_\ell = -0.901 \pm 0.018$  and  $b_\ell = 1.003 \pm 0.001$ .

The matrix elements  $A_{mn}$  are different from zero only for  $n \geq 2m$  and the associated matrix  $S_0$  is therefore nilpotent with  $S_0^l = 0$  and  $l = \log_2(N) \ll N$ . This triangular matrix structure can be seen in Fig. 42(a) which shows the amplitudes of  $S$ . The vertical gray/green lines correspond to the extra contribution due to the dangling nodes. These  $l$  nonvanishing eigenvalues of  $S$  can be efficiently calculated as the zeros of the reduced polynomial (11) up to  $N = 10^9$  with  $l = 29$ . For  $N = 10^9$  the largest eigenvalues are  $\lambda_1 = 1$ ,  $\lambda_{2,3} \approx -0.27178 \pm i0.42736$ ,  $\lambda_4 \approx -0.17734$ , and  $|\lambda_j| < 0.1$  for  $j \geq 5$ . The dependence of the eigenvalues on  $N$  seems to scale with the parameter  $1/\ln(N)$  for  $N \rightarrow \infty$  and in particular  $\gamma_2(N) = -2 \ln |\lambda_2(N)| \approx 1.020 + 7.14/\ln N$  (Frahm, Chepelienskii, and Shepelyansky, 2012). Therefore the first eigenvalue is separated from the

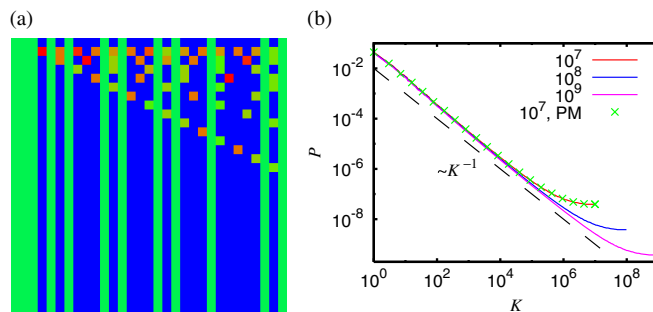


FIG. 42 (color online). (a) The Google matrix of integers. The amplitudes of matrix elements  $S_{mn}$  are shown by color black (blue) for minimal zero elements and gray (red) maximal unity elements, with  $1 \leq n \leq 31$  corresponding to the  $x$  axis (with  $n = 1$  corresponding to the left column) and  $1 \leq m \leq 31$  for the  $y$  axis (with  $m = 1$  corresponding to the upper row). (b) The full lines correspond to the dependence of the PageRank probability  $P(K)$  on index  $K$  for the matrix sizes  $N = 10^7$ ,  $10^8$ , and  $10^9$  with the PageRank evaluated by the exact expression  $P \propto \sum_{j=0}^{l-1} v^{(j)}$ . The gray (green) crosses correspond to the PageRank obtained by the power method for  $N = 10^7$ ; the dashed straight line shows the Zipf law dependence  $P \sim 1/K$ . From Frahm, Chepelienskii, and Shepelyansky, 2012.

second eigenvalue and one can choose the damping factor  $\alpha = 1$  without any problems to define a unique PageRank.

The large values of  $N$  are possible because the vector iteration  $v^{(j+1)} = S_0 v^{(j)}$  can actually be computed without storing the  $N_\ell \sim N \ln N$  nonvanishing elements of  $S_0$  by using

$$v_n^{(j+1)} = \sum_{m=2}^{[N/n]} \frac{M(mn, m)}{Q(mn)} v_{mn}^{(j)}, \quad \text{if } n \geq 2 \quad (13)$$

and  $v_1^{(j+1)} = 0$  (Frahm, Chepelienskii, and Shepelyansky, 2012). The initial vector is given by  $v^{(0)} = e/N$  and  $Q(n) = \sum_{m=2}^{n-1} M(n, m)$  is the number of divisors of  $n$  (taking into account the multiplicity). The multiplicity  $M(mn, n)$  can be recalculated during each iteration and one needs only to store  $N(\ll N_\ell)$  integer numbers  $Q(n)$ . It is also possible to reformulate Eq. (13) in a different way without using  $M(mn, n)$  (Frahm, Chepelienskii, and Shepelyansky, 2012). The vectors  $v^{(j)}$  allow one to compute the coefficients  $c_j = d^T v^{(j)}$  in the reduced polynomial and the PageRank  $P \propto \sum_{j=0}^{l-1} v^{(j)}$ . Figure 42(b) shows the PageRank for  $N \in \{10^7, 10^8, 10^9\}$  obtained in this way and for comparison also the result of the power method for  $N = 10^7$ .

Actually Fig. 43 shows that in the sum  $P \propto \sum_{j=0}^{l-1} v^{(j)}$  the first three terms already give a quite satisfactory approximation to the PageRank allowing a further analytical simplified evaluation (Frahm, Chepelienskii, and Shepelyansky, 2012) with the result  $P(n) \approx C_N/b_n n$  for  $n \ll N$ , where  $C_N$  is the normalization constant and  $b_n = 2$  for prime numbers  $n$  and  $b_n = 6 - \delta_{p_1, p_2}$  for numbers  $n = p_1 p_2$  being a product of two prime numbers  $p_1$  and  $p_2$ . The behavior  $P(n)n \approx C_N/b_n$ , which takes approximately constant values on several branches, is also visible in Fig. 43 with  $C_N/b_n$  decreasing if  $n$  is a product of many prime numbers. The numerical

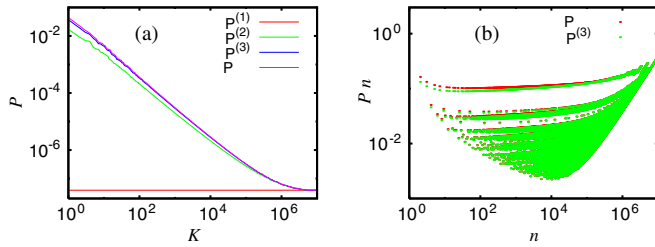


FIG. 43 (color online). (a) Comparison of the first three PageRank approximations  $P^{(i)} \propto \sum_{j=0}^{i-1} v^{(j)}$  for  $i = 1, 2, 3$  and the exact PageRank dependence  $P(K)$ . (b) Comparison of the dependence of the rescaled probabilities  $nP$  and  $nP^{(3)}$  on  $n$ . Both panels correspond to the case  $N = 10^7$ . From Frahm, Chepelyanskii, and Shepelyansky, 2012.

results up to  $N = 10^9$  show that the numbers  $n$ , corresponding to the leading PageRank values for  $K = 1, 2, \dots, 32$ , are  $n = 2, 3, 5, 7, 4, 11, 13, 17, 6, 19, 9, 23, 29, 8, 31, 10, 37, 41, 43, 14, 47, 15, 53, 59, 61, 25, 67, 12, 71, 73, 22$ , and 21 with about 30% of nonprimes among these values (Frahm, Chepelyanskii, and Shepelyansky, 2012).

A simplified model for the network for integer numbers with  $M(n, m) = 1$  if  $m$  is the divisor of  $n$  and  $1 < m < n$  has also been studied with similar results (Frahm, Chepelyanskii, and Shepelyansky, 2012).

### C. Citation network of Physical Review

Citation networks for Physical Review and other scientific journals can be defined by taking published articles as nodes and linking an article A to another article B if A cites B. PageRank and a similar analysis of such networks are efficient to determine influential articles (Redner, 1998, 2005; Newman, 2001; Radicchi *et al.*, 2009).

In a citation network links go mostly from newer to older articles and therefore such networks have, apart from the dangling node contributions, typically also a (nearly) triangular structure as can be seen in Fig. 44 which shows a coarse-grained density of the corresponding Google matrix for the citation network of Physical Review from the very beginning until 2009 (Frahm, Eom, and Shepelyansky, 2014). However, due to the delay of the publication process in certain rare instances a published paper may cite another paper that is actually published a little later and sometimes two papers may even mutually cite each other. Therefore the matrix structure is not exactly triangular but in the coarse-grained density in Fig. 44 the rare “future citations” are not well visible.

The nearly triangular matrix structure implies large dimensional Jordan blocks associated with the eigenvalue  $\lambda = 0$ . This creates the Jordan error enhancement (12) with severe numerical problems for an accurate computation of eigenvalues in the range  $|\lambda| < 0.3$ – $0.4$  when using the Arnoldi method with standard double-precision arithmetic (Frahm, Eom, and Shepelyansky, 2014).

One can eliminate the small number of future citations (12 126 which is 0.26% of the total number of links  $N_\ell = 4\,691\,015$ ) and determine the complex eigenvalue spectrum of a triangular reduced citation network using the semi-analytical theory presented in Sec XII.B. It turns out that in this

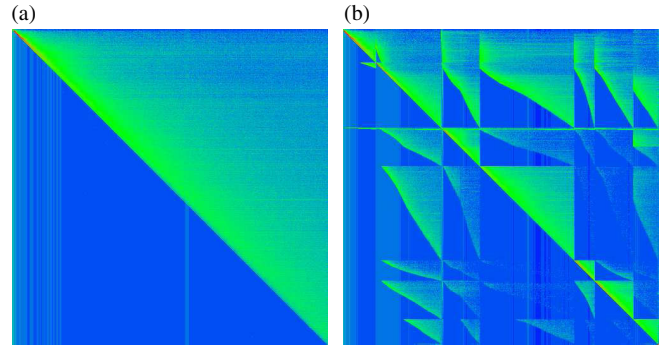


FIG. 44 (color online). Different representations of the Google matrix structure for the Physical Review network until 2009. (a) Density of matrix elements  $G_{tt}$  in the basis of the publication time index  $t$  (and  $t'$ ). (b) Density of matrix elements in the basis of journal ordering according to Phys. Rev. Series I, Phys. Rev., Phys. Rev. Lett., Rev. Mod. Phys., Phys. Rev. A, B, C, D, E, Phys. Rev. STAB, Phys. Rev. STPER, and with time index ordering inside each journal. Note that the journals Phys. Rev. Series I, Phys. Rev. STAB, and Phys. Rev. STPER are not clearly visible due to a small number of published papers. Also Rev. Mod. Phys. appears only as a thick line with 2–3 pixels (out of 500) due to a limited number of published papers. The different blocks with triangular structure correspond to clearly visible seven journals with considerable numbers of published papers. Both panels show the coarse-grained density of matrix elements on  $500 \times 500$  square cells for the entire network. Color shows the density of matrix elements (of  $G$  at  $\alpha = 1$ ) changing from black (blue) for minimum zero value to gray (red) maximum value. From Frahm, Eom, and Shepelyansky, 2014.

case the matrix  $S_0$  is nilpotent  $S_0^l = 0$  with  $l = 352$  which is much smaller than the total network size  $N = 463\,348$ . The 352 nonvanishing eigenvalues can be determined numerically as the zeros of the polynomial (11), but due to an alternate sign problem with a strong loss of significance it is necessary to use the high-precision library GMP with 256 binary digits (Frahm, Eom, and Shepelyansky, 2014).

The semi-analytical theory can also be generalized to the case of nearly triangular networks, i.e., the full citation network including the future citations. In this case the matrix  $S_0$  is no longer nilpotent but one can still generalize the arguments of the previous section and discuss the two cases, where the quantity  $C = d^T \psi$  either vanishes (eigenvectors of the first group) or is different from zero (eigenvectors of the second group). The eigenvalues  $\lambda$  for the first group, which may now be different from zero, can be determined by a quite complicated but numerically very efficient procedure using the subspace eigenvalues of  $S$  and degenerate subspace eigenvalues of  $S_0$  (due to the absence of dangling node contributions the matrix  $S_0$  produces much larger invariant subspaces than  $S$ ) (Frahm, Eom, and Shepelyansky, 2014). The eigenvalues of the second group are given as the complex zeros of the rational function:

$$\mathcal{R}(\lambda) = 1 - d^T \frac{\mathbb{1}}{\lambda \mathbb{1} - S_0} e/N = 1 - \sum_{j=0}^{\infty} c_j \lambda^{-1-j} \quad (14)$$

with  $c_j$  given as in Eq. (11) and now the series is not finite since  $S_0$  is not nilpotent. For the citation network of Physical

Review the coefficients  $c_j$  behave as  $c_j \propto \rho_1^j$ , where  $\rho_1 \approx 0.902$  is the largest eigenvalue of the matrix  $S_0$  with an eigenvector nonorthogonal to  $d$ . Therefore the series in Eq. (14) converges well for  $|\lambda| > \rho_1$  but in order to determine the spectrum the rational function  $\mathcal{R}(\lambda)$  needs to be evaluated for smaller values of  $|\lambda|$ . This problem can be solved by interpolating  $\mathcal{R}(\lambda)$  with (another) rational function using a certain number of support points on the complex unit circle, where Eq. (14) converges well, and determining the complex zeros, well inside the unit circle, of the numerator polynomial using again the high-precision library GMP (Frahm, Eom, and Shepelyansky, 2014). In this way using 16 384 binary digits one may obtain 2500 reliable eigenvalues of the second group.

The numerical high-precision spectra obtained by the semianalytic methods for both cases, triangular reduced and full citation network, are shown in Fig. 45. Note that it is also possible to implement the Arnoldi method using the high-precision library GMP for both cases and the resulting eigenvalues coincide very accurately with the semianalytic spectra for both cases (Frahm, Eom, and Shepelyansky, 2014).

When the spectrum of  $G$  is determined with good accuracy we can test the validity of the fractal Weyl law (5) changing the matrix size  $N_t$  by considering articles published from the beginning to a certain time moment  $t$  measured in years. The data presented in Fig. 46 show that the network size grows approximately exponentially as  $N_t = 2^{(t-t_0)/\tau}$  with the fit parameters  $t_0 = 1791$  and  $\tau = 11.4$ . The time interval considered in Fig. 46 is  $1913 \leq t \leq 2009$  since the first data point corresponds to  $t = 1913$  with  $N_t = 1500$  papers published between 1893 and 1913. The results, for the number  $N_\lambda$  of eigenvalues with  $|\lambda_i| > \lambda$ , show that its growth is well described by the relation  $N_\lambda = a(N_t)^\nu$  for the range when

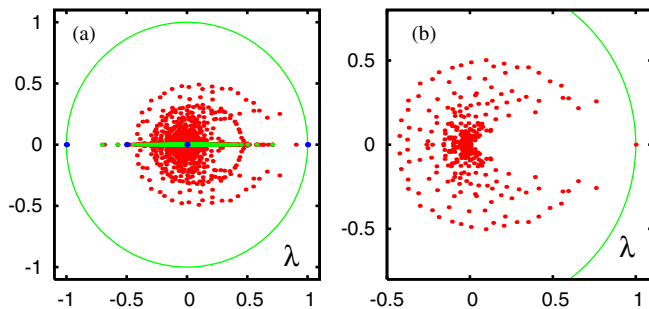


FIG. 45 (color online). (a) Most accurate spectrum of eigenvalues for the full Physical Review network; the gray (red) dots represent the core space eigenvalues obtained by the rational interpolation method with the numerical precision of  $p = 16\,384$  binary digits,  $n_R = 2500$  eigenvalues; light gray (green) dots show the degenerate subspace eigenvalues of the matrix  $S_0$  which are also eigenvalues of  $S$  with a degeneracy reduced by one (eigenvalues of the first group); black (blue) dots show the direct subspace eigenvalues of  $S$ . (b) Spectrum of numerically accurate 352 nonvanishing eigenvalues of the Google matrix for the triangular reduced Physical Review network determined by the Newton-Maehly method applied to the reduced polynomial (11) with a high-precision calculation of 256 binary digits; note the absence of subspace eigenvalues for this case. In both panels the gray (green) curves represent the unit circles. From Frahm, Eom, and Shepelyansky, 2014.

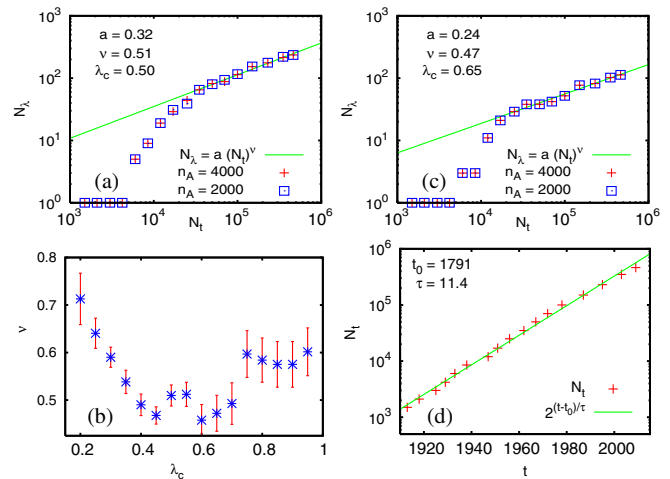


FIG. 46 (color online). Data for the whole citation network of Physical Review at different moments of time. (a) [or (c)] The number  $N_\lambda$  of eigenvalues with  $\lambda_c \leq \lambda \leq 1$  for  $\lambda_c = 0.50$  (or  $\lambda_c = 0.65$ ) vs the effective network size  $N_t$ , where the nodes with publication times after a cut time  $t$  are removed from the network. The gray (green) line shows the fractal Weyl law  $N_\lambda = a(N_t)^\nu$  with parameters  $a = 0.32 \pm 0.08$  ( $a = 0.24 \pm 0.11$ ) and  $\nu = 0.51 \pm 0.02$  ( $\nu = 0.47 \pm 0.04$ ) obtained from a fit in the range  $3 \times 10^4 \leq N_t < 5 \times 10^5$ . The number  $N_\lambda$  includes both exactly determined invariant subspace eigenvalues and core space eigenvalues obtained from the Arnoldi method with double precision (52 binary digits) for  $n_A = 4000$  [gray (red) crosses] and  $n_A = 2000$  [black (blue) squares]. (b) Exponent  $\nu$  with error bars obtained from the fit  $N_\lambda = a(N_t)^\nu$  in the range  $3 \times 10^4 \leq N_t < 5 \times 10^5$  vs the cut value  $\lambda_c$ . (d) The effective network size  $N_t$  vs cut time  $t$  (in years). The gray (green) line shows the exponential fit  $2^{(t-t_0)/\tau}$  with  $t_0 = 1791 \pm 3$  and  $\tau = 11.4 \pm 0.2$  representing the number of years after which the size of the network (number of papers published in all Physical Review journals) is effectively doubled. From Frahm, Eom, and Shepelyansky, 2014.

the number of articles becomes sufficiently large  $3 \times 10^4 \leq N_t < 5 \times 10^5$ . This range is not very large and probably due to that there is a certain dependence of the exponent  $\nu$  on the range parameter  $\lambda_c$ . At the same time we note that the maximal matrix size  $N$  studied here is probably the largest one used in numerical studies of the fractal Weyl law. We have  $0.47 < \nu < 0.6$  for all  $\lambda_c \geq 0.4$  that is definitely smaller than unity and thus the fractal Weyl law is well applicable to the Physical Review network. The value of  $\nu$  increases up to 0.7 for the data points with  $\lambda_c < 0.4$  but this is due to the fact that  $N_\lambda$  also includes some numerically incorrect eigenvalues related to the numerical instability of the Arnoldi method at standard double precision (52 binary digits) as discussed previously.

We conclude that the most appropriate choice for the description of the data is obtained at  $\lambda_c = 0.4$  which from one side excludes small, partly numerically incorrect, values of  $\lambda$  and on the other side gives sufficiently large values of  $N_\lambda$ . Here we have  $\nu = 0.49 \pm 0.02$  corresponding to the fractal dimension  $d = 0.98 \pm 0.04$ . Furthermore, for  $0.4 \leq \lambda_c \leq 0.7$  we have a rather constant value  $\nu \approx 0.5$  with  $d_f \approx 1.0$ . Of course, it would be interesting to extend this analysis to a

larger size  $N$  of citation networks of various type and not only for Physical Review. We expect that the fractal Weyl law is a generic feature of citation networks.

Further studies of the citation network of Physical Review concern the properties of eigenvectors (different from the PageRank) associated with relatively large complex eigenvalues, the fractal Weyl law, the correlations between PageRank and CheiRank (see also Sec. IV.C), and the notion of “ImpactRank” (Frahm, Eom, and Shepelyansky, 2014). To define the ImpactRank one may ask the question how a paper influences or has been influenced by other papers. For this one considers an initial vector  $v_0$ , localized on one node or paper. Then the modified Google matrix  $\tilde{G} = \gamma G + (1 - \gamma)v_0 e^T$  (with a damping factor  $\gamma \sim 0.5-0.9$ ) produces a “PageRank”  $v_f$  by the propagator  $v_f = (1 - \gamma)/(1 - \gamma G)v_0$ . In the vector  $v_f$  the leading nodes or papers have strongly influenced the initial paper represented in  $v_0$ . Doing the same for  $G^*$  one obtains a vector  $v_f^*$ , where the leading papers have been influenced by the initial paper represented in  $v_0$ . This procedure has been applied to certain historically important papers (Frahm, Eom, and Shepelyansky, 2014).

In summary, the results of this section show that the phenomenon of the Jordan error enhancement (12), induced by finite accuracy of computations with a finite number of digits, can be resolved by advanced numerical methods described previously. Thus the accurate eigenvalues  $\lambda$  can be obtained even for the most difficult case of quasitriangular matrices. Note that for other networks such as the WWW of UK universities, Wikipedia, and Twitter, the triangular structure of  $S$  is much less pronounced (see, e.g., Fig. 1) that gives a reduction of Jordan blocks so that the Arnoldi method with double precision computes accurate values of  $\lambda$ .

### XIII. RANDOM MATRIX MODELS OF MARKOV CHAINS

#### A. Albert-Barabási model of directed networks

There are various preferential attachment models generating complex scale-free networks (Albert and Barabási, 2002; Dorogovtsev, 2010). Such undirected networks are generated by the Albert-Barabási (AB) procedure (Albert and Barabási, 2000) which builds networks by an iterative process. Such a procedure has been generalized to generate directed networks in Giraud, Georgeot, and Shepelyansky (2009) with the aim to study properties of the Google matrix of such networks. The procedure works as follows: starting from  $m$  nodes, at each step  $m$  links are added to the existing network with probability  $p$ , or  $m$  links are rewired with probability  $q$ , or a new node with  $m$  links is added with probability  $1 - p - q$ . In each case the end node of new links is chosen with preferential attachment, i.e., with probability  $(k_i + 1)/\sum_j (k_j + 1)$ , where  $k_i$  is the total number of ingoing and outgoing links of node  $i$ . This mechanism generates directed networks having the small-world and scale-free properties, depending on the values of  $p$  and  $q$ . The results are averaged over  $N_r$  random realizations of the network to improve the statistics.

The studies (Giraud, Georgeot, and Shepelyansky, 2009) are done mainly for  $m = 5$ ,  $p = 0.2$  and two values of  $q$  corresponding to scale-free ( $q = 0.1$ ) and exponential

( $q = 0.7$ ) regimes of link distributions [see Fig. 1 in Albert and Barabási (2000) for undirected networks]. For the generated directed networks at  $q = 0.1$ , one finds properties close to the behavior for the WWW with the cumulative distribution of ingoing links showing algebraic decay  $P_c^{\text{in}}(k) \sim 1/k$  and average connectivity  $\langle k \rangle \approx 6.4$ . For  $q = 0.7$  one finds  $P_c^{\text{in}}(k) \sim \exp(-0.03k)$  and  $\langle k \rangle \approx 15$ . For outgoing links, the numerical data are compatible with an exponential decay in both cases with  $P_c^{\text{out}}(k) \sim \exp(-0.6k)$  for  $q = 0.1$  and  $P_c^{\text{out}}(k) \sim \exp(-0.1k)$  for  $q = 0.7$ . Small variations of parameters  $m$ ,  $p$ ,  $q$  near the chosen values do not qualitatively affect the properties of the  $G$  matrix.

It is found that the eigenvalues of  $G$  for the AB model have one  $\lambda = 1$  with all other  $|\lambda_i| < 0.3$  at  $\alpha = 0.85$  [see Fig. 1 in Giraud, Georgeot, and Shepelyansky (2009)]. This distribution shows no significant modification with the growth of matrix size  $2^{10} \leq N \leq 2^{14}$ . However, the values of IPR  $\xi$  are growing with  $N$  for typical values  $|\lambda| \sim 0.2$ . This indicates a delocalization of corresponding eigenstates at large  $N$ . At the same time the PageRank probability is well described by the algebraic dependence  $P \sim 1/K$  with  $\xi$  being practically independent of  $N$ .

These results for the directed AB model network shows that it captures certain features of real directed networks as, e.g., a typical PageRank decay with the exponent  $\beta \approx 1$ . However, the spectrum of  $G$  in this model is characterized by a large gap between  $\lambda = 1$  and other eigenvalues which have  $\lambda \leq 0.35$  at  $\alpha = 1$ . This feature is drastically different with spectra of such typical networks at the WWW of universities, Wikipedia, and Twitter (see Figs. 17, 22, and 32). In fact the AB model has no subspaces and no isolated or weakly coupled communities. In this network all sites can be reached from a given site in a logarithmic number of steps that generates a large gap in the spectrum of the Google matrix and a rapid relaxation to the PageRank eigenstate. In real networks there are plenty of isolated or weakly coupled communities and the introduction of a damping factor  $\alpha < 1$  is necessary to have a single PageRank eigenvalue at  $\lambda = 1$ . Thus the results obtained by Giraud, Georgeot, and Shepelyansky (2009) show that the AB model is not able to capture the important spectral features of real networks.

Additional studies by Giraud, Georgeot, and Shepelyansky (2009) analyzed the model of a real WWW university network with rewiring procedure of links, which consists of randomizing the links of the network keeping fixed the number of links at any given node. Starting from a single network, this creates an ensemble of randomized networks of the same size, where each node has the same number of ingoing and outgoing links as for the original network. The spectrum of such randomly rewired networks is also characterized by a large gap in the spectrum of  $G$  showing that rewiring destroys the communities existing in the original networks. The spectrum and eigenstate properties are studied in the related work on various real networks of moderate size  $N < 2 \times 10^4$  which have no spectral gap (Georgeot, Giraud, and Shepelyansky, 2010).

#### B. Random matrix models of directed networks

Previously we saw that the standard models of scale-free networks are not able to reproduce the typical properties of the

spectrum of Google matrices of real large-scale networks. At the same time we believe that it is important to find realistic matrix models of the WWW and other networks. Here we discuss certain results for certain random matrix models of  $G$ .

Analytical and numerical studies of random unistochastic or orthostochastic matrices of size  $N = 3$  and 4 lead to triplet and cross structures in the complex eigenvalue spectra (Zyczkowski *et al.*, 2003); see also Fig. 18. However, the size of such matrices is too small.

Here we consider other examples of random matrix models of Perron-Frobenius operators characterized by non-negative matrix elements and column sums normalized to unity. We call these models random Perron-Frobenius matrices (RPFM). A number of RPFM, with arbitrary size  $N$ , can be constructed by drawing  $N^2$  independent matrix elements  $0 \leq G_{ij} \leq 1$  from a given distribution  $p(G_{ij})$  with finite variance  $\sigma^2 = \langle G_{ij}^2 \rangle - \langle G_{ij} \rangle^2$  and normalizing the column sums to unity (Frahm, Eom, and Shepelyansky, 2014). The average matrix  $\langle G_{ij} \rangle = 1/N$  is just a projector on the vector  $e$  (with unity entries on each node, see also Sec. XII.A) and has the two eigenvalues  $\lambda_1 = 1$  (of multiplicity 1) and  $\lambda_2 = 0$  (of multiplicity  $N - 1$ ). Using an argument of degenerate perturbation theory on  $\delta G = G - \langle G \rangle$  and known results on the eigenvalue density of nonsymmetric random matrices (Guhr, Mueller-Groeling, and Weidenmueller, 1998; Mehta, 2004; Akemann, Baik, and Francesco, 2011) one finds that an arbitrary realization of  $G$  has the leading eigenvalue  $\lambda_1 = 1$  and the other eigenvalues are uniformly distributed on the complex unit circle of radius  $R = \sqrt{N}\sigma$  (see Fig. 47).

Choosing different distributions  $p(G_{ij})$  one obtains different variants of the model (Frahm, Eom, and Shepelyansky, 2014), for example,  $R = 1/\sqrt{3N}$  using a full matrix with uniform  $G_{ij} \in [0, 2/N]$ . Sparse models with  $Q \ll N$  nonvanishing elements per column can be modeled by a distribution, where the probability of  $G_{ij} = 0$  is  $1 - Q/N$  and for nonzero  $G_{ij}$  (either uniform in  $[0, 2/Q]$  or constant  $1/Q$ ) is  $Q/N$  leading to  $R = 2/\sqrt{3Q}$  (for uniform nonzero elements) or  $R = 1/\sqrt{Q}$  (for constant nonzero elements). The circular eigenvalue density with these values of  $R$  is also very well confirmed by numerical simulations in Fig. 47. Another case is a power law  $p(G) = D/(1 + aG)^{-b}$  (for  $0 \leq G \leq 1$ ) with  $D$  and  $a$  to be determined by normalization and the average  $\langle G_{ij} \rangle = 1/N$ . For  $b > 3$  this case is similar to a full matrix with  $R \sim 1/\sqrt{N}$ . However, for  $2 < b < 3$  one finds that  $R \sim N^{1-b/2}$ .

The situation changes when one imposes a triangular structure on  $G$  in which case the complex spectrum of  $\langle G \rangle$  is already quite complicated and, due to nondegenerate perturbation theory, close to the spectrum of  $G$  with modest fluctuations, mostly for the smallest eigenvalues (Frahm, Eom, and Shepelyansky, 2014). Following the previous discussion about triangular networks (with  $G_{ij} = 0$  for  $i \geq j$ ) we also numerically study a triangular RPFM, where for  $j \geq 2$  and  $i < j$  the matrix elements  $G_{ij}$  are uniformly distributed in the interval  $[0, 2/(j-1)]$  and for  $i \geq j$  we have  $G_{ij} = 0$ . When the first column is empty, that means it corresponds to a dangling node and it needs to be replaced by  $1/N$  entries. For the triangular RPFM the situation changes

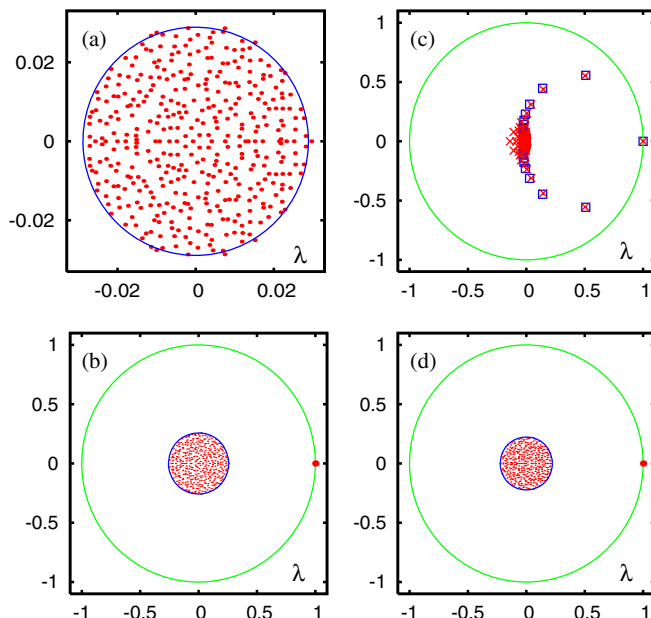


FIG. 47 (color online). (a) The spectrum [gray (red) dots] of one realization of a full uniform RPFM with dimension  $N = 400$  and matrix elements uniformly distributed in the interval  $[0, 2/N]$ ; the black (blue) outer circle represents the theoretical spectral border with radius  $R = 1/\sqrt{3N} \approx 0.02887$ . The unit eigenvalue  $\lambda = 1$  is not shown due to the zoomed presentation range. (c) The spectrum of one realization of triangular RPFM [gray (red) crosses] with nonvanishing matrix elements uniformly distributed in the interval  $[0, 2/(j-1)]$  and a triangular matrix with nonvanishing elements  $1/(j-1)$  [black (blue) squares]; here  $j = 2, 3, \dots, N$  is the index number of nonempty columns and the first column with  $j = 1$  corresponds to a dangling node with elements  $1/N$  for both triangular cases. (b), (d) The complex eigenvalue spectrum [gray (red) dots] of a sparse RPFM with dimension  $N = 400$  and  $Q = 20$  nonvanishing elements per column at random positions. (b) [or (d)] corresponds to the case of uniformly distributed nonvanishing elements in the interval  $[0, 2/Q]$  (constant nonvanishing elements being  $1/Q$ ); the black (blue) small circle represents the theoretical spectral border with radius  $R = 2/\sqrt{3Q} \approx 0.2582$  ( $R = 1/\sqrt{Q} \approx 0.2236$ ). (b), (d)  $\lambda = 1$  is shown by a larger red dot for better visibility. The unit circle is shown by the gray (green) curve [(b)–(d)]. From Frahm, Eom, and Shepelyansky, 2014.

completely since here the average matrix  $\langle G_{ij} \rangle = 1/(j-1)$  (for  $i < j$  and  $j \geq 2$ ) has already a nontrivial structure and eigenvalue spectrum. Therefore the argument of degenerate perturbation theory which allows one to apply the results of standard full nonsymmetric random matrices does not apply here. In Fig. 47 one clearly sees that for  $N = 400$  the spectra for one realization of a triangular RPFM and its average are very similar for the eigenvalues with large modulus but both do not have at all a uniform circular density in contrast to the RPFM models without the triangular constraint discussed previously. For the triangular RPFM the PageRank behaves as  $P(K) \sim 1/K$  with the ranking index  $K$  being close to the natural order of nodes  $\{1, 2, 3, \dots\}$  that reflects the fact that the node 1 has the maximum of  $N - 1$  incoming links, etc.

These results show that it is not so simple to propose a good random matrix model which captures the generic spectral

features of real directed networks. We think that investigations in this direction should be continued.

### C. Anderson delocalization of PageRank?

The phenomenon of Anderson localization of electron transport in disordered materials (Anderson, 1958) is now a well-known effect studied in detail in physics (Evers and Mirlin, 2008). In one and two dimensions even a small disorder leads to an exponential localization of electron diffusion that corresponds to an insulating phase. Thus, even if classical electron dynamics is diffusive and delocalized over the whole space, the effects of quantum interference generates a localization of all eigenstates of the Schrödinger equation. In higher dimensions a localization is preserved at sufficiently strong disorder, while a delocalized metallic phase appears for a disorder strength being smaller than a certain critical value dependent on the Fermi energy of electrons. This phenomenon is rather generic and we can expect that a somewhat similar delocalization transition can appear in the small-world networks.

Indeed, it is useful to consider the 1D Anderson model on a ring with a certain number of shortcut links, described by the Schrödinger equation

$$\epsilon_n \psi_n + V(\psi_{n+1} + \psi_{n-1}) + V \sum_S (\psi_{n+S} + \psi_{n-S}) = E \psi_n, \quad (15)$$

where  $\epsilon_n$  are random on site energies homogeneously distributed within the interval  $-W/2 \leq \epsilon_n \leq W/2$ , and  $V$  is the hopping matrix element. The sum over  $S$  is taken over randomly established shortcuts from a site  $n$  to any other random site of the network. The number of such shortcuts is  $S_{\text{tot}} = p_\ell L$ , where  $L$  is the total number of sites on a ring and  $p_\ell$  is the density of shortcut links. This model was introduced by Chepelienskii and Shepelyansky (2001). The numerical study, reported there, showed that the level-spacing statistics  $p(s)$  for this model has a transition from the Poisson distribution  $p_{\text{Pois}}(s) = \exp(-s)$ , typical for the Anderson localization phase, to the Wigner surmise distribution  $p_{\text{Wig}}(s) = (\pi s/2) \exp(-\pi s^2/4)$ , typical for the Anderson metallic phase (Guhr, Mueller-Groeling, and Weidenmueller, 1998; Evers and Mirlin, 2008). The numerical diagonalization was done via the Lanczos algorithm for sizes up to  $L = 32\,000$  and the typical parameter range  $0.005 \leq p_\ell < 0.1$  and  $1 \leq W/V \leq 4$ . An example of the variation of  $p_\ell(s)$  with a decrease of  $W/V$  is shown in Fig. 48(a). We see that the Wigner surmise provides a good description of the numerical data at  $W/V = 1$ , when the maximal localization length  $\ell_1 \approx 96(V/W)^2 \approx 96$  in the 1D Anderson model (Evers and Mirlin, 2008) is much smaller than the system size  $L$ .

To identify a transition from one limiting case  $p_{\text{Pois}}(s)$  to another  $p_{\text{Wig}}(s)$  it is convenient to introduce the parameter  $\eta_s = \int_0^{s_0} [p(s) - p_{\text{Wig}}(s)] ds / \int_0^{s_0} [p_{\text{Pois}}(s) - p_{\text{Wig}}(s)] ds$ , where  $s_0 = 0.4729\dots$  is the intersection point of  $p_{\text{Pois}}(s)$  and  $p_{\text{Wig}}(s)$ . In this way  $\eta_s$  varies from 1 [for  $p(s) = p_{\text{Pois}}(s)$ ] to 0 [for  $p(s) = p_{\text{Wig}}(s)$ ] (Shepelyansky, 2001). From the variation of  $\eta_s$  with system parameters and size  $L$ , the critical

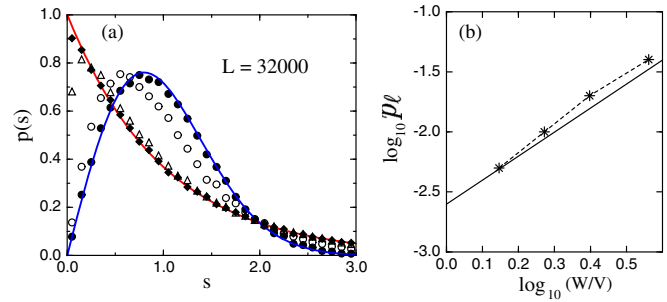


FIG. 48 (color online). (a) The gray (red) and black (blue) curves represent the Poisson and Wigner surmise distributions. Diamonds, triangles, open circles, and black solid circles represent, respectively, the level-spacing statistics  $p(s)$  at  $W/V = 4, 3, 2, 1$ ;  $p_\ell = 0.02$ ,  $L = 32\,000$ ; averaging is done over 60 network realizations. (b) Stars give dependence of  $p_\ell$  on a disorder strength  $W/V$  at the critical point when  $\eta_\ell(W, p_\ell) = 0.8$ , and  $p_\ell = 0.005, 0.01, 0.02, 0.04$  at fixed  $L = 8\,000$ ; the straight line corresponds to  $p_\ell = p_c = 1/4\ell_1 \approx (W/V)^2/400$ ; the dashed curve is to guide the eye. From Chepelienskii and Shepelyansky, 2001.

density  $p_\ell = p_c$  can be determined by the condition  $\eta_s(p_c, W/V) = \eta_c = 0.8 = \text{const}$  being independent of  $L$ . The obtained dependence of  $p_c$  on  $W/V$  obtained at a fixed critical point  $\eta_c = 0.8$  is shown in Fig. 48(b). The Anderson delocalization transition takes place when the density of shortcuts becomes larger than a critical density  $p_\ell > p_c \approx 1/(4\ell_1)$ , where  $\ell_1 \approx 96(V/W)^2$  is the length of Anderson localization in 1D. A simple physical interpretation of this result is that the delocalization takes place when the localization length  $\ell_1$  becomes larger than a typical distance  $1/(4p_\ell)$  between shortcuts. Further studies of the time evolution of the wave function  $\psi_n(t)$  and IPR  $\xi$  variation also confirmed the existence of quantum delocalization transition on this quantum small-world network (Giraud, Georgeot, and Shepelyansky, 2005).

Thus the results obtained for the quantum small-world networks (Chepelienskii and Shepelyansky, 2001; Giraud, Georgeot, and Shepelyansky, 2005) show that the Anderson transition can take place in such systems. However, the above model represents an undirected network corresponding to a symmetric matrix with a real spectrum while the typical directed networks are characterized by asymmetric matrix  $G$  and complex spectrum. The possibility of the existence of localized states of  $G$  for the WWW networks was also discussed by Perra *et al.* (2009) but the fact that in a typical case the spectrum of  $G$  is complex has not been analyzed in detail.

Previously we saw certain indications of the possibility of an Anderson-type delocalization transition for eigenstates of the  $G$  matrix. Our results show that certain eigenstates in the core space are exponentially localized [see, e.g., Fig. 19(b)]. Such states are localized only on a few nodes touching other nodes of network only by an exponentially small tail. A similar situation appears in the 1D Anderson model if absorption is introduced on one end of the chain. Then the eigenstates located far away from this place feel this absorption only by exponentially small tails so that the imaginary part of the eigenenergy has for such far away states only an

exponentially small imaginary part. It is natural to expect that such localization can be destroyed by some parameter variation. Indeed, certain eigenstates with  $|\lambda| < 1$  for the directed network of the AB model have IPR  $\xi$  growing with the matrix size  $N$  [see Sec. XIII.A and Giraud, Georgeot, and Shepelyansky (2009)] even if for the PageRank the values of  $\xi$  remain independent of  $N$ . The results for the Ulam network from Figs. 13 and 14 provide an example of directed network where the PageRank vector becomes delocalized when the damping factor is decreased from  $\alpha = 0.95$  to 0.85 (Zhirov, Zhirov, and Shepelyansky, 2010). This example demonstrates the possibility of PageRank delocalization but a deeper understanding of the conditions required for such a phenomenon to occur are still lacking. The main difficulty is the absence of well-established random matrix models which have properties similar to the available examples of real networks.

Indeed, for Hermitian and unitary matrices the theories of random matrices, mesoscopic systems, and quantum chaos allow one to capture the main universal properties of spectra and eigenstates (Guhr, Mueller-Groeling, and Weidenmueller, 1998; Mehta, 2004; Evers and Mirlin, 2008; Haake, 2010; Akemann, Baik, and Francesco, 2011). For asymmetric Google matrices the spectrum is complex and at the moment there are no good random matrix models which would allow one to perform analytical analysis of various parameter dependencies. It is possible that non-Hermitian Anderson models in 1D, which naturally generates a complex spectrum and may have delocalized eigenstates, will provide new insights in this direction (Goldsheid and Khoruzhenko, 1998). We note that the recent random Google matrix models studied by Zhirov and Shepelyansky (2015) give indications of the appearance of the Anderson transition for Google matrix eigenstates and a mobility edge contour in a plane of complex eigenvalues. Such a delocalization transition cannot be attributed to the percolation since in the small-world networks there are only 6 degrees of separation between nodes (Watts and Strogatz, 1998; Dorogovtsev, 2010).

#### XIV. OTHER EXAMPLES OF DIRECTED NETWORKS

##### A. Brain neural networks

von Neumann (1958) in 1958 traced first parallels between architecture of the computer and the brain. Since that time computers became an unavoidable element of the modern society forming a computer network connected by the WWW with about  $4 \times 10^9$  indexed web pages spread all over the world (see, e.g., <http://www.worldwidewebsite.com/>). This number starts to become comparable with  $10^{10}$  neurons in a human brain, where each neuron can be viewed as an independent processing unit connected with about  $10^4$  other neurons by synaptic links (Sporns, 2007). About 20% of these links are unidirectional (Felleman and van Essen, 1991) and hence the brain can be viewed as a directed network of neuron links. At present, more and more experimental information about neurons and their links becomes available and the investigations of properties of neuronal networks attract an active interest (Bullmore and Sporns, 2009; Zuo *et al.*, 2012). The fact that enormous sizes of the WWW and brain networks are comparable gives an idea that the Google matrix analysis should find useful application in brain science as is the case for the WWW.

First applications of methods of the Google matrix methods to brain neural networks was done by Shepelyansky and Zhirov (2010b) for a large-scale thalamocortical model (Izhikevich and Edelman, 2008) based on experimental measures in several mammalian species. The model spans three anatomic scales. (i) It is based on global (white-matter) thalamocortical anatomy obtained by means of diffusion tensor imaging of a human brain. (ii) It includes multiple thalamic nuclei and six-layered cortical microcircuitry based on *in vitro* labeling and three-dimensional reconstruction of single neurons of cat visual cortex. (iii) It has 22 basic types of neurons with appropriate laminar distribution of their branching dendritic trees. According to Izhikevich and Edelman (2008) the model exhibits behavioral regimes of normal brain activity that were not explicitly built in but emerged spontaneously as the result of interactions among anatomical and dynamic processes.

The model studied by Shepelyansky and Zhirov (2010b) contains  $N = 10^4$  neurons with  $N_\ell = 1\,960\,108$ . The results obtained show that PageRank and CheiRank vectors have rather large  $\xi$  being comparable to the whole network size at  $\alpha = 0.85$ . The corresponding probabilities have flat dependence on their indices showing that they are close to a delocalized regime. We attribute these features to a rather large number of links per node  $\zeta \approx 196$  being even larger than for the Twitter network. At the same time the PageRank-CheiRank correlator is rather small  $\kappa = -0.065$ . Thus this network is structured in such a way that functions related to order signals (outgoing links of CheiRank) and signals bringing orders (ingoing links of PageRank) are well separated and independent of each other as is the case for the Linux Kernel software architecture. The spectrum of  $G$  has a gapless structure showing that long-living excitations can exist in this neuronal network.

Of course, model systems of neural networks can provide a number of interesting insights but it is much more important to study examples of real neural networks. Kandiah and Shepelyansky (2014) performed such an analysis for the neural network of *C. elegans* (a worm). The full connectivity of this directed network is known and well documented at WormAtlas (Altun *et al.*, 2012). The number of linked neurons (nodes) is  $N = 279$  with the number of synaptic connections and gap junctions (links) between them being  $N_\ell = 2990$ .

The Google matrix  $G$  of *C. elegans* is constructed using the connectivity matrix elements  $S_{ij} = S_{\text{syn},ij} + S_{\text{gap},ij}$ , where  $S_{\text{syn}}$  is an asymmetric matrix of synaptic links whose elements are 1 if neuron  $j$  connects to neuron  $i$  through a chemical synaptic connection and 0 otherwise. The matrix part  $S_{\text{gap}}$  is a symmetric matrix describing gap junctions between pairs of cells,  $S_{\text{gap},ij} = S_{\text{gap},ji} = 1$  if neurons  $i$  and  $j$  are connected through a gap junction and 0 otherwise. Then the matrices  $G$  and  $G^*$  are constructed following the standard rule (1) at  $\alpha = 0.85$ . The connectivity properties of this network are similar to those of the WWW of Cambridge and Oxford with approximately the same number of links per node.

The spectra of  $G$  and  $G^*$  are shown in Fig. 49 with corresponding IPR values of eigenstates. The imaginary part of  $\lambda$  is relatively small  $|\text{Im}(\lambda)| < 0.2$  due to a large fraction of symmetric links. The second by modulus eigenvalues are



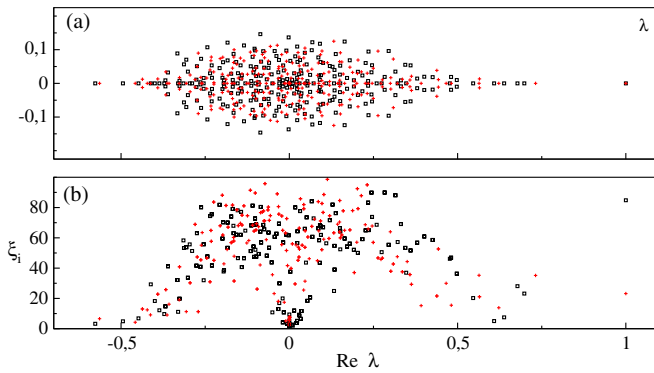


FIG. 49 (color online). (a) Spectrum of eigenvalues  $\lambda$  for the Google matrices  $G$  and  $G^*$  at  $\alpha = 0.85$  for the neural network of *C. elegans* [black and gray (red) symbols]. (b) Values of IPR  $\xi_i$  of eigenvectors  $\psi_i$  are shown as a function of corresponding  $\text{Re } \lambda$  (the same colors). From Kandiah and Shepelyansky, 2014.

$\lambda_2 = 0.8214$  for  $G$  and  $\lambda_2 = 0.8608$  for  $G^*$ . Thus the network relaxation time  $\tau = 1/|\ln \lambda_2|$  is approximately 5, 6.7 iterations of  $G, G^*$ . Certain IPR values  $\xi_i$  of eigenstates of  $G, G^*$  have rather large  $\xi \approx N/3$  while others have  $\xi$  located only on about ten nodes.

We have a large value  $\xi \approx 85$  for PageRank and a more moderate value  $\xi \approx 23$  for CheiRank vectors. Here we have the algebraic decay exponents being  $\beta \approx 0.33$  for  $P(K)$  and  $\beta \approx 0.50$  for  $P^*(K^*)$ . Of course, the network size is not large and these values are only approximate. However, they indicate an interchange between PageRank and CheiRank showing the importance of outgoing links. It is possible that such an inversion is related to a significant importance of outgoing links in neural systems: in a sense such links transfer orders, while ingoing links bring instructions to a given neuron from other neurons. The correlator  $\kappa = 0.125$  is small and thus the network structure allows one to perform a control of information flow in a more efficient way without interference of errors between orders and executions. We saw already in Sec. VII.A that such a separation of concerns emerges in the software architecture. It seems that the neural networks also adopt such a structure.

We note that a somewhat similar situation appears for networks of business process management where principals of a company are located at the top CheiRank position while the top PageRank positions belong to company contacts (Abel and Shepelyansky, 2011). Indeed, a case study of a real company structure analyzed by Abel and Shepelyansky (2011) also stress the importance of company managers who transfer orders to other structural units. For this network the correlator is also small being  $\kappa = 0.164$ . We expect that brain neural networks may have certain similarities with company organization.

Each neuron  $i$  belongs to two ranks  $K_i$  and  $K_i^*$  and it is convenient to represent the distribution of neurons on the PageRank-CheiRank plane  $(K, K^*)$  shown in Fig. 50. The plot confirms that there are little correlations between both ranks since the points are scattered over the whole plane. Neurons ranked at top  $K$  positions of PageRank have their soma located mainly in both extremities of the worm (head and tail) showing that neurons in those regions have important

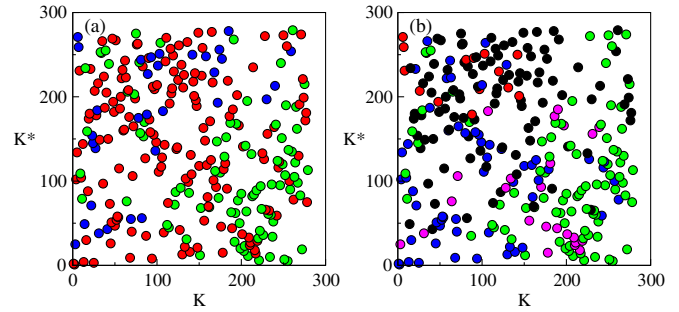


FIG. 50 (color online). The PageRank-CheiRank plane  $(K, K^*)$  showing distribution of neurons according to their ranking. (a) Soma region coloration—head (gray/red), middle (light gray/green), and tail (dark gray/blue). (b) Neuron-type coloration—sensory (gray/red), motor (light gray/green), interneuron (dark gray/blue), polymodal (light-dark gray/purple), and unknown (black). The classifications and colors are given according to the WormAtlas (Altun *et al.*, 2012). From Kandiah and Shepelyansky, 2014.

connections coming from many other neurons which control head and tail movements. This tendency is even more visible for neurons at top  $K^*$  positions of CheiRank but with a preference for head and middle regions. In general, neurons, that have their soma in the middle region of the worm, are quite highly ranked in CheiRank but not in PageRank. The neurons located at the head region have top positions in CheiRank and also PageRank, while the middle region has some top CheiRank indexes but rather large indexes of PageRank [Fig. 50(a)]. The neuron-type coloration [Fig. 50(b)] also reveals that sensory neurons are at top PageRank positions but at rather large CheiRank indexes, whereas in general motor neurons are in the opposite situation.

Top nodes of PageRank and CheiRank favor important signal relaying neurons such as *AVA* and *AVB* that integrate signals from crucial nodes and in turn pilot other crucial nodes. Neurons *AVAL, AVAR, AVBL, AVBR, and AVEL, AVER* are considered to belong to the rich club analyzed by Towlson *et al.* (2013). The top neurons in the 2DRank are *AVAL, AVAR, AVBL, AVBR, and PVCR* that correspond to a dominance of interneurons. More details can be found in Kandiah and Shepelyansky (2014).

The technological progress allows one to obtain more and more detailed information about neural networks (Bullmore and Sporns, 2009; Zuo *et al.*, 2012; Towlson *et al.*, 2013) even if it is not easy to get information about link directions. As a result we expect that the methods of directed network analysis described here will find useful future applications for brain neural networks.

## B. Google matrix of DNA sequences

The approaches of the Markov chains and the Google matrix can also be efficiently used for the analysis of statistical properties of DNA sequences. The Ensemble Genome data sets are publicly available at <http://www.ensembl.org/>. The analysis of Poincaré recurrences in these DNA sequences (Frahm and Shepelyansky, 2012b) shows their similarities with the statistical properties of recurrences for dynamical

trajectories in the Chirikov standard map and other symplectic maps (Frahm and Shepelyansky, 2010). Indeed, a DNA sequence can be viewed as a long symbolic trajectory and, hence, the Google matrix, constructed from it, highlights the statistical features of DNA from a new viewpoint.

An important step in the statistical analysis of DNA sequences was done by Mantegna *et al.* (1995) applying methods of statistical linguistics and determining the frequency of various words composed of up to seven letters. First order Markovian models have also been proposed and briefly discussed in this work. The Google matrix analysis provides a natural extension of this approach. Thus the PageRank eigenvector gives the most frequent words of a given length. The spectrum and eigenstates of  $G$  characterize the relaxation processes of different modes in the Markov process generated by a symbolic DNA sequence. Thus the comparison of word ranks of different species allows one to identify their proximity.

The statistical analysis is done for DNA sequences of the species: Homo sapiens (HS, human), Canis familiaris (CF, dog), Loxodonta africana (LA, elephant), Bos Taurus (BT, bull), and Danio rerio (DR, zebrafish) (Kandiah and Shepelyansky, 2013). For HS, DNA sequences are represented as a single string of length  $L \approx 1.5 \times 10^{10}$  base pairs (bp) corresponding to five individuals. Similar data are obtained for BT ( $2.9 \times 10^9$  bp), CF ( $2.5 \times 10^9$  bp), LA ( $3.1 \times 10^9$  bp), and DR ( $1.4 \times 10^9$  bp). All strings are composed of four letters  $A$ ,  $G$ ,  $G$ , and  $T$  and undetermined letter  $N_l$ . The strings can be found from Kandiah and Shepelyansky (2013).

For a given sequence we fix the words  $W_k$  of  $m$  letters length corresponding to the number of states  $N = 4^m$ . We consider that there is a transition from a state  $j$  to state  $i$  inside this basis  $N$  when we move along the string from left to right going from a word  $W_k$  to the next word  $W_{k+1}$ . This transition adds one unit in the transition matrix element  $T_{ij} \rightarrow T_{ij} + 1$ . The words with letter  $N_l$  are omitted; the transitions are counted only between nearby words not separated by words with  $N_l$ . There are approximately  $N_t \approx L/m$  such transitions for the whole length  $L$  since the fraction of undetermined letters  $N_l$  is small. Thus we have  $N_t = \sum_{i,j=1}^N T_{ij}$ . The Markov matrix of transitions  $S_{ij}$  is obtained by normalizing matrix elements in such a way that their sum in each column is equal to unity  $S_{ij} = T_{ij}/\sum_i T_{ij}$ . If there are columns with all zero elements (dangling nodes), then zeros of such columns are replaced by  $1/N$ . Then the Google matrix  $G$  is constructed from  $S$  by the standard rule (1). It is found that the spectrum of  $G$  has a significant gap and a variation of  $\alpha$  in a range (0.5,1) does not significantly affect the PageRank probability. Thus all DNA results are shown at  $\alpha = 1$ .

The image of matrix elements  $G_{KK'}$  is shown in Fig. 51 for HS with  $m = 6$ . We see that almost all of the matrix is full which is drastically different from the WWW and other networks considered previously. Analysis of the statistical properties of matrix elements  $G_{ij}$  shows that their integrated distribution follows a power law as shown in Fig. 52. Here  $N_g$  is the number of matrix elements of the matrix  $G$  with values  $G_{ij} > g$ . The data show that the number of nonzero matrix elements  $G_{ij}$  is very close to  $N^2$ . The main fraction of

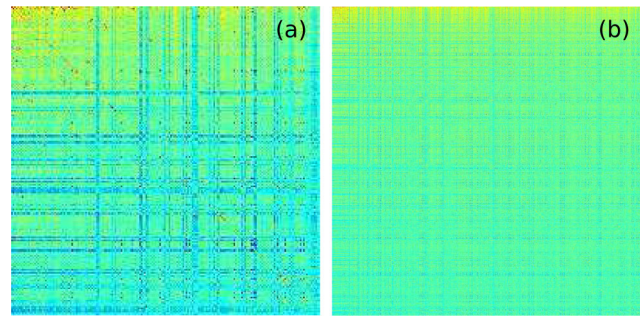


FIG. 51 (color online). DNA Google matrix of Homo sapiens (HS) constructed for words of six-letters length. Matrix elements  $G_{KK'}$  are shown in the basis of the PageRank index  $K$  (and  $K'$ ). Here  $x$  and  $y$  axes show  $K$  and  $K'$  within the ranges (a)  $1 \leq K, K' \leq 200$  and (b)  $1 \leq K, K' \leq 1000$ . The element  $G_{11}$  at  $K = K' = 1$  is placed at the top-left corner. Color marks the amplitude of matrix elements changing from black (blue) for the minimum zero value to gray (red) at the maximum value. From Kandiah and Shepelyansky, 2013.

elements has values  $G_{ij} \leq 1/N$  (some elements  $G_{ij} < 1/N$  since for certain  $j$  there are many transitions to some node  $i'$  with  $T_{i'j} \gg N$  and, e.g., only one transition to other  $i''$  with  $T_{i''j} = 1$ ). At the same time there are also transition elements  $G_{ij}$  with large values whose fraction decays in an algebraic law  $N_g \approx AN/g^{\nu-1}$  with some constant  $A$  and an exponent  $\nu$ . The fit of numerical data in the range  $-5.5 < \log_{10} g < -0.5$  of algebraic decay gives for  $m = 6$ :  $\nu = 2.46 \pm 0.025$  (BT),  $2.57 \pm 0.025$  (CF),  $2.67 \pm 0.022$  (LA),  $2.48 \pm 0.024$  (HS), and  $2.22 \pm 0.04$  (DR). For the HS case we find  $\nu = 2.68 \pm 0.038$  at  $m = 5$  and  $\nu = 2.43 \pm 0.02$  at  $m = 7$  with the average  $A \approx 0.003$  for  $m = 5, 6$ , and  $7$ . There are visible oscillations in the algebraic decay of  $N_g$  with  $g$  but in global we see that on average all species are well described by a universal decay law with the exponent  $\nu \approx 2.5$ . For comparison we also show the distribution  $N_g$  for the WWW networks of the University of Cambridge and Oxford in year 2006.

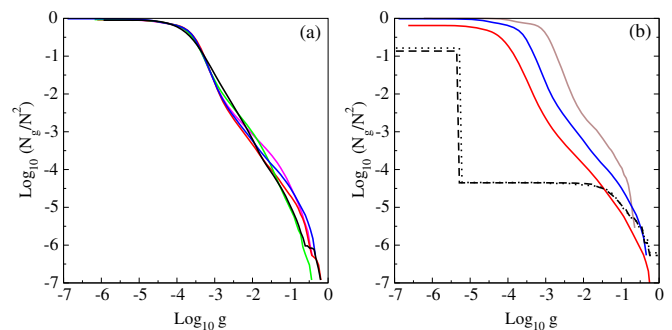


FIG. 52 (color online). Integrated fraction  $N_g/N^2$  of Google matrix elements with  $G_{ij} > g$  as a function of  $g$ . (a) Various species with six-letters word length: elephant LA (green), zebrafish DR (black), dog CF (red), bull BT (magenta), and Homo sapiens HS (blue) (from left to right at  $y = -5.5$ ). (b) Data for HS sequence with words of length  $m = 5$  (brown),  $6$  (blue),  $7$  (red) (from right to left at  $y = -2$ ); for comparison black dashed and dotted curves show the same distribution for the WWW networks of Universities of Cambridge and Oxford in 2006, respectively. From Kandiah and Shepelyansky, 2013.

We see that in these cases the distribution  $N_g$  has a very short range in which the decay is at least approximately algebraic [ $-5.5 < \log_{10}(N_g/N^2) < -6$ ]. In contrast to that for the DNA sequences we have a large range of algebraic decay.

Since in each column we have the sum of all elements equal to unity we can say that the differential fraction  $dN_g/dg \propto 1/g^\nu$  gives the distribution of outgoing matrix elements which is similar to the distribution of outgoing links extensively studied for the WWW networks. Indeed, for the WWW networks all links in a column are considered to have the same weight so that these matrix elements are given by an inverse number of outgoing links with the decay exponent  $\nu \approx 2.7$ . Thus, the obtained data show that the distribution of DNA matrix elements is similar to the distribution of outgoing links in the WWW networks. Indeed, for outgoing links of the Cambridge and Oxford networks the fit of numerical data gives the exponents  $\nu = 2.80 \pm 0.06$  (Cambridge) and  $2.51 \pm 0.04$  (Oxford).

As discussed previously, on average the probability of the PageRank vector is proportional to the number of ingoing links that works satisfactorily for sparse  $G$  matrices. For DNA we have a situation where the Google matrix is almost full and zero matrix elements are practically absent. In such a case an analog of the number of ingoing links is the sum of ingoing matrix elements  $g_s = \sum_{j=1}^N G_{ij}$ . The integrated distribution of ingoing matrix elements with the dependence of  $N_s$  on  $g_s$  is shown in Fig. 53. Here  $N_s$  is defined as the number of nodes with the sum of ingoing matrix elements being larger than  $g_s$ . A significant part of this dependence, corresponding to large values of  $g_s$  and determining the PageRank probability decay, is well described by a power law  $N_s \approx BN/g_s^{\mu-1}$ . The fit of data at  $m = 6$  gives  $\mu = 5.59 \pm 0.15$  (BT),  $4.90 \pm 0.08$  (CF),  $5.37 \pm 0.07$  (LA),  $5.11 \pm 0.12$  (HS), and  $4.04 \pm 0.06$  (DR). For the HS case at  $m = 5, 7$  we find, respectively,  $\mu = 5.86 \pm 0.14$  and  $4.48 \pm 0.08$ . For HS and other species we have on average  $B \approx 1$ .

For the WWW one usually has  $\mu \approx 2.1$ . Indeed, for the ingoing matrix elements of the Cambridge and Oxford networks we find, respectively, the exponents  $\mu = 2.12 \pm 0.03$  and  $2.06 \pm 0.02$  (see curves in Fig. 53). For the ingoing links distribution of the Cambridge and Oxford networks we obtain,

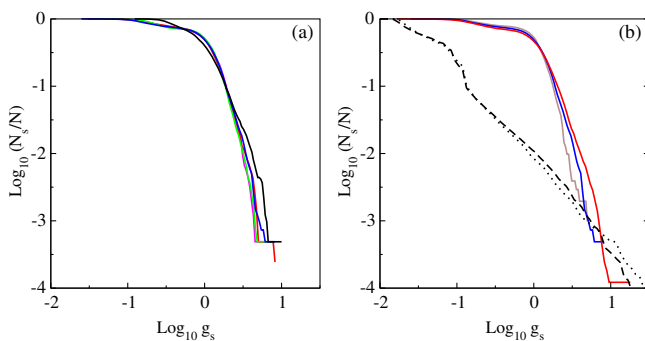


FIG. 53 (color online). Integrated fraction  $N_s/N$  of the sum of ingoing matrix elements with  $\sum_{j=1}^N G_{i,j} \geq g_s$ . (a), (b) The same cases as in Fig. 52 in the same colors. The dashed and dotted curves are shifted on the  $x$  axis by one unit left to fit the figure scale. From Kandiah and Shepelyansky, 2013.

respectively,  $\mu = 2.29 \pm 0.02$  and  $2.27 \pm 0.02$  which are close to the usual WWW value  $\mu \approx 2.1$ . In contrast the exponent  $\mu$  for DNA Google matrix elements gets a significantly larger value  $\mu \approx 5$ . This feature marks a significant difference between the DNA and WWW networks.

The PageRank vector can be obtained by a direct diagonalization. The dependence of probability  $P$  on index  $K$  is shown in Fig. 54 for various species and different word length  $m$ . The probability  $P(K)$  describes the steady state of random walks on the Markov chain and thus it gives the frequency of the appearance of various words of length  $m$  in the whole sequence  $L$ . The frequencies or probabilities of words appearance in the sequences were obtained by Mantegna *et al.* (1995) by a direct counting of words along the sequence (the available sequences  $L$  were shortened at that time). Both methods are mathematically equivalent and indeed our distributions  $P(K)$  are in good agreement with those found by Mantegna *et al.* (1995) even if now we have significantly better statistics.

The decay of  $P$  with  $K$  can be described by a power law  $P \sim 1/K^\beta$ . Thus, for example, for the HS sequence at  $m = 7$  we find  $\beta = 0.357 \pm 0.003$  for the fit range  $1.5 \leq \log_{10} K \leq 3.7$  that is rather close to the exponent found in Mantegna *et al.* (1995). Since on average the PageRank probability is proportional to the number of ingoing links, or the sum of ingoing matrix elements of  $G$ , one has the relation between the exponent of PageRank  $\beta$  and the exponent of ingoing links (or matrix elements)  $\beta = 1/(\mu - 1)$ . Indeed, for the HS DNA case at  $m = 7$  we have  $\mu = 4.48$  that gives  $\beta = 0.29$  being close to the above value of  $\beta = 0.357$  obtained from the direct fit of the  $P(K)$  dependence. The agreement is not so perfect since there is a visible curvature in the log-log plot of  $N_s$  vs  $g_s$  and also since a small value of  $\beta$  gives a moderate variation of  $P$  that produces a reduction of accuracy of the numerical fit procedure. In spite of this only approximate agreement we conclude that in global the relation between  $\beta$  and  $\mu$  works correctly.

It is interesting to plot a PageRank index  $K_s(i)$  of a given species  $s$  versus the index  $K_{hs}(i)$  of HS for the same word  $i$ . For identical sequences one should have all points on a

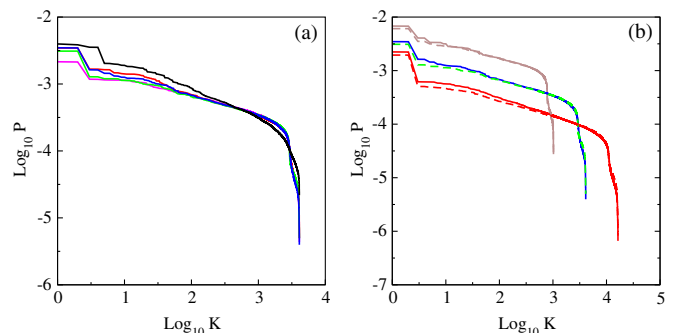


FIG. 54 (color online). Dependence of the PageRank probability  $P(K)$  on the PageRank index  $K$ . (a) Data for different species for word length of six letters: zebrafish DR (black), dog CF (red), Homo sapiens HS (blue), elephant LA (green), and bull BT (magenta) (from top to bottom at  $x = 1$ ). (b) Data for HS (full curve) and LA (dashed curve) for word length  $m = 5$  (brown), 6 (blue/green), and 7 (red) (from top to bottom at  $x = 1$ ). From Kandiah and Shepelyansky, 2013.

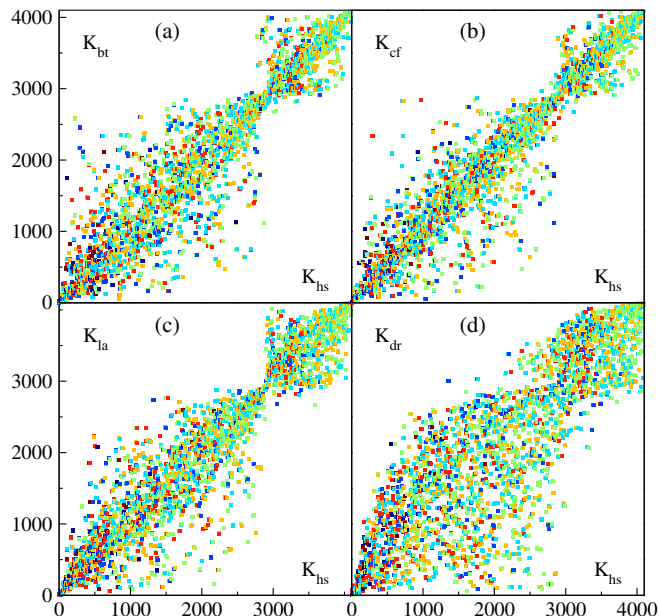


FIG. 55 (color online). PageRank proximity  $K - K$  plane diagrams for different species in comparison with *Homo sapiens*: (a) the  $x$  axis shows PageRank index  $K_{hs}(i)$  of a word  $i$  and the  $y$  axis shows the PageRank index of the same word  $i$  with  $K_{bt}(i)$  of bull, (b)  $K_{cf}(i)$  of dog, (c)  $K_{la}(i)$  of elephant, and (d)  $K_{dr}(i)$  of zebrafish; here the word length is  $m = 6$ . The colors of the symbols mark the purine content in a word  $i$  (fractions of letters  $A$  or  $G$  in any order); the color varies from gray (red) at maximal content, via brown, yellow, green, and light blue, to black (blue) at minimal zero content. From Kandiah and Shepelyansky, 2013.

diagonal, while the deviations from the diagonal characterize the differences between species. The examples of such PageRank proximity  $K - K$  diagrams are shown in Fig. 55 for words at  $m = 6$ . A visual impression is that the CF case has less deviations from the HS rank compared to BT and LA. The nonmammalian DR case has the most strong deviations from the HS rank.

The fraction of purine letters  $A$  or  $G$  in a word of  $m = 6$  letters is shown by color in Fig. 55 for all words ranked by PageRank index  $K$ . We see that these letters are approximately homogeneously distributed over the whole range of  $K$  values. To determine the proximity between different species or different HS individuals we compute the average dispersion

$$\sigma(s_1, s_2) = \sqrt{\frac{1}{N} \sum_{i=1}^N [K_{s_1}(i) - K_{s_2}(i)]^2} \quad (16)$$

between two species (individuals)  $s_1$  and  $s_2$ . Comparing the words with length  $m = 5, 6,$  and  $7$  we find that the scaling  $\sigma \propto N$  works with good accuracy (about 10% when  $N$  is increased by a factor of 16). To represent the result in a form independent of  $m$  we compare the values of  $\sigma$  with the corresponding random model value  $\sigma_{rnd}$ . This value is computed assuming a random distribution of  $N$  points in a square  $N \times N$  when only one point appears in each column and each line (e.g., at  $m = 6$  we have  $\sigma_{rnd} \approx 1673$  and  $\sigma_{rnd} \propto N$ ). The dimensionless dispersion is

then given by  $\zeta(s_1, s_2) = \sigma(s_1, s_2) / \sigma_{rnd}$ . From the ranking of different species we obtain the following values at  $m = 6$ :  $\zeta(CF, BT) = 0.308$ ;  $\zeta(LA, BT) = 0.324$ ,  $\zeta(LA, CF) = 0.303$ ;  $\zeta(HS, BT) = 0.246$ ,  $\zeta(HS, CF) = 0.206$ ,  $\zeta(HS, LA) = 0.238$ ;  $\zeta(DR, BT) = 0.425$ ,  $\zeta(DR, CF) = 0.414$ ,  $\zeta(DR, LA) = 0.422$ , and  $\zeta(DR, HS) = 0.375$  (other  $m$  have similar values). According to this statistical analysis of PageRank proximity between species we find that the  $\zeta$  value is minimal between CF and HS showing that these two are the most similar species among those considered here. Comparison of two HS individuals gives the value  $\zeta(HS1, HS2) = 0.031$  being significantly smaller than the proximity correlator between different species (Kandiah and Shepelyansky, 2012).

The spectrum of  $G$  was analyzed in detail by Kandiah and Shepelyansky (2012). It was shown that it has a relatively large gap due to which there is a relatively rapid relaxation of probability of a random surfer to the PageRank values.

### C. Gene regulation networks

At present the analysis of gene transcription regulation networks and recovery of their control biological functions is an active research field of bioinformatics (Milo *et al.*, 2002). Here, following Ermann, Chepelienskii, and Shepelyansky (2012), we provide two simple examples of a 2DRanking analysis for gene transcriptional regulation networks of *Escherichia Coli* [ $N = 423$ ,  $N_\ell = 519$  (Shen-Orr *et al.*, 2002)] and yeast [ $N = 690$ ,  $N_\ell = 1079$  (Milo *et al.*, 2002)]. In the construction of the  $G$  matrix the outgoing links to all nodes in each column are taken with the same weight  $\alpha = 0.85$ .

The distribution of nodes in the PageRank-Cheirank plane is shown in Fig. 56. The top five nodes, with their operon names, are given there for indices of PageRank  $K$ , Cheirank  $K^*$ , and 2DRank  $K_2$ . This ranking selects operons with the most high functionality in communication ( $K^*$ ), popularity ( $K$ ), and those that combine both features ( $K_2$ ). For these networks the correlator  $\kappa$  is close to zero ( $\kappa = -0.0645$  for *Escherichia Coli* and  $\kappa = -0.0497$  for yeast; see Fig. 6) that

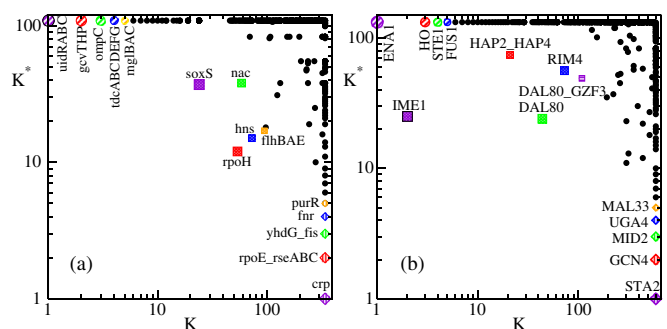


FIG. 56 (color online). Distribution of nodes in the PageRank-Cheirank plane ( $K, K^*$ ) for (a) *Escherichia Coli* v1.1 and (b) yeast gene transcription networks [network data are taken from Milo *et al.* (2002), Shen-Orr *et al.* (2002), and Alon (2014)]. The nodes with the top five probability values of PageRank, Cheirank, and 2DRank are labeled by their corresponding operon (node) names; they correspond to the five lowest values of indices  $K, K_2, K^*$ . From Ermann, Chepelienskii, and Shepelyansky, 2012.

indicates the statistical independence between outgoing and ingoing links being quite similar to the case of the PCN for the Linux Kernel. This shows that a slightly negative correlator  $\kappa$  is a generic property for the data flow network of control and regulation systems. A similar situation appears for networks of business process management and brain neural networks. Thus it is possible that the networks performing control functions are characterized in general by small correlator  $\kappa$  values. We expect that the 2DRanking will find further useful applications for large-scale gene regulation networks.

#### D. Networks of game go

The complexity of the well-known game go is such that no computer program has been able to beat a good player, in contrast with chess where world champions have been bested by game simulators. It is partly due to the fact that the total number of possible allowed positions in go is about  $10^{171}$ , compared to, e.g., only  $10^{50}$  for chess (Tromp and Farneback, 2007).

It has been argued that the complex network analysis can give useful insights for a better understanding of this game. With this aim a network, modeling the game of go, was defined by a statistical analysis of the databases of several important historical professional and amateur Japanese go tournaments (Georgeot and Giraud, 2012). In this approach moves and nodes are defined as all possible patterns in  $3 \times 3$  plaquettes on a go board of  $19 \times 19$  intersections. Taking into account all possible obvious symmetry operations the number of nonequivalent moves is reduced to  $N = 1107$ . Moves which are close in space (typically a maximal distance of four intersections) are assumed to belong to the same tactical fight generating transitions on the network.

Using the historical data of many games, the transition probabilities between the nodes may be determined leading to a directed network with a finite size Perron-Frobenius operator which can be analyzed by tools of PageRank, CheiRank, complex eigenvalue spectrum, properties of certain selected eigenvectors, and also certain other quantities (Georgeot and Giraud, 2012; Kandiah, Georgeot, and Giraud, 2014). The studies are done for plaquettes of different sizes with the corresponding network size changing from  $N = 1107$  for plaquette squares with  $3 \times 3$  intersections up to maximal  $N = 193\,995$  for diamond-shape plaquettes with  $3 \times 3$  intersections plus the four at distance two from the center in the four directions left, right, top, down. It is shown that the PageRank leads to a frequency distribution of moves which obeys a Zipf law with exponents close to unity but this exponent may slightly vary if the network is constructed with shorter or longer sequences of successive moves. The important nodes in certain eigenvectors may correspond to certain strategies, such as protecting a stone and eigenvectors are also different between amateur and professional games. It is also found that the different phases of the game go are characterized by a different spectrum of the  $G$  matrix. The results obtained show that with the help of the Google matrix analysis it is possible to extract communities of moves which share some common properties.

Georgeot and Giraud (2012) and Kandiah, Georgeot, and Giraud (2014) argued that the Google matrix analysis can find a number of interesting applications in the theory of games and the human decision-making processes.

#### E. Opinion formation on directed networks

Understanding the nature and origins of mass opinion formation is an outstanding challenge of democratic societies (Zaller, 1999). In the last few years the enormous development of such social networks as LiveJournal, Facebook, Twitter, and VKONTAKTE, with up to hundreds of millions of users, has demonstrated the growing influence of these networks on social and political life. The small-world scale-free structure of the social networks, combined with their rapid communication facilities, leads to a very fast information propagation over networks of electors, consumers, and citizens, making them very active on instantaneous social events. This invokes the need for new theoretical models which would allow one to understand the opinion formation process in modern society in the 21st century.

The important steps in the analysis of opinion formation have been done with the development of various voter models, described in great detail by Castellano, Fortunato, and Loreto (2009) and Krapivsky, Redner, and Ben-Naim (2010). This research field became known as sociophysics (Galam, 1986, 2008). Here, following Kandiah and Shepelyansky (2012), we analyze the opinion formation process introducing several new aspects which take into account the generic features of social networks. First we analyze the opinion formation on real directed networks such as the WWW of the Universities of Cambridge and Oxford (2006), Twitter (2009), and LiveJournal. This allows us to incorporate the correct scale-free network structure instead of unrealistic regular lattice networks, often considered in voter models. Second, we assume that the opinion at a given node is formed by the opinions of its linked neighbors weighted with the PageRank probability of these network nodes. The introduction of such a weight represents the reality of social networks, where network nodes are characterized by the PageRank vector which provides a natural ranking of node importance, or elector or society member importance. In a certain sense, the top nodes of PageRank correspond to a political elite of the social network whose opinion influences the opinions of other members of the society (Zaller, 1999). Thus the proposed PageRank opinion formation (PROF) model takes into account the situation in which an opinion of an influential friend from high ranks of the society counts more than an opinion of a friend from a lower society level. We argue that the PageRank probability is the most natural form of ranking of society members. Indeed, the efficiency of a PageRank rating had been well demonstrated for various types of scale-free networks.

The PROF model is defined in the following way. In agreement with the standard PageRank algorithm we determine the probability  $P(K_i)$  for each node ordered by PageRank index  $K_i$  (using  $\alpha = 0.85$ ). In addition, a network node  $i$  is characterized by an Ising spin variable  $\sigma_i$  which can take value  $+1$  or  $-1$ , coded also by red or blue color, respectively. The sign of a node  $i$  is determined by its direct neighbors  $j$ , which have PageRank probabilities  $P_j$ . For that we compute the sum  $\Sigma_i$  over all directly linked neighbors  $j$  of node  $i$ :

$$\begin{aligned} \Sigma_i = & a \sum_j (P^+_{j,\text{in}} - P^-_{j,\text{in}}) \\ & + b \sum_j (P^+_{j,\text{out}} - P^-_{j,\text{out}}), \quad a + b = 1, \quad (17) \end{aligned}$$

where  $P_{j,\text{in}}$  and  $P_{j,\text{out}}$  denote the PageRank probability  $P_j$  of a node  $j$  pointing to node  $i$  (ingoing link) and a node  $j$  to which node  $i$  points to (outgoing link), respectively. Here the two parameters  $a$  and  $b$  are used to tune the importance of ingoing and outgoing links with the imposed relation  $a + b = 1$  ( $0 \leq a, b \leq 1$ ). The values  $P^+$  and  $P^-$  correspond to red and blue nodes, and the spin  $\sigma_i$  takes the value 1 or  $-1$ , respectively, for  $\Sigma_i > 0$  or  $\Sigma_i < 0$ . In a certain sense we can say that a large value of parameter  $b$  corresponds to a conformist society in which an elector  $i$  takes an opinion of other electors to which he or she points. In contrast, a large value of  $a$  corresponds to a tenacious society in which an elector  $i$  mainly takes the opinion of those electors who point to him or her. A standard random number generator is used to create an initial random distribution of spins  $\sigma_i$  on a given network. The time evolution then is determined by Eq. (17) applied to each spin one by one. When all  $N$  spins are turned following Eq. (17) a time unit  $t$  is changed to  $t \rightarrow t + 1$ . Up to  $N_r = 10^4$  random initial generations of spins are used to obtain statistically stable results. We present results for the number of red nodes since other nodes are blue.

The main part of studies is done for the WWW of Cambridge and Oxford discussed previously. We start with a random realization of a given fraction of red nodes  $f_i = f(t = 0)$  in which evolution in time converges to a steady state with a final fraction of red nodes  $f_f$  approximated after time  $t_c \approx 10$ . However, different initial realizations with the same  $f_i$  value evolve to different final fractions  $f_f$  clearly showing a bistability phenomenon. To analyze how the final fraction of red nodes  $f_f$  depends on its initial fraction  $f_i$ , we study the time evolution  $f(t)$  for a large number  $N_r$  of initial random realizations of colors following it up to the convergence time for each realization. We found that the final red nodes are homogeneously distributed in the PageRank index  $K$ . Thus there is no specific preference for top society levels for an initial random distribution. The probability distribution  $W_f$  of final fractions  $f_f$  is shown in Fig. 57 as a function of initial fraction  $f_i$  at  $a = 0.1$ . The results show the two main features of the model: a small fraction of red opinion is completely suppressed if  $f_i < f_c$  and its larger fraction dominates completely for  $f_i > 1 - f_c$ ; there is a bistability phase for the initial opinion range  $f_b \leq f_i \leq 1 - f_b$ . Of course, there is symmetry with respect to the exchange of red and blue colors. For the small value  $a = 0.1$  we have  $f_b \approx f_c$  with  $f_c \approx 0.25$ . For the larger value  $a = 0.9$  we have  $f_c \approx 0.35$  and  $f_b \approx 0.45$  (Kandiah and Shepelyansky, 2012).

Our interpretation of these results is the following. For small values of  $a \ll 1$  the opinion of a given society member is determined mainly by the PageRank of neighbors to whom he or she points (outgoing links). The PageRank probability  $P$  of nodes to which many nodes point is usually high, since  $P$  is proportional to the number of ingoing links. Thus at  $a \ll 1$  the society is composed of members who form their opinion by listening to an elite opinion. In such a society its elite with one

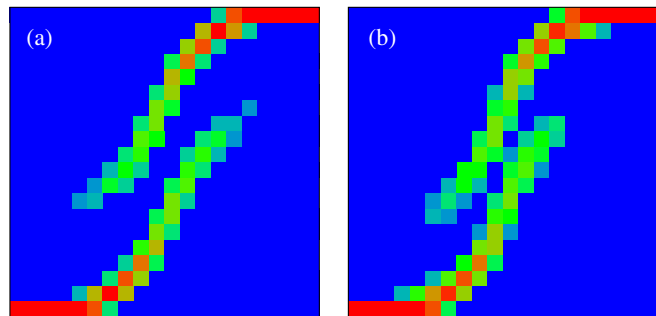


FIG. 57 (color online). Density plot of probability  $W_f$  to find a final red fraction  $f_f$ , shown on the  $y$  axis, in dependence on an initial red fraction  $f_i$ , shown on the  $x$  axis; data are shown inside the unit square  $0 \leq f_i, f_f \leq 1$ . The values of  $W_f$  are defined as a relative number of realizations found inside each of  $20 \times 20$  cells which cover the whole unit square. Here  $N_r = 10^4$  realizations of randomly distributed colors are used to obtain  $W_f$  values; for each realization the time evolution is followed up the convergence time with up to  $t = 20$  iterations.; (a) Cambridge network and (b) Oxford network at  $a = 0.1$ . The probability  $W_f$  is proportional to color changing from zero (black/blue) to unity (gray/red). From Kandiah and Shepelyansky, 2012.

color opinion can impose this opinion on a large fraction of the society. Indeed, the direct analysis of the case, where the top  $N_{\text{top}} = 2000$  nodes of PageRank index have the same red color, shows that this 1% of the society elite can impose its opinion to about 50% of the whole society at small  $a$  values (conformist society) while at large  $a$  values (tenacious society) this fraction drops significantly [see Fig. 4 in Kandiah and Shepelyansky (2012)]. We attribute this to the fact that in Fig. 57 we start with a randomly distributed opinion, since the opinion of the elite has two fractions of two colors this creates a bistable situation when the two fractions of society follow the opinions of this divided elite, which makes the situation bistable on a larger interval of  $f_i$  compared to the case of a tenacious society at  $a \rightarrow 1$ . In Eq. (17) when we replace  $P$  by 1 then the bistability disappears.

However, a detailed understanding of the opinion formation on directed networks still waits its development. Indeed, the results of the PROF model for the LiveJournal and Twitted networks show that the bistability in these networks practically disappears. Also for the Twitter network studied in Sec. X.A, the elite of  $N_{\text{top}} = 35\,000$  (about 0.1% of the whole society) can impose its opinion to 80% of the society at small  $a < 0.15$  and to about 30% for  $a > 0.15$  (Kandiah and Shepelyansky, 2012). It is possible that a large number of links between top PageRank nodes in Twitter creates a stronger tendency to a totalitarian opinion formation comparing to the case of university networks. At the same time the studies of opinion formation with the PROF model on the Ulam networks (Chakhmakhchyan and Shepelyansky, 2013), which do not have a large number of links, show practically no bistability in opinion formation. It is expected that a small number of loops is at the origin of such a difference with respect to university networks. Various extensions and properties of the PROF model are discussed by Eom and Shepelyansky (2015).

Finally we discuss a more generic version of opinion formation called the PROF-Sznajd model (Kandiah and

Shepelyansky, 2012). Indeed, we see that in the PROF model on university network opinions of small groups of red nodes with  $f_i < f_c$  are completely suppressed that seems to not be very realistic. In fact, the Sznajd model (Sznajd-Weron and Sznajd, 2000) features the idea of resistant groups of a society and thus incorporates a well-known trade union principle “United we stand, divided we fall.” Usually the Sznajd model is studied on regular lattices. Its generalization for directed networks is done on the basis of the notion of groups of nodes  $N_g$  at each discrete time step  $\tau$ .

The evolution of group is defined by the following rules:

- (a) We pick in the network by random a node  $i$  and consider the polarization of  $N_g - 1$  the highest PageRank nodes pointing to it.
- (b) If node  $i$  and all other  $N_g - 1$  nodes have the same color (same polarization), then these  $N_g$  nodes form a group whose effective PageRank value is the sum of all the member values  $P_g = \sum_{j=1}^{N_g} P_j$ .
- (c) Consider all the nodes pointing to any member of the group and check all these nodes  $n$  directly linked to the group: if an individual node PageRank value  $P_n$  is less than the defined above  $P_g$ , the node joins the group by taking the same color (polarization) as the group nodes and increases  $P_g$  by the value of  $P_n$ ; if that is not the case, a node is left unchanged.

The above time step is repeated many times during time  $\tau$ , counting the number of steps and choosing a random node  $i$  on each next step.

The time evolution of this PROF-Sznajd model converges to a steady state after  $\tau \approx 10N$  steps. This is compatible with the results obtained for the PROF model. However, the statistical fluctuations in the steady-state regime are present keeping the color distribution only on average. The dependence of the final fraction of red nodes  $f_f$  on its initial value  $f_i$  is shown by the density plot of probability  $W_f$  in Fig. 58 for the university networks. The probability  $W_f$  is obtained from many initial random realizations in a similar way to the case of Fig. 57. We see that there is a significant difference compared to the PROF model: now even at small values of  $f_i$  we find small but finite values of  $f_f$ , while in the PROF model the red color disappears at  $f_i < f_c$ . This feature is related to the essence of the Sznajd model: here even small groups can resist against the totalitarian opinion. Other features of Fig. 58 are similar to those found for the PROF model: we again observe bistability of opinion formation. The number of nodes  $N_g$ , which form the group, does not significantly affect the distribution  $W_f$  (for studied  $3 \leq N_g \leq 13$ ).

The previous studies of opinion formation models on scale-free networks show that the society elite, corresponding to the top PageRank nodes, can impose its opinion on a significant fraction of the society. However, for a homogeneous distribution of two opinions, there exists a bistability range of opinions which depends on a conformist parameter characterizing the opinion formation. The proposed PROF-Sznajd model shows that totalitarian opinions can be escaped from by small sub-communities. The enormous development of social networks in the last few years definitely shows that the analysis of opinion formation on such networks requires further investigation.

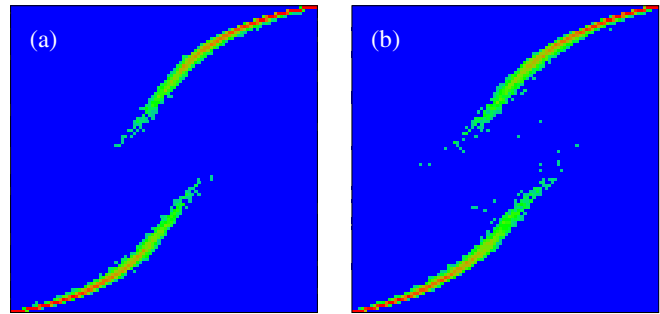


FIG. 58 (color online). The PROF-Sznajd model, option 1: density plot of probability  $W_f$  to find a final red fraction  $f_f$ , shown on the  $y$  axis, in dependence on an initial red fraction  $f_i$ , shown on the  $x$  axis; data are shown inside the unit square  $0 \leq f_i, f_f \leq 1$ . The values of  $W_f$  are defined as a relative number of realizations found inside each of  $100 \times 100$  cells which cover the whole unit square. Here  $N_r = 10^4$  realizations of randomly distributed colors are used to obtain  $W_f$  values; for each realization the time evolution follows the convergence time with up to  $\tau = 10^7$  steps. (a) Cambridge network, (b) Oxford network; here  $N_g = 8$ . The probability  $W_f$  is proportional to color changing from zero (black/blue) to unity (gray/red). From Kandiah and Shepelyansky, 2012.

## XV. DISCUSSION

Previously we considered many examples of real directed networks where the Google matrix analysis finds useful applications. The examples belong to various sciences varying from the WWW, social and Wikipedia networks, software architecture to world trade, games, DNA sequences, and Ulam networks. It is clear that the concept of Markov chains and Google matrix represents the mathematical foundation of directed network analysis.

For Hermitian and unitary matrices there are now many universal concepts, developed in theoretical physics, so that the main properties of such matrices are well understood. Indeed, such characteristics as level-spacing statistics, localization and delocalization properties of eigenstates, Anderson transition (Anderson, 1958), and quantum chaos features can be well handled by various theoretical methods (Guhr, Mueller-Groeling, and Weidenmueller, 1998; Mehta, 2004; Evers and Mirlin, 2008; Haake, 2010; Akemann, Baik, and Francesco, 2011). A number of generic models has been developed in this area allowing one to understand the main effects via numerical simulations and analytical tools.

In contrast to the previous cases of Hermitian or unitary matrices, the studies of matrices of Markov chains of directed networks are now only at their initial stage. In this review, for examples of real networks we illustrated certain typical properties of such matrices. Among them there is the fractal Weyl law, which has certain traces in the field of quantum chaotic scattering, but the main parts of the features are new ones. In fact, the spectral properties of Markov chains had not been investigated on a large scale. We try here to provide an introduction to the properties of such matrices which contain all information about large-scale directed networks. The Google matrix is like *The Library of Babel* (Borges, 1962), which contains everything. Unfortunately, we are still not able

to find generic Markov matrix models which reproduce the main features of the real networks. Among them there is the possible spectral degeneracy at damping  $\alpha = 1$ , the absence of a spectral gap, and the algebraic decay of eigenvectors. Because of the absence of such generic models it is still difficult to capture the main properties of real directed networks and to understand or predict their variations with a change of network parameters. At the moment the main part of real networks have an algebraic decay of the PageRank vector with an exponent  $\beta \approx 0.5-1$ . However, certain examples of Ulam networks (see Figs. 13 and 14) show that a delocalization of the PageRank probability over the whole network can take place. Such a phenomenon looks to be similar to the Anderson transition for electrons in disordered solids. It is clear that if an Anderson delocalization of the PageRank would take place, as a result of further developments of the WWW, the search engines based on the PageRank would lose their efficiency since the ranking would become very sensitive to various fluctuations. In a sense the whole world would go blind the day such a delocalization takes place. Because of that a better understanding of the fundamental properties of Google matrices and their dependences on various system parameters have a high practical significance. We believe that the theoretical research in this direction should be actively continued. In many respects, as *The Library of Babel*, the Google matrix still keeps its secrets to be discovered by researchers from various fields of science. We hope that further research will allow one “to formulate a general theory of the Library and solve satisfactorily the problem which no conjecture had deciphered: the formless and chaotic nature of almost all the books” (Borges, 1962).

#### ACKNOWLEDGMENTS

We are grateful to our colleagues M. Abel, A. D. Chepelianskii, Y.-H. Eom, B. Georgeot, O. Giraud, V. Kandiah, and O. V. Zhirov for fruitful collaborations on the topics included in this review. We also thank our partners of the EC FET open project NADINE A. Benczúr, N. Litvak, S. Vigna, and colleague A. Kaltenbrunner for illuminating discussions. Our special thanks go to Debora Donato for her insights at our initial stage of this research. Our research presented here is supported in part by the European Commission Future and Emerging Technologies (EC FET) Open project “New tools and algorithms for directed network analysis” (NADINE No. 288956). This work was granted access to the HPC resources of CALMIP (Toulouse) under the allocation 2012-P0110. We also thank the United Nations Statistics Division for provided help and friendly access to the UN COMTRADE database.

#### REFERENCES

- Abel, M. W., and D. L. Shepelyansky, 2011, *Eur. Phys. J. B* **84**, 493.
- Akemann, G., J. Baik, and Ph. Di Francesco, 2011, *The Oxford Handbook of Random Matrix Theory* (Oxford University Press, Oxford).
- Albert, R., and A.-L. Barabási, 2000, *Phys. Rev. Lett.* **85**, 5234.
- Albert, R., and A.-L. Barabási, 2002, *Rev. Mod. Phys.* **74**, 47.
- Alon, U., 2014, <http://www.weizmann.ac.il/mcb/UriAlon/>.
- Altun, Z. F., L. A. Herndon, C. Crocker, R. Lints, and D. H. Hall, 2012, Eds., *WormAtlas*, <http://www.wormatlas.org>.
- Anderson, P. W., 1958, *Phys. Rev.* **109**, 1492.
- Aragón, P., D. Laniado, A. Kaltenbrunner, and Y. Volkovich, 2012, *Proceedings of the 8th WikiSym2012* (ACM, New York), Vol. 19, [arXiv:1204.3799v2](https://arxiv.org/abs/1204.3799v2).
- Arnoldi, W. E., 1951, *Q. Appl. Math.* **9**, 17.
- Barigozzi, M., G. Fagiolo, and D. Garlaschelli, 2010, *Phys. Rev. E* **81**, 046104.
- Bascompte, J., P. Jordano, C. J. Melian, and J. M. Olesen, 2003, *Proc. Natl. Acad. Sci. U.S.A.* **100**, 9383.
- Bastolla, U., M. A. Pascual-Garcia, A. Ferrera, B. Luque, and J. Bascompte, 2009, *Nature (London)* **458**, 1018.
- Blank, M., G. Keller, and J. Liverani, 2002, *Nonlinearity* **15**, 1905.
- Bohigas, O., M.-J. Giannoni, and C. Schmit, 1984, *Phys. Rev. Lett.* **52**, 1.
- Borges, J. L., 1962, *The Library of Babel (Ficciones)* (Grove Press, New York).
- Brin, M., and G. Stuck, 2002, *Introduction to Dynamical Systems* (Cambridge University Press, Cambridge, UK).
- Brin, S., and L. Page, 1998, *Comp. Networks ISDN Syst.* **30**, 107.
- Bruzda, W., M. Smaczyński, V. Cappellini, H.-J. Sommers, and K. Zyczkowski, 2010, *Phys. Rev. E* **81**, 066209.
- Bullmore, E., and O. Sporns, 2009, *Nat. Rev. Neurosci.* **10**, 312.
- Burgos, E., H. Ceva, L. Hernández, R. P. J. Perazzo, M. Devoto, and D. Medan, 2008, *Phys. Rev. E* **78**, 046113.
- Burgos, E., H. Ceva, R. P. J. Perazzo, M. Devoto, D. Medan, M. Zimmermann, and A. M. Delbue, 2007, *J. Theor. Biol.* **249**, 307.
- Caldarelli, G., 2003, *Scale-free networks* (Oxford University Press, Oxford).
- Capocci, A., V. D. P. Servedio, F. Colaiori, L. S. Buriol, D. Donato, S. Leonardi, and G. Caldarelli, 2006, *Phys. Rev. E* **74**, 036116.
- Castellano, C., S. Fortunato, and V. Loreto, 2009, *Rev. Mod. Phys.* **81**, 591.
- Central Intelligence Agency, 2009, *The CIA World Factbook 2010* (Skyhorse Publ., New York).
- Chakhmakhchyan, L., and D. L. Shepelyansky, 2013, *Phys. Lett. A* **377**, 3119.
- Chen, N., N. Litvak, and M. Olvera-Cravioto, 2014, [arXiv:1408.3610](https://arxiv.org/abs/1408.3610).
- Chepelianskii, A. D., 2010, [arXiv:1003.5455](https://arxiv.org/abs/1003.5455).
- Chepelianskii, A. D., and D. L. Shepelyansky, 2001, <http://www.quantware.ups-tlse.fr/talks-posters/chepelianskii2001.pdf>.
- Chirikov, B. V., 1979, *Phys. Rep.* **52**, 263.
- Chirikov, B. V., and D. Shepelyansky, 2008, *Scholarpedia* **3**, 3550.
- Cornfeld, I. P., S. V. Fomin, and Y. G. Sinai, 1982, *Ergodic Theory* (Springer, New York).
- Craig, B., and G. von Peter, 2010, *Interbank tiering and money center bank* (Discussion paper N 12/2010, Deutsche Bundesbank).
- De Benedictis, L., and L. Tajoli, 2011, *The World Economy* **34**, 1417 [<http://onlinelibrary.wiley.com/journal/10.1111/%28ISSN%291467-9701>].
- Dijkstra, E. W., 1982, *Selected Writing on Computing: A Personal Perspective* (Springer-Verlag, New York).
- Dimassi, M., and J. Sjöstrand, 1999, *Spectral Asymptotics in the Semiclassical Limit* (Cambridge University Press, Cambridge, England).
- Donato, D., L. Laura, S. Leonardi, and S. Milozzi, 2004, *Eur. Phys. J. B* **38**, 239.
- Dorogovtsev, S., 2010, *Lectures on Complex Networks* (Oxford University Press, Oxford).
- Dorogovtsev, S. N., A. V. Goltsev, and J. F. F. Mendes, 2008, *Rev. Mod. Phys.* **80**, 1275.



- Eom, Y.-H., P. Aragón, D. Laniado, A. Kaltenbrunner, S. Vigna, and D. L. Shepelyansky, 2015, *PLoS One* **10**, e0114825.
- Eom, Y.-H., K. M. Frahm, A. Benczúr, and D. L. Shepelyansky, 2013, *Eur. Phys. J. B* **86**, 492.
- Eom, Y.-H., and D. L. Shepelyansky, 2013, *PLoS One* **8**, e74554.
- Eom, Y.-H., and D. L. Shepelyansky, 2015, *Physica (Amsterdam)* **436A**, 707.
- Ermann, L., A. D. Chepelianskii, and D. L. Shepelyansky, 2011, *Eur. Phys. J. B* **79**, 115.
- Ermann, L., A. D. Chepelianskii, and D. L. Shepelyansky, 2012, *J. Phys. A* **45**, 275101.
- Ermann, L., K. M. Frahm, and D. L. Shepelyansky, 2013, *Eur. Phys. J. B* **86**, 193.
- Ermann, L., K. M. Frahm, and D. L. Shepelyansky, 2015, color figures are available in open access at arXiv-preprint <http://arxiv.org/pdf/1409.0428v2.pdf>.
- Ermann, L., and D. L. Shepelyansky, 2010a, *Phys. Rev. E* **81**, 036221.
- Ermann, L., and D. L. Shepelyansky, 2010b, *Eur. Phys. J. B* **75**, 299.
- Ermann, L., and D. L. Shepelyansky, 2011, *Acta Phys. Pol. A* **120**, A158.
- Ermann, L., and D. L. Shepelyansky, 2012, *Physica (Amsterdam)* **241D**, 514.
- Ermann, L., and D. L. Shepelyansky, 2013, *Phys. Lett. A* **377**, 250.
- Ermann, L., and D. L. Shepelyansky, 2015, *Eur. Phys. J. B* **88**, 84.
- Evers, F., and A. D. Mirlin, 2008, *Rev. Mod. Phys.* **80**, 1355.
- Felleman, D. J., and D. C. van Essen, 1991, *Cereb. Cortex* **1**, 1.
- Fogaras, D., 2003, in *Innovative Internet Community Systems*, edited by T. Bohme, G. Heyer, and H. Unger, Lecture Notes in Computer Science Vol. 2877 (Springer-Verlag, Berlin/Heidelberg), p. 65 [[http://link.springer.com/chapter/10.1007/978-3-540-39884-4\\_6#page-2](http://link.springer.com/chapter/10.1007/978-3-540-39884-4_6#page-2)].
- Fortunato, S., 2010, *Phys. Rep.* **486**, 75.
- Frahm, K. M., A. D. Chepelianskii, and D. L. Shepelyansky, 2012, *J. Phys. A* **45**, 405101.
- Frahm, K. M., Y.-H. Eom, and D. L. Shepelyansky, 2014, *Phys. Rev. E* **89**, 052814.
- Frahm, K. M., B. Georgeot, and D. L. Shepelyansky, 2011, *J. Phys. A* **44**, 465101.
- Frahm, K. M., and D. L. Shepelyansky, 2009, *Phys. Rev. E* **80**, 016210.
- Frahm, K. M., and D. L. Shepelyansky, 2010, *Eur. Phys. J. B* **76**, 57.
- Frahm, K. M., and D. L. Shepelyansky, 2012a, *Eur. Phys. J. B* **85**, 355.
- Frahm, K. M., and D. L. Shepelyansky, 2012b, *Phys. Rev. E* **85**, 016214.
- Frahm, K. M., and D. L. Shepelyansky, 2013, *Eur. Phys. J. B* **86**, 322.
- Frahm, K. M., and D. L. Shepelyansky, 2014, *Eur. Phys. J. B* **87**, 93.
- Franceschet, M., 2011, *Commun. ACM* **54**, 92.
- Froyland, G., and K. Padberg, 2009, *Physica (Amsterdam)* **238D**, 1507.
- Galam, S., 1986, *J. Math. Psychol.* **30**, 426.
- Galam, S., 2008, *Int. J. Mod. Phys. C* **19**, 409.
- Gamow, G. A., 1928, *Z. Phys.* **51**, 204.
- Gantmacher, F. R., 2000, *The Theory of Matrices*, Vol. 2 (AMS Chelsea Publ., New York).
- Garlaschelli, D., and M. I. Loffredo, 2005, *Physica (Amsterdam)* **355A**, 138.
- Garratt, R. J., L. Mahadeva, and K. Svirydzenka, 2011, Mapping systemic risk in the international banking network (Working paper N 413, Bank of England).
- Gaspard, P., 1998, *Chaos, Scattering and Statistical Mechanics* (Cambridge University Press, Cambridge, England).
- Gaspard, P., 2014, *Scholarpedia* **9**, 9806.
- Georgeot, B., and O. Giraud, 2012, *Europhys. Lett.* **97**, 68002.
- Georgeot, B., O. Giraud, and D. L. Shepelyansky, 2010, *Phys. Rev. E* **81**, 056109.
- Giraud, O., B. Georgeot, and D. L. Shepelyansky, 2005, *Phys. Rev. E* **72**, 036203.
- Giraud, O., B. Georgeot, and D. L. Shepelyansky, 2009, *Phys. Rev. E* **80**, 026107.
- Goldshaid, I. Y., and B. A. Khoruzhenko, 1998, *Phys. Rev. Lett.* **80**, 2897.
- Golub, G. H., and C. Greif, 2006, *BIT* **46**, 759.
- Guhr, T., A. Mueller-Groeling, and H. A. Weidenmueller, 1998, *Phys. Rep.* **299**, 189.
- Haake, F., 2010, *Quantum Signatures of Chaos* (Springer-Verlag, Berlin).
- Hart, M. H., 1992, *The 100: Ranking of the Most Influential Persons in History* (Citadel Press, New York).
- He, J., and M. W. Deem, 2010, *Phys. Rev. Lett.* **105**, 198701.
- Hrisitidis, V., H. Hwang, and Y. Papakonstantinou, 2008, *ACM Transactions on Database Systems* **33**, 1.
- Izhikevich, E. M., and G. M. Edelman, 2008, *Proc. Natl. Acad. Sci. U.S.A.* **105**, 3593.
- Jelenkovic, P. R., and M. Olvera-Cravioto, 2013, *Springer Proceedings in Mathematics & Statistics*, edited by G. Alsmeyer, and M. Löwe (Springer, Berlin), Vol. 53, p. 159 [<http://link.springer.com/book/10.1007/978-3-642-38806-4#page=161>].
- Kandiah, V., H. Escaith, and D. L. Shepelyansky, 2015, *Eur. Phys. J. B* **88**, 186; arXiv:1507.03278.
- Kandiah, V., B. Georgeot, and O. Giraud, 2014, *Eur. Phys. J. B* **87**, 246.
- Kandiah, V., and D. L. Shepelyansky, 2012, *Physica (Amsterdam)* **391A**, 5779.
- Kandiah, V., and D. L. Shepelyansky, 2013, *PLoS One* **8**, e61519.
- Kandiah, V., and D. L. Shepelyansky, 2014, *Phys. Lett. A* **378**, 1932.
- Kernighan, B. W., and D. M. Ritchie, 1978, *The C Programming Language* (Prentice Hall, Englewood Cliffs, NJ).
- Kleinberg, J. M., 1999, *J. ACM* **46**, 604.
- Krapivsky, P. L., S. Redner, and E. Ben-Naim, 2010, *A Kinetic View of Statistical Physics* (Cambridge University Press, Cambridge, UK).
- Krugman, P. R., M. Obstfeld, and M. Melitz, 2011, *International Economics: Theory & Policy* (Prentice Hall, New Jersey).
- Landau, L. D., and E. M. Lifshitz, 1989, *Quantum Mechanics* (Nauka, Moscow).
- Langville, A. M., and C. D. Meyer, 2006, *Google's PageRank and Beyond: The Science of Search Engine Rankings* (Princeton University Press, Princeton, NJ).
- Li, T.-Y., 1976, *J. Approx. Theory* **17**, 177.
- Lichtenberg, A. J., and M. A. Lieberman, 1992, *Regular and Chaotic Dynamics* (Springer, Berlin).
- Linux Kernel, 2010, releases are downloaded from <http://www.kernel.org/>.
- Litvak, N., W. R. W. Scheinhardt, and Y. Volkovich, 2008, in *Algorithms and Models for the Web-Graph*, Lecture Notes in Computer Science Vol. 4936 (Springer, Berlin/Heidelberg), p. 72.
- Lu, W. T., S. Sridhar, and M. Zworski, 2003, *Phys. Rev. Lett.* **91**, 154101.
- Mantegna, R. N., S. V. Buldyrev, A. L. Goldberger, S. Havlin, C.-K. Peng, M. Simons, and H. E. Stanley, 1995, *Phys. Rev. E* **52**, 2939.
- Markov, A. A., 1906, *Izvestiya Fiziko-matematicheskogo obschestva pri Kazanskom universitete, 2-ya seriya* (in Russian) **15**, 135.
- May, R. M., 2001, *Stability and Complexity in Model Ecosystems* (Princeton University Press, Princeton, NJ).

- Mehta, M. L., 2004, *Random Matrices* (Elsevier-Academic Press, Amsterdam).
- Memmott, J., N. M. Waser, and M. V. Price, 2004, *Proc. R. Soc. B* **271**, 2605.
- Meusel, R., S. Vigna, O. Lehmberg, and C. Bizer, 2015, *J. Web Sci.* **1**, 33.
- Milo, R., S. Shen-Orr, S. Itzkovitz, N. Kashtan, D. Chklovskii, and U. Alon, 2002, *Science* **298**, 824.
- Muchnik, L., R. Itzhack, S. Solomon, and Y. Louzoun, 2007, *Phys. Rev. E* **76**, 016106.
- Newman, M. E. J., 2001, *Proc. Natl. Acad. Sci. U.S.A.* **98**, 404.
- Newman, M. E. J., 2003, *SIAM Rev.* **45**, 167.
- Newman, M. E. J., 2010, *Networks: An Introduction* (Oxford University Press, Oxford, UK).
- Nonnenmacher, S., J. Sjostrand, and M. Zworski, 2014, *Ann. Math.* **179**, 179.
- Nonnenmacher, S., and M. Zworski, 2007, *Commun. Math. Phys.* **269**, 311.
- Olesen, J. M., J. Bascompte, Y. L. Dupont, and P. Jordano, 2007, *Proc. Natl. Acad. Sci. U.S.A.* **104**, 19891.
- Pandurangan, G., P. Raghavan, and E. Upfal, 2006, *Internet Math.* **3**, 1.
- Perra, N., V. Zlatic, A. Chessa, C. Conti, D. Donato, and G. Caldarelli, 2009, *Europhys. Lett.* **88**, 48002.
- Radicchi, F., S. Fortunato, B. Markines, and A. Vespignani, 2009, *Phys. Rev. E* **80**, 056103.
- Redner, S., 1998, *Eur. Phys. J. B* **4**, 131.
- Redner, S., 2005, *Phys. Today* **58**, No. 6, 49.
- Rezende, E. L., J. E. Lavabre, P. R. Guimaraes, P. Jordano, and J. Bascompte, 2007, *Nature (London)* **448**, 925.
- Rodríguez-Gironés, M. A., and L. Santamaría, 2006, *J. Biogeography* **33**, 924.
- Saverda, S., D. B. Stouffer, B. Uzzi, and J. Bascompte, 2011, *Nature (London)* **478**, 233.
- Serra-Capizzano, S., 2005, *SIAM J. Matrix Anal. Appl.* **27**, 305.
- Serrano, M. A., M. Boguna, and A. Vespignani, 2007, *J. Econ. Interact. Coord.* **2**, 111.
- Shen-Orr, A., R. Milo, S. Mangan, and U. Alon, 2002, *Nat. Genet.* **31**, 64.
- Shepelyansky, D., 2015, Top 100 historical figures of Wikipedia, <https://hal.archives-ouvertes.fr/hal-01184245/>.
- Shepelyansky, D. L., 2001, *Phys. Scr.* **2001**, 112.
- Shepelyansky, D. L., 2008, *Phys. Rev. E* **77**, 015202(R).
- Shepelyansky, D. L., and O. V. Zhironov, 2010a, *Phys. Rev. E* **81**, 036213.
- Shepelyansky, D. L., and O. V. Zhironov, 2010b, *Phys. Lett. A* **374**, 3206.
- Sjöstrand, J., 1990, *Duke Math. J.* **60**, 1.
- SJR, 2007, SCImago, SJR SCImago Journal & Country, Rank <http://www.scimagojr.com>.
- Skiena, S., and C. B. Ward, 2014, *Who's Bigger?: Where Historical Figures Really Rank* (Cambridge University Press, New York), <http://www.whoisbigger.com/>.
- Song, C., S. Havlin, and H. A. Makse, 2005, *Nature (London)* **433**, 392.
- Soramäki, K., M. L. Bech, J. Arnold, R. J. Glass, and W. E. Beyeler, 2007, *Physica (Amsterdam)* **379A**, 317.
- Sporns, O., 2007, *Scholarpedia* **2**, 4695.
- Stewart, G. W., 2001, *Matrix Algorithms Vol. II: Eigensystems* (SIAM, Philadelphia, PA).
- Sznajd-Weron, K., and J. Sznajd, 2000, *Int. J. Mod. Phys. C* **11**, 1157.
- Towlson, E. K., P. E. Vértes, S. E. Ahnert, W. R. Schafer, and E. T. Bullmore, 2013, *J. Neurosci.* **33**, 6380.
- Tromp, J., and G. Farneback, 2007, in *Computers and Games*, Lecture Notes in Computer Science Vol. 4630 (Springer-Verlag, Berlin/Heidelberg), p. 84 [<http://link.springer.com/book/10.1007/978-3-540-75538-8>].
- Ulam, S., 1960, *A Collection of Mathematical Problems*, Interscience Tracts in Pure and Applied Mathematics (Interscience, New York).
- UN COMTRADE, 2011, United Nations Commodity Trade Statistics Database, <http://comtrade.un.org/db/>.
- Vázquez, D. P., and M. A. Aizen, 2004, *Ecology* **85**, 1251.
- Vigna, S., 2013, [arXiv:0912.0238v13](https://arxiv.org/abs/0912.0238v13).
- von Neumann, J., 1958, *The Computer and The Brain* (Yale University Press, New Haven, CT).
- Watts, D. J., and S. H. Strogatz, 1998, *Nature (London)* **393**, 440.
- Weyl, H., 1912, *Math. Ann.* **71**, 441.
- Zaller, J. R., 1999, *The Nature and Origins of Mass Opinion* (Cambridge University Press, Cambridge, UK).
- Zhironov, A. O., O. V. Zhironov, and D. L. Shepelyansky, 2010, *Eur. Phys. J. B* **77**, 523.
- Zhironov, O. V., and D. L. Shepelyansky, 2015, *Ann. Phys. (Berlin)* (to be published).
- Zipf, G. K., 1949, *Human Behavior and the Principle of Least Effort* (Addison-Wesley, Boston).
- Zlatic, V., M. Bozicevic, H. Stefancic, and M. Domazet, 2006, *Phys. Rev. E* **74**, 016115.
- Zuo, X.-N., R. Ehmke, M. Mennes, D. Imperati, F. X. Castellanos, O. Sporns, and M. P. Milham, 2012, *Cereb. Cortex* **22**, 1862.
- Zworski, M., 1999, *Not. Am. Math. Soc.* **46**, 319 [<http://www.ams.org/notices/199903/zworski.pdf>].
- Zyczkowski, K., M. Kus, W. Slomczynski, and H.-J. Sommers, 2003, *J. Phys. A* **36**, 3425.